การวิเคราะห์แบบความโค้งมากของโครงข้อแข็งยืดหยุ่นเชิงเส้นสองมิติ

ด้วยวิธีการรวมสติฟเนสโดยตรง

นายจงค์อาพล ดวรหวัน

LARGE CURVATURE ANALYSIS OF TWO-DIMENSIONAL LINEAR ELASTIC FRAMES BY DIRECT STIFFNESS METHOD

Mr. Jongaphonh Douanevanh

A Thesis Submitted in Partial Fulfillment of the Requirements

for the Degree of Master of Engineering Program in Civil Engineering

Department of Civil Engineering

Faculty of Engineering

Chulalongkorn University

Academic Year 2011

Thesis Title	LARGE CURVATURE ANALYSIS OF TWO-DIMENSIONAL LINEAR ELASTIC FRAMES BY DIRECT STIFFNESS METHOD
By	Mr. Jongaphonh Douanevanh
Field of Study	Civil Engineering
Thesis Advisor	Assistant Professor Jaroon Rungamornrat, Ph.D.
Thesis Co-advisor	Khampaseuth Thepvongsa, D.Eng.

Accepted by the Faculty of Engineering, Chulalongkorn University in Partial Fulfillment of the Requirements for the Master's Degree

………………………………….Dean of the Faculty of Engineering

(Associate Professor Boonsom Lerdhirunwong, Dr.Ing.)

THESIS COMMITTEE

………………………………………….. Chairman

(Professor Teerapong Senjuntichai, Ph.D.)

………………………………………..……. Thesis Advisor

(Assistant Professor Jaroon Rungamornrat, Ph.D.)

………………………………………..……. Thesis Co-advisor

(Khampaseuth Thepvongsa, D.Eng.)

……………………………………………….. Examiner

(Akhrawat Lenwari, Ph.D.)

……………………………………………….. External Examiner

(Punchet Thammarak, Ph.D.)

iv

iv

จงค์อาพล ดวรหวัน : การวิเคราะห์แบบความโค้งมากของโครงข้อแข็งยืดหยุ่นเชิงเส้นสองมิติด้วยวิธี
การรวมสติฟเนสโดยตรง. (LARGE CURVATURE ANALYSIS OF TWO-
DIMENSIONAL LINEAR ELASTIC FRAMES BY DIRECT STIFFNESS
METHOD) อ.ที่ปรึกษาวิทยานิพนธ์หลัก : ผศ. ดร. จรูญ รุ่งอมรรัตน์, อ.ที่ปรึกษาวิทยานิพนธ์ร่วม :
ดร.คำประเสิรฐ เทพวงษา, 74 หน้า.

วิทยานิพนธ์นี้ นำเสนอระเบียบวิธีกึ่งเชิงวิเคราะห์ที่มีประสิทธิภาพโดยอาศัยหลักการการหมุนร่วมและ
การรวมสติฟเนสโดยตรงสำหรับการวิเคราะห์การเปลี่ยนตำแหน่งและการหมุนมากของโครงข้อแข็งยืดหยุ่นเชิง
เส้นยืดหดตัวได้แบบสองมิติที่มีเรขาคณิตและรับแรงกระทำแบบทั่วไป ระเบียบวิธีที่พัฒนาขึ้นใช้ขั้นตอนมาตรา
ฐานของการรวมสติฟเนสโดยตรงในการพัฒนาสมการกำกับของทั้งโครงสร้างอย่างเป็นระบบ โดยในการพัฒนา
สมการกำกับนั้น เซตของสมการเชิงอนุพันธ์ไร้เชิงเส้นที่ได้จากความสัมพันธ์แบบแม่นตรงระหว่างความโค้งและ
การเปลี่ยนตำแหน่งถูกนำมาใช้สำหรับพัฒนาเซตของสมการกำกับเชิงพีชคณิตไร้เชิงเส้นที่สมมูลกันสำหรับชิ้น
ส่วนตรงสม่ำเสมอ สมการกำกับดังกล่าวนี้ ได้ถูกนำมาใช้เพื่อหาความสัมพันธ์ระหว่างแรงและการเปลี่ยนตำ
แหน่งรวมทั้งเมทริกซ์เกรเดียนท์ของชิ้นส่วนในระบบพิกัดหมุนร่วม ผลที่ได้ดังกล่าวนี้ สามารถนำไปใช้ร่วมกับ
เทคนิคการหมุนร่วมเพื่อพัฒนาความสัมพันธ์ระหว่างแรงและการเปลี่ยนตำแหน่งและเมทริกซ์สติฟเนสสัมผัส
แบบแม่นตรงสำหรับชิ้นส่วนทั่วไป เมทริกซ์สติฟเนสสัมผัสแบบแม่นตรงและแรงคงค้างแบบแม่นตรงของ
โครงสร้างสามารถคำนวณได้โดยอาศัยหลักการรวมโดยตรง สององค์ประกอบหลังนี้ มีความสำคัญมากในขั้น
ตอนการหาผลเฉลยของระบบสมการไร้เชิงเส้นขนาดใหญ่โดยระเบียบวิธีการทำซ้ำของนิวตันราฟสัน เพื่อยืนยัน
ความถูกต้องของแบบจำลองทางคณิตศาสตร์และโปรแกรมคอมพิวเตอร์ที่พัฒนาขึ้นได้ทำการวิเคราะห์
โครงสร้างตัวอย่างจำนวนมากและเปรียบเทียบผลที่ได้กับผลเฉลยอ้างอิงจากการทดลองเชิงตัวเลขดังกล่าวสรุป
ได้ว่าระเบียบวิธีที่นำเสนอนี้ ให้ผลเฉลยเชิงตัวเลขที่มีความถูกต้องสูงเทียบเท่าผลเฉลยเชิงวิเคราะห์โดยไม่
จำเป็นต้องใช้ชิ้นส่วนย่อยจำนวนมาก

ภาควิชา ....วิศวกรรมโยธา.................... ลายมือชื่อนิสิต ....
สาขาวิชา ....วิศวกรรมโยธา.................... ลายมือชื่อ อ.ที่ปรึกษาวิทยานิพนธ์หลัก ....
ปีการศึกษา ....2554.................... ลายมือชื่อ อ.ที่ปรึกษาวิทยานิพนธ์ร่วม ....

5270717421 : MAJOR CIVIL ENGINEERING

KEYWORDS : LARGE DISPLACEMENT AND ROTATION / ELASTICA / CO-ROTATIONAL FORMULATION / ELEMENT TANGENT STIFFNESS MATRIX / NEWTON-RAPHSON ITERATION

JONGAPHONH DOUANEVANH : LARGE CURVATURE ANALYSIS OF TWO-DIMENSIONAL LINEAR ELASTIC FRAMES BY DIRECT STIFFNESS METHOD. ADVISOR : ASST. PROF. JAROON RUNGAMORNRAT, Ph.D., CO-ADVISOR : KHAMPASEUTH THEPVONGSA, D.Eng., 74 pp.

This thesis presents an efficient semi-analytical technique based upon the co-rotational formulation and the direct stiffness strategy for large displacement and rotation analysis of two-dimensional, linearly elastic, extensible frames of general geometries and subjected to general loading conditions. The technique exploits the standard direct stiffness procedure to systematically set up the governing equations for the entire structure. In the formulation, a set of nonlinear differential equations derived from the exact curvature-displacement relationship is employed to construct an equivalent set of nonlinear algebraic equations governing the behavior of a straight prismatic member. Such governing equations are employed first to obtain the force-displacement relation and the corresponding gradient matrix for a member in its co-rotational coordinate system. Such basic results are then utilized along with the co-rotational approach to develop the exact element tangent stiffness matrix and the force-displacement relation for a generic member. The direct assembly algorithm is then used to obtain the exact tangent stiffness matrix and exact load residuals for the structure. These two components are essential in the solution procedure for a large system of nonlinear equations by Newton-Raphson iterative scheme. Several examples have been selected in the numerical experiments to verify both the formulation and implementation and it can be concluded that the proposed technique yields numerical results comparable to analytical solutions without refining the discretization.

Department: ......Civil Engineering...... Student 's Signature: ……………………..

Field of Study: ...Civil Engineering...... Advisor 's Signature: ………………..……..

Academic Year: ………2011…………..... Co-advisor 's Signature: …………..……...

ACKNOWLEDGEMENTS

CONTENTS

LIST OF FIGURES

LIST OF ABBREVIATIONS

A   - cross-sectional area

E   - Young's modulus

I   - moment of inertia of the cross section

L   - length of member

$\hat{d}^*$ - normalized projected length

f_x^* - resultant internal force in x^*-direction

f_{xi}^* - member end force in x^*-direction at node i

$\hat{f}_x^*$ - normalized resultant internal force in x^*-direction

$\hat{f}_{xi}^*$ - normalized member end force in x^*-direction at node i

f_y^* - resultant internal force in y^*-direction

f_{yi}^* - member end force in y^*-direction at node i

$\hat{f}_y^*$ - normalized resultant internal force in y^*-direction

$\hat{f}_{yi}^*$ - normalized member end force in y^*-direction at node i

m^* - bending moment

m_i^* - member end moment at node i

$\hat{m}^*$ - normalized bending moment

$\hat{m}_i^*$ - normalized member end moment at node i

$\bar{n}$ - axial force resultant at interior point

$\bar{s}$ - shear force resultant at interior point

u - displacement in x-direction

$\hat{u}_i^*$ - normalized displacement of node i in x^*-direction

$\hat{\bar{u}}^*$ - normalized displacement at interior point in x^*-direction

v - displacement in y-direction

$\hat{v}_i^*$ - normalized displacement of node i in y^*-direction

$\hat{\bar{v}}^*$ - normalized displacement at interior point in y^*-direction

θ_i^* - rotation at node i

θ_z^* - rotation at inflection point

$\bar{\theta}$ - rotation at interior point

β - chord rotation

φ - angle between the local x-axis and the global X-axis

ε_0 - axial strain of member

ξ - normalized length

ϑ - moment-dependence function

$\boldsymbol{f}^*$ - vector of member end forces in co-rotational coordinate system

$\boldsymbol{f}^l$ - vector of member end forces in local coordinate system

$\boldsymbol{f}^g$ - vector of member end forces in global coordinate system

$\boldsymbol{k}^*$ - gradient matrix in co-rotational coordinate system

$\boldsymbol{k}^l$ - local element tangent stiffness matrix

$\boldsymbol{k}^g$ - global element tangent stiffness matrix

$\boldsymbol{K}^T$ - tangent stiffness matrix of structure

$\boldsymbol{Q}$ - transformation matrix (local to global coordinate systems)

$\boldsymbol{P}$ - structure load vector

$\boldsymbol{T}$ - transformation matrix (co-rotational to local coordinate systems)

$\boldsymbol{u}^*$ - vector of member end displacement in co-rotational coordinate system

$\boldsymbol{u}^l$ - vector of member end displacement in local coordinate system

$\boldsymbol{u}^g$ - vector of member end displacement in global coordinate system

$\boldsymbol{U}$ - vector of degrees of freedom of structure

CHAPTER I

INTRODUCTION

1.1 General

During the past four decades, applications of highly flexible components in various civil engineering structures and infrastructural systems have been well-recognized, for instance, suspension cables in suspension and cable stayed bridges, power-line cables for electric transmission, marine pipes for transporting oil and natural gas from the underneath ocean floor to the production platforms or drilling ships, and membrane roofs made of very thin components. In addition, various parts of machines and aerospace vehicles have generally been designed to function under conditions vulnerable to experience significant change of their configurations. For examples, leaf springs in the car suspension systems, helicopter rotor blades, wind turbine blades, and components in aircraft structures have been often designed up to the post-buckling limit state and the high-altitude long-endurance aircraft has also been designed to resist a wing tip deflection up to 25% of the wing span (Henderson, 1990; Frank, 2007). Furthermore, due to the rapid growth in the space technology, highly flexible components have been increasingly employed to achieve the optimal design solution in the minimization of both the size and weight of space structures.

In the analysis of such highly flexible structures, conventional techniques based upon linearized mathematical models (known as the linear analyses) are of very limited capability and generally predicts responses that are of insufficient accuracy especially when the displacement, rotation and deformation of those structures are relatively large. Another crucial drawback of the linear analysis is that it provides either inadequate or no information about the stability behavior of investigated structures (e.g. bifurcation or critical loads, stability status of structures, post-buckling behavior, etc.). In design practices, such stability information has been found essential and played a central role in the design of certain structural members such as columns,

beam-columns, and axially dominated thin plate and shell structures. The limitation of the linear analysis is also apparent when it is applied to very slender structures (cables and mooring systems) whose configuration and geometry can be substantially changed under regular service conditions.

To enhance the modeling capability and improve the accuracy of predicted responses of structures experiencing significant change of their configurations, mathematical models integrating essential components capable of treating the present geometric nonlinearity are required. A simple model that has been widely used to account for the axial-bending interaction in the study of beam-columns and the determination of buckling loads of axially loaded structures is the second-order analysis. Besides its simplicity and successful applications to the buckling and P-delta analysis, the technique has found lack of capability to analyze structures undergoing large displacement and rotation (e.g. post-buckling responses) due to its simplified kinematics. In such class of problems, the geometric nonlinearity plays a major role in the key governing equations and cannot sufficiently be captured by low-order, approximate kinematics. As a result, mathematical models based upon the exact relation between displacements and deformations have become an attractive alternative to resolve all those limitations and, in addition, allow various responses and behavior of structures to be thoroughly investigated.

Besides vast capabilities gained, use of exact kinematics to model geometric nonlinearity has, at the same time, posed several mathematical and computational challenges due to its complexity. Although this type of analysis has a very long history heading back to Euler and Lagrange's era and its framework has been nowadays well-established due to the emergence of powerful computing devices and reliable numerical techniques, rigorous investigations in this area are still required to further improve and enhance the modeling capability, computational efficiency and quality of solutions. The key motivation of the present study is to develop a simple, efficient and accurate technique that is capable of performing large-displacement-and-rotation analysis of structures of various geometries and subjected to general loading conditions. In the subsequent section, results from extensive literature survey are presented in order to demonstrate the historical development and current advance in

this specific area and clearly identify the originality and contribution of the current study.

1.2 Background and Review

Literature review has been extensively conducted with the primary focus on the development of analytical, semi-analytical and numerical techniques that are capable of performing the analysis of two-dimensional skeleton structures undergoing large displacement and rotation. Results from the review have been organized into three separate parts regarding to the structural configuration and the extensibility assumption considered in each investigation.

1.2.1. Inextensible Single Member

An elastica problem (i.e. a problem of finding the *exact* elastic or deformed shape of structures) has been introduced by Euler since his first investigation in 1744. In his study, both the direct approach and a method of final cause have been employed to determine exact elastic curves of a single straight member under different loading conditions. It should be noted, however, that preceding the work of Euler, James Bernoulli (1691) also attempted to determine the shape of a bent cantilever beam. Although his obtained result was incorrect due to an erroneous assumption on the axis of rotation of the cross section, his statement regarding the proportionality between the curvature and bending moment at any point was correct and used later by Euler in his study of elastica. After Euler's work in 1744, Daniel Bernoulli demonstrated that the final elastic curve of a bending beam minimizes the bending strain energy. He also suggested that the calculus of variations can be applied along with such minimization criteria to find the shape of the elastic curve for a given member length and boundary conditions. Lagrange (1770) followed the Euler's direct approach with the independent variable measured along the unstressed configuration being chosen in his analysis and his analytical solutions were presented in term of elliptic integrals. Later, Kirchoff (1859) made a significant progress by introducing an analogy between a problem of finding elastic curve of a cantilever column and a problem of a pendulum. With such analogy, a closed-form solution could also be obtained in terms of elliptic

integrals. Due to complexity posed by the exact curvature-displacement relation, solutions of elastica problems in its early age have been limited to very simple structures under certain loading conditions.

Due to the emergence of powerful computing devices and reliable numerical techniques, the analysis capability has been significantly enhanced and a broader class of complex and more practical elastica problems can be solved. Nowadays, the large displacement and rotation analysis has gained significant attention and been used extensively to investigate various aspects of post-buckling behavior of structures. Certain relevant works have been summarized and briefly discussed here with a primary objective to present a series of historical breakthrough and, at the same time, to identify the current gap of knowledge and the original aspect of the current investigation.

Rao and Rao (1989) investigated the large deflections of a cantilever beam subjected to a rotational distributed load. In their work, the fourth-order Runge-Kutta integration scheme was employed to solve a second-order nonlinear integro-differential equation. By assuming a special function form of the distributed load in terms of the Dirac-delta distribution, results for a beam under a rotational concentrated load were readily obtained. They also pointed out that the proposed technique involved less computational cost and yielded numerical results that are in good agreement with existing benchmark solutions. Wang (1997) employed a numerical procedure based on the perturbation technique to explore the post-buckling behavior of a prismatic, simply-supported column clamped at one end and subjected to a concentrated load at the other end. Later, Lee (2001) investigated the post-buckling behavior of a prismatic cantilever column under the combined action between the uniformly distributed load and a concentrated load at the tip. In this study, Butcher's fifth-order Runge-Kutta method was utilized to construct the numerical solutions and the good agreement with existing results was concluded. Madhusudan et al. (2003) employed the dynamic formulation to derive governing equations for the post-buckling of a cantilever column with variable cross-section and subjected to the distributed axial load and concentrated load at the tip. A fourth-order

Runge-Kutta integration scheme was adopted to solve such governing nonlinear differential equations.

In 2007, Shavartman examined the influence of the rotational spring at the base of a cantilever column and the tip follower force on its deformed shape. In the formulation, a governing nonlinear two-point boundary value problem was transformed into an initial value problem by using the change of variables. The final problem was solved by a selected technique that requires no iteration and numerical results were obtained in a more efficient and highly accurate manner than that by the numerical shooting method and the fourth-order Runge-Kutta method. Wang et al. (2008) reexamined a cantilever beam subjected to a concentrated load at the tip. In the analysis, a homotopy analysis method (HAM) was developed to construct an explicit solution of the rotation and displacement at the free end. It was shown from this study that the HAM is a powerful and accurate technique and well-suited for solving strongly nonlinear problems in structural analysis. Benjaree et al. (2008) employed a nonlinear shooting method along with the adomain decomposition to determine the elastic curve of a cantilever beam under arbitrary loading conditions and containing an interior inflection point. Computed results were found comparable to those obtained from a classical elliptic integral technique.

Klubjaidai and Chucheepsakul (2008) employed both the elliptic integral method and the shooting method supplemented by the seventh-order Runge-Kutta integration scheme to study the post-buckling behavior of a circular arch subjected to end forces. Solutions from the two techniques were compared and they were in good agreement. Shavartman (2009) employed a similar technique to that employed by Shavartman (2007) to reinvestigate a non-uniform cantilever beam subjected to two follower forces and similar findings regarding to the accuracy and computational efficiency were concluded. Recently, Chen (2010) employed the moment integral treatment to solve the large deflection of a cantilever beam. Results obtained from the proposed technique were compared with those from the elliptic integral approach and a reliable commercial FEM package, ANSYS$^{©}$. It was concluded that the technique is computationally efficient, yields accurate numerical solutions, and can be applied to

problems involving complex loading conditions and variable beam properties (e.g. cross section and Young's modulus).

1.2.2. Inextensible Multiple Members

It should be remarked that all studies described above are restricted only to structures consisting of a single member. On the basis of extensive literature review, work focusing on the large displacement and rotation analysis of structures consisting of multiple members is still relatively few and some of those investigations are briefly summarized below.

Ohtsuki et al. (2000) performed a large displacement analysis of a square frame with rigid joints. The frame was loaded by a pair of opposite forces at two joints along its diagonal. Analytical solutions in terms of elliptic integrals were derived for the representative flexural quantities such as the arc length, horizontal and vertical displacement, curvature, bending moment, and bending stress. The predicted results were found in very good agreement with experimental data. Dado et al. (2004) investigated the post-buckling behavior of a cantilever column consisting of two segments of different properties connecting by a rotational spring. In their analysis, three methods (including a semi-analytical method based upon the governing equations cast in terms of elliptic integrals and solved by Newton-Raphson technique, a numerical integration technique, and the large displacement finite element analysis by NASTRAN) were employed. Results from their study revealed that the semi-analytical technique was proved to be computationally efficient and accurate in comparison with the other two. Suwansheewasiri and Chucheepsakul (2004) studied the buckling and post-buckling behaviors of a two-member rigid frame of a particular configuration. Solutions of both the symmetric and non-symmetric post-buckling shapes were obtained by using the elliptic integral method.

Later, Dado et al. (2006) performed a large displacement and rotation analysis of a flexible rhombus frame consisting of non-prismatic members connected by rigid joints. The frame was subjected to a pair of opposite diagonal forces. In their work, relations between the displacement at the corner and the applied force are obtained

using a new robust numerical technique based on a representation of an angular deflection of the member by a polynomial function along the deflected beam axis. This new method was compared with classical numerical integration techniques and all results were found in excellent agreement. Hu et al. (2008) employed a differential quadrature element method (DQEM) to study the large displacement structures containing discontinuity conditions. The proposed method seems to be computationally efficient and applicable to large displacement analysis of structures with general configurations; however, the method itself is an approximate scheme and the discretization of the problem must be properly treated in order to obtain converged numerical results. Shatarat et al. (2009) reinvestigated a problem of thin rhombus frame. In their study, the member cross section was assumed to be rectangular, the frame was subjected to two opposite diagonal forces, and both geometrical and material nonlinearities were treated. A semi-analytical solution has been formulated for the relation between the displacement at the corners of the frame and the applied forces. Results were compared with those obtained from ADINA and excellent agreement among those results was observed. Most recently, Rungamornrat and Tangnovarad (2011) proposed a semi-analytical technique based on a co-rotational formulation and a direct stiffness strategy for large displacement and rotation analysis of two-dimensional beams and frames. The element tangent stiffness matrices and load residuals were derived exactly from the governing nonlinear differential equations and used as essential components in a nonlinear solver by Newton-Raphson iteration. From extensive verifications with both analytical and benchmark solutions, their technique yielded highly accurate numerical solutions with independence of the mesh refinement

1.2.3. Extensible Single Member

All studies described in the previous two sub-sections were focused primarily on inextensible structures where the deformation of the neutral axis is fully prevented. It is worth noting that the inextensibility assumption is, to some extent, impractical and can lead to inaccurate predicted results when the axial deformation becomes significant. Various attempts have been devoted to incorporate the extensibility in the

large displacement and rotation analysis and some of those recent studies are summarized below.

Anders et al. (2001) examined both buckling and post buckling behaviors of an extensible beam under an axial compression force. The governing equations were formulated from the principle of virtual work along with Euler-Bernoulli assumption and the close-form solutions were obtained in terms of elliptic integrals. In this study, they showed that the bifurcation load depends primarily on the slenderness of the beam and, for relatively small slenderness ratio, the bifurcation point becomes unstable. Chucheepsakul et al. (2003) employed a variational approach to construct a three-dimensional mathematical model for extensible marine cables with the specified top tension. In their works, the finite element method and the shooting optimization technique were utilized to determine responses of the cables. Li et al. (2005) employed a shooting method along with the numerical integration to investigate the post-buckling behavior of an extensible, hinged-fixed beam under the uniformly distributed follower force. Recently, Mazzilli (2009) employed a method of multiple scales to study buckling and post-buckling behavior of an extensible rod under five end conditions. Results from this study indicated that the multiple scale method was robust and yielded sufficiently accurate approximate solutions. Recently, Sepahi et al. (2010) applied the differential quadrature method (DQM) to investigate the buckling and post-buckling of an extensible cantilever beam with variable cross section and subjected to both a concentrated axial load at its free end and a non-uniformly distributed axial load. Results obtained from this particular technique were in very good agreement with analytical solutions from the elliptic integral method and numerical solutions from other methods such as shooting and multiple scale methods. The DQM was also exploited by Sepahi et al. (2010) to solve a post-buckling problem of a hinged-fixed column under the terminal forces and its self weight. Again, the DQM was found computationally promising and yielded sufficiently accurate numerical solutions. It is noted by passing that large displacement and rotation analysis of extensible structures has also been studied within the context of thermal loadings, for instance, Shirong et al. (2000) in the study of thermal post-buckling of

uniformly heated elastic rods by using the shooting method and other related works by Shirong et al. (2003), Vaz and Solano (2003) and Saha and Ali (2009).

While various studies described above have already integrated the extensibility into the mathematical model, they were still focused only on structures consisting of a single member. Work towards the treatment of structures of arbitrary geometry and subjected to general loading conditions is still limited and this, therefore, necessitates further investigations. It should be noted again that ability to incorporate the member extensibility in the modeling allows complex and more practical structures to be investigated since, in real structures, both the axial and flexural rigidities of their components remain finite.

1.3 Research Objectives

The key objective of the present study is to develop a systematic, efficient and accurate technique capable of performing large displacement and rotation analysis of two-dimensional, extensible, linearly elastic frames of general geometries and subjected to general loading conditions. The computational behaviors of the proposed technique such as the accuracy and computational efficiency are to be explored.

1.4 Scopes of Research

The proposed investigation is to be carried out within following context and assumptions:
1) frames are two-dimensional and can be discretized into straight prismatic members that are free of interior loads;
2) each member is made of a homogeneous, isotropic, linearly elastic material;
3) direction of all applied loads are fully fixed during their applications; and
4) shear deformation is neglected.

1.5 Methodology

The co-rotational formulation and the direct stiffness strategy are integrated to establish a semi-analytical technique capable of performing large displacement and rotation analysis. The methodology can be described in details as follows:

1) three basic equations in structural mechanics (i.e. equilibrium equations in the deformed state, moment-curvature relationship, and exact kinematics among the curvature, rotation and displacement) are combined into a set of governing nonlinear ordinary differential equations for a straight member;

2) a direct integration technique is utilized to transform a set of governing nonlinear ordinary differential equations into an equivalent set of governing nonlinear algebraic equations for a straight member;

3) the force-displacement relationship in the co-rotational axis is developed by specializing a set of governing nonlinear algebraic equations to a simply-supported member and the corresponding exact gradient matrix is derived using the chain rule for differentiation along with implicit differentiations;

4) a co-rotational approach is employed to derive the force-displacement relationship and the exact tangent stiffness matrix of a member in the local coordinate system;

5) standard transformations and direct assembly procedure are utilized to relate the displacements and applied loads in the structure level and to construct the structure tangent stiffness matrix and exact load residual vector;

6) a standard Newton-Ralphson technique is employed to solve a system of nonlinear algebraic equations; and

7) all computational procedures are implemented in terms of an in-house computer code and tested with reliable benchmark solutions.

CHAPTER II

BASIC EQUATIONS

This chapter summarizes the problem statement, key assumptions underlying the mathematical model, and the formulation of a set of governing differential equations for a straight member undergoing large displacement and rotation.

2.1 Problem Statement and Basic Assumptions

The problem statement is to develop an accurate and computationally efficient technique that is capable of modeling two-dimensional frames undergoing large displacement and rotation. The geometry and loading conditions of the frame are assumed to be general except that it can be discretized into straight, prismatic members that are free of interior loads as shown schematically in Figure 2.1. In the development of a mathematical model and a set of governing differential equations, following essential components and certain assumptions are employed: (i) all members are made of an isotropic, linearly elastic material; (ii) equilibrium is enforced in the deformed state; (iii) the displacement, rotation and curvature are related by exact kinematics; (iv) directions of all applied loads are fully fixed during their applications; (v) shear deformation is neglected while axial deformation of the centroid of any cross section is allowed; and (vi) the cross section remains plane after undergoing deformation.
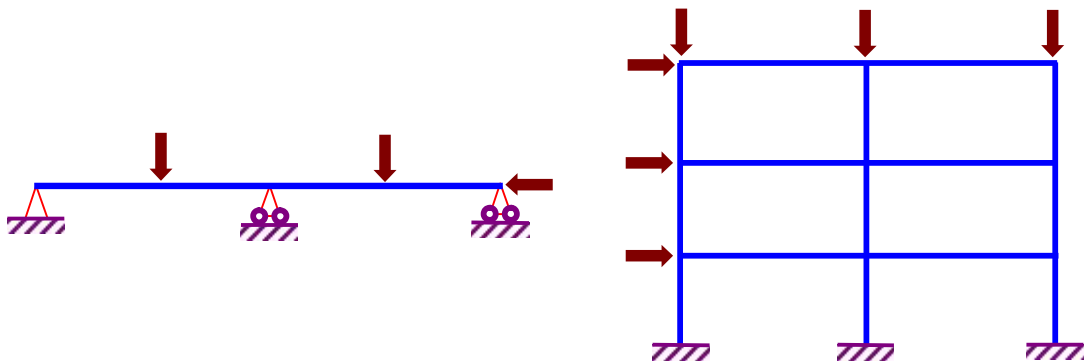
Figure 2.1 Schematic of two-dimensional, extensible, linearly elastic frames

2.2 Basic Governing Equations for Straight Prismatic Member

Consider a straight, prismatic member of length L, cross-sectional area A, and moment of inertia I, and made of a linearly elastic material of Young's modulus E. An undeformed configuration of this member, represented by a line connecting the centroid of all cross sections, occupies a straight line defined by $x \in [0, L]$ and $y = 0$. Due to the action of applied loads, the member moves to a new configuration, termed the deformed configuration, as shown in Figure 2.2(a). Any cross section in the undeformed state, represented by its centroid $(S, 0)$, displaces to a new position in the deformed state, represented by $(S + u, v)$ where $u = u(S)$ and $v = v(S)$ are the x-component and y-component of the displacement at the point $(S, 0)$, respectively. Also, let define $f_x = f_x(S), f_y = f_y(S)$, and $m = m(S)$ as a resultant internal force in the x-direction, a resultant internal force in the y-direction, and a resultant bending moment at the cross section $(S, 0)$, respectively.

Let dS be an infinitesimal element in the undeformed state occupying a straight line connecting the cross section $(S, 0)$ and $(S + dS, 0)$ and ds be the same element in the deformed state occupying a curve connecting points $(S + u, v)$ and $(S + dS + u + du, v + dv)$ as shown in Figure 2.2(a).

(a)   (b)
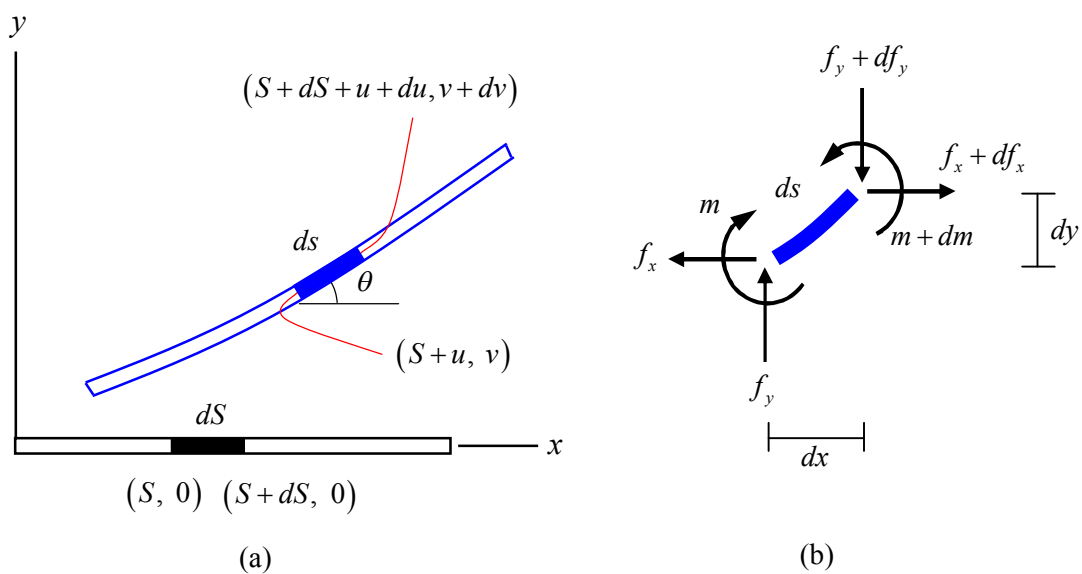
Figure 2.2 (a) Undeformed and deformed configurations of straight prismatic segment and (b) free body diagram of infinitesimal deformed element ds

Upon considering geometry of the deformed element ds, it leads to following three geometric relations:

$$\sin\theta = \frac{1}{1+\varepsilon_0}\frac{dv}{dS} \tag{2.1}$$

$$\cos\theta = \frac{1}{1+\varepsilon_0}\left(1+\frac{du}{dS}\right) \tag{2.2}$$

$$\frac{ds}{dS} = 1+\varepsilon_0 \tag{2.3}$$

where ε_0 is the (engineering) axial strain at the centroid of the cross section and θ denotes the rotation at any cross section.

By enforcing equilibrium of the deformed element ds (see Figure 2.2(b) for its free body diagram), following ordinary differential equations are obtained

$$\frac{df_x}{dS} = 0 \tag{2.4}$$

$$\frac{df_y}{dS} = 0 \tag{2.5}$$

$$\frac{dm}{dS} = f_y\frac{dx}{dS} + f_x\frac{dy}{dS} \tag{2.6}$$

Upon exploiting the assumption (vi) along with the linear stress-strain relationship, the axial strain ε_0 can be related to the axial force n by

$$\varepsilon_0 = \frac{n}{EA} \tag{2.7}$$

where the axial force n (i.e. a resultant internal force normal to the cross section in the deformed state) can be expressed in terms of the internal forces f_x and f_y as

$$n = f_x\cos\theta - f_y\sin\theta \tag{2.8}$$

By exploiting the assumptions (v) and (vi) along with the linear stress-strain relationship, the bending moment m can be related directly to the spatial rate of change of the rotation θ by

$$m = EI \frac{d\theta}{dS} \tag{2.9}$$

By substituting (2.9) into the moment equilibrium equation (2.6) and combining (2.7) and (2.8), it results in

$$EI \frac{d^2\theta}{dS^2} = f_y \left(1 + \frac{du}{dS}\right) + f_x \frac{dv}{dS} \tag{2.10}$$

$$\varepsilon_0 = \frac{f_x}{EA} \cos\theta - \frac{f_y}{EA} \sin\theta \tag{2.11}$$

With use of the geometric relations (2.1) and (2.2) along with the expression (2.11), equation (2.10) becomes

$$EI \frac{d^2\theta}{dS^2} = \left(1 + \frac{f_x}{EA}\cos\theta - \frac{f_y}{EA}\sin\theta\right)\left(f_x \sin\theta + f_y \cos\theta\right) \tag{2.12}$$

By defining non-dimensional parameters $\hat{f}_x = f_x L^2 / EI$, $\hat{f}_y = f_y L^2 / EI$, $\xi = S/L$ and $\alpha = I/AL^2$, the relations (2.11) and (2.12) can be expressed in a non-dimensional form as

$$\varepsilon_0 = \varepsilon_0\left(\theta; \hat{f}_x, \hat{f}_y\right) = \alpha\left(\hat{f}_x \cos\theta - \hat{f}_y \sin\theta\right) \tag{2.13}$$

$$\frac{d^2\theta}{d\xi^2} = \hat{f}_x \sin\theta + \hat{f}_y \cos\theta + \alpha\left(\frac{\hat{f}_x^2 - \hat{f}_y^2}{2}\sin 2\theta + \hat{f}_x \hat{f}_y \cos 2\theta\right) \tag{2.14}$$

To suit the direct integration of the differential equation (2.14), a term on its left hand side is first re-expressed as

$$\frac{d^2\theta}{d\xi^2} = \frac{d}{d\xi}\left(\frac{d\theta}{d\xi}\right) = \frac{d\theta}{d\xi}\frac{d}{d\theta}\left(\frac{d\theta}{d\xi}\right) = \frac{1}{2}\frac{d}{d\theta}\left(\frac{d\theta}{d\xi}\right)^2 \tag{2.15}$$

With use of (2.15), equation (2.14) can directly be integrated to obtain

$$\left(\frac{d\theta}{d\xi}\right)^2 = C - 2\hat{f}_x\cos\theta + 2\hat{f}_y\sin\theta - \alpha\left(\frac{\hat{f}_x^2 - \hat{f}_y^2}{2}\right)\cos 2\theta + \alpha\hat{f}_x\hat{f}_y\sin 2\theta \tag{2.16}$$

where C is an arbitrary constant of integration that can be determined from the boundary condition. It should be apparent from (2.9) that the normalized derivative $d\theta/d\xi$ possesses an identical sign to that of the normalized bending moment $\hat{m} = mL/EI$. Equation (2.16) can therefore be uniquely solved to obtain

$$\frac{d\xi}{d\theta} = \frac{\vartheta(\hat{m})}{\sqrt{C - 2\hat{f}_x\cos\theta + 2\hat{f}_y\sin\theta - \alpha\left(\dfrac{\hat{f}_x^2 - \hat{f}_y^2}{2}\right)\cos 2\theta + \alpha\hat{f}_x\hat{f}_y\sin 2\theta}} \tag{2.17}$$

where $\vartheta(\hat{m})$ is a moment-dependent function defined by

$$\vartheta(\hat{m}) = \begin{cases} 1 & , & \hat{m} > 0 \\ -1 & , & \hat{m} < 0 \end{cases} \tag{2.18}$$

By combining the geometric relations (2.1) and (2.2) with the equation (2.17), we then obtain the governing ordinary differential equations for the displacement u and v as

$$\frac{d\hat{v}}{d\theta} = \frac{\vartheta(\hat{m})\left[\sin\theta(1+\varepsilon_0)\right]}{\sqrt{C - 2\hat{f}_x\cos\theta + 2\hat{f}_y\sin\theta - \alpha\left(\dfrac{\hat{f}_x^2 - \hat{f}_y^2}{2}\right)\cos 2\theta + \alpha\hat{f}_x\hat{f}_y\sin 2\theta}} \tag{2.19}$$

$$\frac{d\hat{u}}{d\theta} = \frac{\vartheta(\hat{m})\left[\cos\theta(1+\varepsilon_0) - 1\right]}{\sqrt{C - 2\hat{f}_x\cos\theta + 2\hat{f}_y\sin\theta - \alpha\left(\dfrac{\hat{f}_x^2 - \hat{f}_y^2}{2}\right)\cos 2\theta + \alpha\hat{f}_x\hat{f}_y\sin 2\theta}} \tag{2.20}$$

where $\hat{u} = u/L$ and $\hat{v} = v/L$ are the normalized displacement in the *x*-direction and *y*-direction, respectively. A set of three basic governing differential equations (2.17), (2.19) and (2.20) forms a basis for the development of the force-displacement relation for a simply-supported element presented in the subsequent chapter.

CHAPTER III

FORMULATION OF MEMBER AND STRUCTURE EQUATIONS

This chapter presents the development of force-displacement relation and the corresponding tangent stiffness matrix for a member in following three different cases: a simply-supported member, a generic member in its local coordinate system and a generic member in its global coordinate system. A set of governing ordinary differential equations established in the previous chapter is utilized to set up an equivalent set of governing nonlinear algebraic equations. Results for the simply-support member are then utilized as a basis for the development of results for the generic member in the local coordinate system via the co-rotational technique. Standard coordinate transformations are employed to obtain both the force-displacement relation and the global element tangent stiffness matrix in the global coordinate system. A standard assembly procedure is finally employed to form the load-displacement relation and the tangent stiffness matrix for a structure.

3.1 Force-displacement Relation for Simply-supported Element
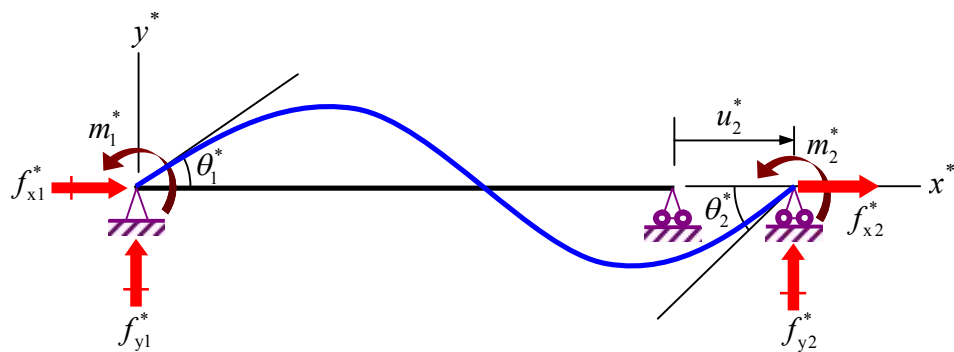
Figure 3.1 Simply-supported member subjected to end force and end moments $\{f_{x2}^*, m_1^*, m_2^*\}$ respectively

Let's consider a simply-supported member of length L, cross-sectional area A, moment of inertia I, and Young's modulus E. Let $\{x^*, y^*, z^*\}$ denote a Cartesian coordinate system as shown in Figure 3.1. It should be remarked that this particular

coordinate system is identical to the co-rotational coordinate system of this member since the x-axis always connects both ends of the member. The left end of a member is a pinned-support and subjected to a moment m_1^* in the z-direction while its right end is a roller support and subjected to a force f_{x2}^* in the x-direction and a moment m_2^* in the z-direction. Boundary conditions associated with the prescribed displacements are given by

$$u(0) = 0, \tag{3.1}$$

$$v(0) = 0, \tag{3.2}$$

$$v(L) = 0 \tag{3.3}$$

whereas boundary conditions associated with the applied force f_{x2}^* and moments m_1^* and m_2^* are given by

$$\frac{d\theta}{d\xi}(0) = \hat{m}_1^* = \frac{m_1^* L}{EI}, \tag{3.4}$$

$$\frac{d\theta}{d\xi}(L) = \hat{m}_2^* = \frac{m_2^* L}{EI}, \tag{3.5}$$

$$\hat{f}_x(L) = \hat{f}_{x2}^* = \frac{f_{x2}^* L^2}{EI}. \tag{3.6}$$

By enforcing the boundary conditions (3.5) and (3.6) along with the fact that f_x is constant throughout the member, the constant C in equation (2.16) can be obtained as

$$C = \hat{m}_2^{*2} + 2\hat{f}_{x2}^* \cos\theta_2^* - 2\hat{f}_y \sin\theta_2^* + \alpha\left(\frac{\hat{f}_{x2}^{*2} - \hat{f}_y^2}{2}\right)\cos 2\theta_2^* - \alpha\hat{f}_{x2}^*\hat{f}_y \sin 2\theta_2^* \tag{3.7}$$

where θ_2^* is the rotation at the right end of the member. By substituting the constant C from (3.7) into the governing equations for the rotation, the displacement in the y-direction and the displacement in the x-direction (2.17), (2.19) and (2.20) respectively, it leads to a set of governing nonlinear ordinary differential equations:

$$\frac{d\xi}{d\theta} = \vartheta(\hat{m}) F\left(\theta, \theta_2^*; \hat{f}_{x2}^*, \hat{f}_y, \hat{m}_2^*\right) , \tag{3.8}$$

$$\frac{d\hat{v}}{d\theta} = \vartheta(\hat{m})\left[\sin\theta(1+\varepsilon_0)\right] F\left(\theta, \theta_2^*; \hat{f}_{x2}^*, \hat{f}_y, \hat{m}_2^*\right) , \tag{3.9}$$

$$\frac{d\hat{u}}{d\theta} = \vartheta(\hat{m})\left[\cos\theta(1+\varepsilon_0)-1\right] F\left(\theta, \theta_2^*; \hat{f}_{x2}^*, \hat{f}_y, \hat{m}_2^*\right). \tag{3.10}$$

where the function F is defined by

$$F\left(\theta, \theta_2^*; \hat{f}_{x2}^*, \hat{f}_y, \hat{m}_2^*\right) = \frac{1}{\sqrt{i + \alpha j}} \tag{3.11}$$

$$i = \hat{m}_2^{*2} + 2\hat{f}_{x2}^*\left(\cos\theta_2^* - \cos\theta\right) - 2\hat{f}_y\left(\sin\theta_2^* - \sin\theta\right) \tag{3.12}$$

$$j = \frac{1}{2}\left(\hat{f}_{x2}^{*2} - \hat{f}_y^2\right)\left(\cos 2\theta_2^* - \cos 2\theta\right) - \hat{f}_{x2}^*\hat{f}_y\left(\sin 2\theta_2^* - \sin 2\theta\right) \tag{3.13}$$

By imposing the moment boundary condition at the left end (3.4), it leads to an addition equation:

$$\begin{aligned}
&\hat{m}_2^{*2} - \hat{m}_1^{*2} + 2\hat{f}_{x2}^*\left(\cos\theta_2^* - \cos\theta_1^*\right) - 2\hat{f}_y\left(\sin\theta_2^* - \sin\theta_1^*\right) \\
&+ \frac{1}{2}\alpha\left(\hat{f}_{x2}^{*2} - \hat{f}_y^2\right)\left(\cos 2\theta_2^* - \cos 2\theta_1^*\right) - \alpha\hat{f}_{x2}^*\hat{f}_y\left(\sin 2\theta_2^* - \sin 2\theta_1^*\right) = 0
\end{aligned} \tag{3.14}$$

where θ_1^* is the rotation at the left end of the member. By enforcing overall equilibrium of a member in the deformed configuration, the normalized reactive forces $\hat{f}_{x1}^* = f_{x1}^* L^2 / EI$, $\hat{f}_{y1}^* = f_{y1}^* L^2 / EI$ and $\hat{f}_{y2}^* = f_{y2}^* L^2 / EI$ can be obtained in terms of the normalized applied forces $\{f_{x2}^*, m_1^*, m_2^*\}$ and the end displacement $\hat{u}_2^*$ as

$$\hat{f}_{x1}^* = -\hat{f}_{x2}^* , \tag{3.15}$$

$$\hat{f}_{y1}^* = \frac{\hat{m}_1^* + \hat{m}_2^*}{\hat{d}^*} , \tag{3.16}$$

$$\hat{f}_{y2}^* = -\frac{\hat{m}_1^* + \hat{m}_2^*}{\hat{d}^*} \tag{3.17}$$

where $\hat{d}^* = 1 + \hat{u}_2^*$ and $\hat{u}_2^* = u_2^* / L$.

Upon performing direct integration of (3.8)-(3.10) from $\xi = 0$ to $\xi = \bar{\xi} = \bar{S} / L$ where $\bar{S} \in [0, L]$, it leads to a set of three integral relations that can be used to compute the normalized displacements and the rotation at any cross section at $\bar{S}$ once all unknown quantities at both ends are solved :

$$\int_{\theta_1^*}^{\bar{\theta}} \mathcal{G}(\hat{m}) F\left(\theta , \theta_2^*; \hat{f}_{x2}^*, \hat{f}_y, \hat{m}_2^*\right) d\theta = \bar{\xi} , \tag{3.18}$$

$$\int_{\theta_1^*}^{\bar{\theta}} \mathcal{G}(\hat{m}) \left[\sin\theta\left(1+\varepsilon_0\right)\right] F\left(\theta , \theta_2^*; \hat{f}_{x2}^*, \hat{f}_y, \hat{m}_2^*\right) d\theta = \hat{\bar{v}} , \tag{3.19}$$

$$\int_{\theta_1^*}^{\bar{\theta}} \mathcal{G}(\hat{m}) \left[\cos\theta\left(1+\varepsilon_0\right)-1\right] F\left(\theta , \theta_2^*; \hat{f}_{x2}^*, \hat{f}_y, \hat{m}_2^*\right) d\theta = \hat{\bar{u}} \tag{3.20}$$

where $\bar{\theta}$ is the rotation at $\bar{S}$, $\hat{\bar{u}} = \bar{u} / L$ is the normalized displacement in the x-direction at $\bar{S}$, and $\hat{\bar{v}} = \bar{v} / L$ is the normalized displacement in the y-direction at $\bar{S}$.

By setting $\xi^* = 1$ in (3.18)-(3.20), it leads to an essential and sufficient set of nonlinear algebraic equations for determining the end rotations θ_1^* and θ_2^* and the end displacement u_2^*:

$$\int_{\theta_1^*}^{\theta_2^*} \mathcal{G}(\hat{m}) F\left(\theta , \theta_2^*; \hat{f}_{x2}^*, \hat{f}_y, \hat{m}_2^*\right) d\theta = 1 , \tag{3.21}$$

$$\int_{\theta_1^*}^{\theta_2^*} \mathcal{G}(\hat{m}) \left[\sin\theta\left(1+\varepsilon_0\right)\right] F\left(\theta , \theta_2^*; \hat{f}_{x2}^*, \hat{f}_y, \hat{m}_2^*\right) d\theta = 0 , \tag{3.22}$$

$$\int_{\theta_1^*}^{\theta_2^*} \mathcal{G}(\hat{m}) \left[\cos\theta\left(1+\varepsilon_0\right)-1\right] F\left(\theta , \theta_2^*; \hat{f}_{x2}^*, \hat{f}_y, \hat{m}_2^*\right) d\theta = \hat{u}_2^* \tag{3.23}$$

where the displacement and rotation at the right end, i.e. $\hat{\bar{u}}\left(\bar{\xi} = 1\right) = \hat{u}_2^*$, $\hat{\bar{v}}\left(\bar{\xi} = 1\right) = 0$ and $\bar{\theta}(\bar{\xi} = 1) = \theta_2^*$, have been used.

Now, let's define $\boldsymbol{f}^*$ as a force vector such that $\boldsymbol{f}^* = [\boldsymbol{f}^{p*}\, \boldsymbol{f}^{r*}]^T$ where $\boldsymbol{f}^{p*} = \{\hat{f}^*_{x2}, \hat{m}^*_1, \hat{m}^*_2\}$ is a vector containing force and moments at the free degrees of freedom and $\boldsymbol{f}^{r*} = \{\hat{f}^*_{x1}, \hat{f}^*_{y1}, \hat{f}^*_{y2}\}$ is a vector containing reactive forces at the prescribed degrees of freedom, and let's $\boldsymbol{u}^*$ be a vector of free degrees of freedom defined by $\boldsymbol{u}^* = \{\hat{u}^*_2, \theta^*_1, \theta^*_2\}$. It is evident that once the relation (3.14) is utilized to implicitly define $\hat{f}_y$ in terms of other quantities, the three equations (3.21)-(3.23) now involve only $\boldsymbol{f}^{p*}$ and $\boldsymbol{u}^*$. In the other word, the three equations (3.21)-(3.23) supplemented by the relation (3.14) implicitly define $\boldsymbol{f}^{p*}$ in terms of $\boldsymbol{u}^*$, i.e. $\boldsymbol{f}^{p*} = \boldsymbol{f}^{p*}(\boldsymbol{u}^*)$. By employing (3.15)-(3.17) along with $\boldsymbol{f}^{p*} = \boldsymbol{f}^{p*}(\boldsymbol{u}^*)$, it can be concluded that the reactive forces $\boldsymbol{f}^{r*}$ are also functions of $\boldsymbol{u}^*$, i.e. $\boldsymbol{f}^{r*} = \boldsymbol{f}^{r*}(\boldsymbol{u}^*)$. By integrating above two results, it leads to the implicit force-displacement relation

$$\boldsymbol{f}^* = \boldsymbol{f}^*(\boldsymbol{u}^*) \tag{3.24}$$

The implicit relation (3.24) implies that for a given end displacement and rotation $\boldsymbol{u}^*$, the force vector $\boldsymbol{f}^*$ can always be computed as follows: (i) the end force and moments $\boldsymbol{f}^{p*}$ are obtained by solving a system of nonlinear equations (3.21)-(3.23) with the auxiliary equation (3.14) and (ii) the reactive forces $\boldsymbol{f}^{r*}$ are subsequently computed from (3.15)-(3.17) by the direct substitution. This task is essential in the evaluation of load residuals in the solution procedure discussed later in the next chapter.

Applying Taylor's series expansion to the nonlinear function $\boldsymbol{f}^*$ about any given vector $\boldsymbol{u}^{*0}$ leads to the best linear approximation of $\boldsymbol{f}^*$ in the neighborhood of $\boldsymbol{u}^{*0}$:

$$\boldsymbol{f}^*(\boldsymbol{u}^*) \equiv \boldsymbol{f}^*(\boldsymbol{u}^{*0}) + \boldsymbol{k}^*(\boldsymbol{u}^{*0})(\boldsymbol{u}^* - \boldsymbol{u}^{*0}) \tag{3.25}$$

where the gradient matrix $\boldsymbol{k}^*$ is defined by

$$k^* = \frac{\partial f^*}{\partial u^*} = \begin{bmatrix} k^{p*} \\ k^{r*} \end{bmatrix} \tag{3.26}$$

with k^{p*} denoting the gradient of the force vector f^{p*} with respect to the vector u^* (this matrix is also known as the tangent stiffness matrix with respect to the co-rotational axis) and k^{r*} representing the gradient of the reactive force vector f^{r*} with respect to the vector u^*. The gradient matrix k^{p*} is given explicitly by

$$k^{p*} = \frac{\partial f^{p*}}{\partial u^*} = \begin{bmatrix} \partial \hat{f}_{x2}^* / \partial \hat{u}_2^* & \partial \hat{f}_{x2}^* / \partial \theta_1^* & \partial \hat{f}_{x2}^* / \partial \theta_2^* \\ \partial \hat{m}_1 / \partial \hat{u}_2^* & \partial \hat{m}_1 / \partial \theta_1^* & \partial \hat{m}_1 / \partial \theta_2^* \\ \partial \hat{m}_2 / \partial \hat{u}_2^* & \partial \hat{m}_2 / \partial \theta_1^* & \partial \hat{m}_2 / \partial \theta_2^* \end{bmatrix} \tag{3.27}$$

and the gradient matrix k^{r*} can be expressed explicitly in terms of entries from the gradient matrix k^{p*} as

$$k^{r*} = \frac{1}{\hat{d}^*} \begin{bmatrix} -k_{11}^{p*}\hat{d}^* & -k_{12}^{p*}\hat{d}^* & -k_{13}^{p*}\hat{d}^* \\ -(\hat{m}_1 + \hat{m}_2)/\hat{d}^* & k_{22}^{p*} + k_{32}^{p*} & k_{23}^{p*} + k_{33}^{p*} \\ (\hat{m}_1 + \hat{m}_2)/\hat{d}^* & -k_{22}^{p*} - k_{32}^{p*} & -k_{23}^{p*} - k_{33}^{p*} \end{bmatrix} \tag{3.28}$$

where k_{ij}^{p*} is an entry located at the ith row and j[th] column of the gradient matrix k^{p*}. It is obvious that the main task for computing the gradient matrix k^* is associated with the evaluation of all entries of the sub-matrix k^{p*} and this can be achieved via explicit and implicit differentiations of equations (3.21)-(3.23) along with the additional equation (3.14) as described in the next section.

3.2 Development of Gradient Matrix k^{p*}

The gradient matrix k^{p*} is derived for two different cases, a member containing no inflection point (termed a single curvature member) and a member containing an interior inflection point (termed a double curvature member). These two cases are treated separately since the function F appearing in equations (3.21)-(3.23) possesses distinct behavior. More specifically, the function F is well-behaved

everywhere for the former case whereas it is weakly singular at the location of the inflection point for the latter case. All involved singular integrals for the double curvature member requires some special treatment as described further below. It is worth noting that while results for the case of a member containing an inflection point at its end are not presented, they can readily be obtained via the proper limit process of those for the double curvature member.

3.2.1 Member Containing No Inflection Point

Let's consider a simply-supported member subjected to the end force f_{x2}^* and two opposite, nonzero end moments m_1^* and m_2^* as shown in Figure 3.2. The deformed shape of the member possesses a single curvature. For this particular case, the moment-dependence function $\vartheta(\hat{m})$ takes the value 1 or -1 depending on either the sign of m_1^* or m_2^*; in particular, $\vartheta(\hat{m}) = 1$ for $m_1^* < 0$ and $m_2^* > 0$ and $\vartheta(\hat{m}) = -1$ for $m_1^* > 0$ and and $m_2^* < 0$.
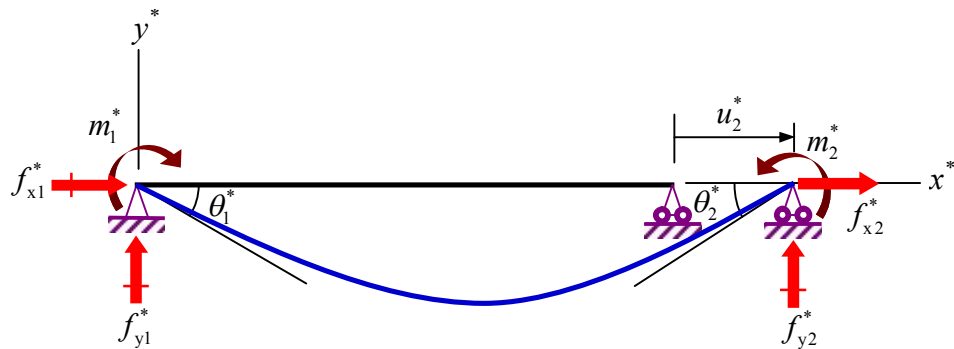
Figure 3.2 Simply-supported member subjected to end force and two opposite, non-zero end moments

For brevity in the presentation of established results, the relation (3.14) and the three nonlinear algebraic equations (3.21)-(3.23) are re-expressed as

$$\Gamma_y(\hat{f}_y, f_{x2}^*, m_1^*, m_2^*, \theta_1^*, \theta_2^*) \equiv \hat{m}_2^{2*} - \hat{m}_1^{2*} + 2\hat{f}_{x2}^*(\cos\theta_2^* - \cos\theta_1^*) - 2\hat{f}_y(\sin\theta_2^* - \sin\theta_1^*)$$
$$+ \frac{1}{2}\alpha(\hat{f}_{x2}^{*2} - \hat{f}_y^2)(\cos 2\theta_2^* - \cos 2\theta_1^*) - \alpha\hat{f}_{x2}^*\hat{f}_y(\sin 2\theta_2^* - \sin 2\theta_1^*) = 0$$

$$(3.29)$$

$$\Gamma_1\left(\theta_1^*,\theta_2^*,\hat{f}_{x2}^*,\hat{f}_y,\hat{m}_2^*\right)\equiv\psi\int_{\theta_1^*}^{\theta_2^*}F\left(\theta\ ,\theta_2^*;\hat{f}_{x2}^*,\hat{f}_y,\hat{m}_2^*\right)d\theta-1=0,\qquad(3.30)$$

$$\Gamma_2\left(\theta_1^*,\theta_2^*,\hat{f}_{x2}^*,\hat{f}_y,\hat{m}_2^*\right)\equiv\psi\int_{\theta_1^*}^{\theta_2^*}\left[\sin\theta\left(1+\varepsilon_0\right)\right]F\left(\theta\ ,\theta_2^*;\hat{f}_{x2}^*,\hat{f}_y,\hat{m}_2^*\right)d\theta=0,\qquad(3.31)$$

$$\Gamma_3\left(\theta_1^*,\theta_2^*,\hat{f}_{x2}^*,\hat{f}_y,\hat{m}_2^*,\hat{u}_2^*\right)\equiv\psi\int_{\theta_1^*}^{\theta_2^*}\left[\cos\theta\left(1+\varepsilon_0\right)-1\right]F\left(\theta\ ,\theta_2^*;\hat{f}_{x2}^*,\hat{f}_y,\hat{m}_2^*\right)d\theta-\hat{u}_2^*=0\qquad(3.32)$$

where $\psi=1$ for $m_1^*<0$ and $m_2^*>0$ and $\psi=-1$ for $m_1^*>0$ and $m_2^*<0$.

It is emphasized that the equation (3.29) implicitly defines $\hat{f}_y$ in terms of $\{f_{x2}^*,m_1^*,m_2^*,\theta_1^*,\theta_2^*\}$, i.e. $\hat{f}_y=\hat{f}_y(f_{x2}^*,m_1^*,m_2^*,\theta_1^*,\theta_2^*)$. Its derivative with respect to those quantities can be obtained by taking implicit differentiation of (3.29) and results are given by

$$\left[\frac{\partial\hat{f}_y}{\partial\boldsymbol{f}^{\mathrm{p}*}}\quad\frac{\partial\hat{f}_y}{\partial\boldsymbol{u}^*}\right]=-\frac{1}{\partial\Gamma_y/\partial\hat{f}_y}\left[\frac{\partial\Gamma_y}{\partial\boldsymbol{f}^{\mathrm{p}*}}\quad\frac{\partial\Gamma_y}{\partial\boldsymbol{u}^*}\right]\qquad(3.33)$$

Terms on the right hand side of (3.33) can be found in Appendix A. By taking derivative of (3.30)-(3.32) with respect to $\hat{u}_2^*$, θ_1^* and θ_2^* along with the implicit function $\hat{f}_y=\hat{f}_y(f_{x2}^*,m_1^*,m_2^*,\theta_1^*,\theta_2^*)$ defined by (3.29), it leads to a system of linear equations for $\boldsymbol{k}^{p*}$

$$\left(\frac{\partial\boldsymbol{\Gamma}}{\partial\boldsymbol{f}^{\mathrm{p}*}}+\frac{\partial\boldsymbol{\Gamma}}{\partial\hat{f}_y}\frac{\partial\hat{f}_y}{\partial\boldsymbol{f}^{\mathrm{p}*}}\right)\boldsymbol{k}^{p*}=-\frac{\partial\boldsymbol{\Gamma}}{\partial\boldsymbol{u}^*}-\frac{\partial\boldsymbol{\Gamma}}{\partial\hat{f}_y}\frac{\partial\hat{f}_y}{\partial\boldsymbol{u}^*}\qquad(3.34)$$

where $\boldsymbol{\Gamma}=\begin{bmatrix}\Gamma_1&\Gamma_2&\Gamma_3\end{bmatrix}^T$ and entries of matrices $\partial\boldsymbol{\Gamma}/\partial\boldsymbol{f}^{\mathrm{p}*}$, $\partial\boldsymbol{\Gamma}/\partial\hat{f}_y$ and $\partial\boldsymbol{\Gamma}/\partial\boldsymbol{u}^*$ are given explicitly in Appendix A. The gradient matrix $\boldsymbol{k}^{p*}$ can therefore be obtained by solving a system of linear equations (3.34).

3.2.2 Member Containing Interior Inflection Point

Let's consider, next, a simply-supported member subjected to the end force f_{x2}^* and the non-zero end moments $\{\hat{m}_1, \hat{m}_2\}$ with the same direction as shown in Figure 3.3. The deformed shape of the member possesses a double curvature with an inflection point located at an interior point $\xi_z \in (0, 1)$. The bending moment disappears at $\xi_z \in (0, 1)$ and $\hat{m}(\xi_1)\hat{m}(\xi_2) < 0$ for $\xi_1 \in [0, \xi_z)$ and $\xi_2 \in (\xi_z, 1]$. The moment-dependence function $\vartheta(\hat{m})$, for this particular case, is discontinuous at ξ_z and takes different values on both sides of the inflection point. For $\hat{m}_1 > 0, \hat{m}_2 < 0$, $\vartheta(\hat{m}) = -1$ for $\xi \in [0, \xi_z)$ and $\vartheta(\hat{m}) = 1$ for $\xi \in (\xi_z, 1]$ and for $\hat{m}_1 < 0, \hat{m}_2 > 0$, $\vartheta(\hat{m}) = 1$ for $\xi \in [0, \xi_z)$ and $\vartheta(\hat{m}) = -1$ for $\xi \in (\xi_z, 1]$. For this particular case, the function F appearing in equations (3.21)-(3.23) is weakly singular at the location of the inflection point and all involved singular integrals must be treated specially and differently from the previous case as described below.
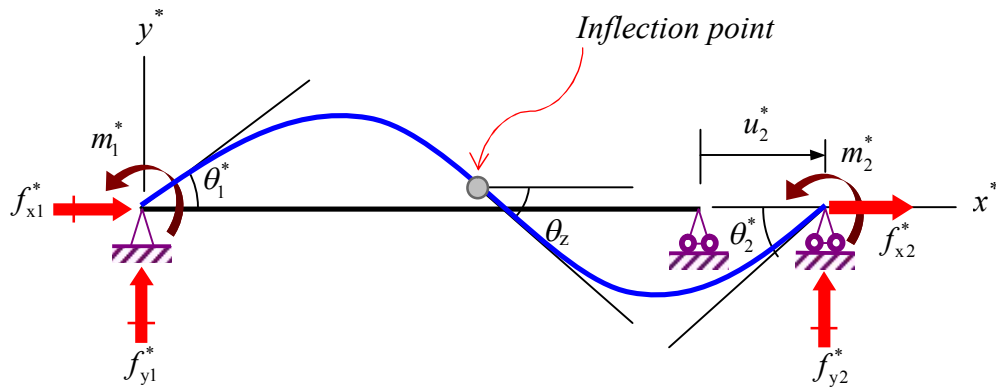

Figure 3.3 Simply-supported member subjected to end force and two non-zero end moments with the same direction

At the inflection point, the bending moment vanishes and this leads to the following condition:

$$\frac{d\theta}{d\xi}(\theta = \theta_z) = 0 \tag{3.35}$$

where θ_z is the rotation of cross section at the inflection point. By substituting the condition (3.35) into (2.16) along with the constant C obtained in (3.7), it leads to

$$\bar{\Gamma}_z(\hat{f}_y,\theta_z,f_{x2}^*,m_1^*,m_2^*,\theta_1^*,\theta_2^*) \equiv \hat{m}_2^{*2} + 2\hat{f}_{x2}^*\left(\cos\theta_2^* - \cos\theta_z\right) - 2\hat{f}\left(\sin\theta_2^* - \sin\theta_z\right)$$
$$+\alpha\left(\frac{\hat{f}_{x2}^{*2} - \hat{f}_y^2}{2}\right)\left(\cos 2\theta_2^* - \cos 2\theta_z\right) - \alpha\hat{f}_{x2}^*\hat{f}_y\left(\sin 2\theta_2^* - \sin 2\theta_z\right) = 0 \tag{3.36}$$

By combining (3.14) and (3.36) yields

$$\bar{\Gamma}_y(\hat{f}_y,\theta_z,f_{x2}^*,m_1^*,m_2^*,\theta_1^*,\theta_2^*) \equiv \hat{m}_1^{*2} + 2\hat{f}_{x2}^*\left(\cos\theta_1^* - \cos\theta_z\right) - 2\hat{f}\left(\sin\theta_1^* - \sin\theta_z\right)$$
$$+\alpha\left(\frac{\hat{f}_{x2}^{*2} - \hat{f}_y^2}{2}\right)\left(\cos 2\theta_1^* - \cos 2\theta_z\right) - \alpha\hat{f}_{x2}^*\hat{f}_y\left(\sin 2\theta_1^* - \sin 2\theta_z\right) = 0 \tag{3.37}$$

By using the relations (3.36) and (3.37), a set of three governing nonlinear algebraic equations (3.21)-(3.23) for the rotation, the displacement in the y-direction and the displacement in the x- direction can be re-expressed as

$$\psi\left[-\int_{\theta_1^*}^{\theta_z} F_z(\theta,\theta_z;\hat{f}_{x2}^*,\hat{f}_y)d\theta + \int_{\theta_z}^{\theta_2^*} F_z(\theta,\theta_z;\hat{f}_{x2}^*,\hat{f}_y)d\theta\right] = 1 \tag{3.38}$$

$$\psi\left\{-\int_{\theta_1^*}^{\theta_z} \left[\sin\theta(1+\varepsilon_0)\right]F_z(\theta,\theta_z;\hat{f}_{x2}^*,\hat{f}_y)d\theta + \int_{\theta_z}^{\theta_2^*} \left[\sin\theta(1+\varepsilon_0)\right]F_z(\theta,\theta_z;\hat{f}_{x2}^*,\hat{f}_y)d\theta\right\} = 0 \tag{3.39}$$

$$\psi\left\{-\int_{\theta_1^*}^{\theta_z} \left[\cos\theta(1+\varepsilon_0)-1\right]F_z(\theta,\theta_z;\hat{f}_{x2}^*,\hat{f}_y)d\theta + \int_{\theta_z}^{\theta^*} \left[\cos\theta(1+\varepsilon_0)-1\right]F_z(\theta,\theta_z;\hat{f}_{x2}^*,\hat{f}_y)d\theta\right\} = \hat{u}_2^* \tag{3.40}$$

where the constant ψ is defined by $\psi = -1$ for $\hat{m}_1^*,\hat{m}_2^* < 0$ and $\psi = 1$ for $\hat{m}_1^*,\hat{m}_2^* > 0$ and the function F_z is defined by

$$F_z(\theta,\theta_z;\hat{f}_{x2}^*,\hat{f}_y) = \frac{1}{\sqrt{i_z + \alpha j_z}} \tag{3.41}$$

$$i_z = \hat{m}_2^{*2} + 2\hat{f}_{x2}^*\left(\cos\theta_z - \cos\theta\right) - 2\hat{f}_y\left(\sin\theta_z - \sin\theta\right) \tag{3.42}$$

$$j_z = \frac{1}{2}\left(\hat{f}_{x2}^{*2} - \hat{f}_y^2\right)\left(\cos 2\theta_z - \cos 2\theta\right) - \hat{f}_{x2}^*\hat{f}_y\left(\sin 2\theta_z - \sin 2\theta\right) \tag{3.43}$$

It is apparent from (3.41) that the function F_z appearing in (3.38)-(3.40) is weakly singular at the inflection point of order $1/\sqrt{\theta-\theta_z}$. To remove such inverted square-root singularity, the change of variable $\phi=\sqrt{\psi\left(\theta-\theta_z\right)}$ is utilized and the governing equations (3.38)-(3.40) now become

$$\bar{\Gamma}_1\left(\hat{f}_{x2}^*,\hat{f}_y,\theta_z,\phi_1,\phi_2\right)\equiv\psi\int_0^{\phi_1}F_\phi\left(\phi,\theta_z,\hat{f}_{x2}^*,\hat{f}_y\right)d\phi+\psi\int_0^{\phi_2}F_\phi\left(\phi,\theta_z,\hat{f}_{x2}^*,\hat{f}_y\right)d\phi-1=0 \tag{3.44}$$

$$\bar{\Gamma}_2\left(\hat{f}_{x2}^*,\hat{f}_y,\theta_z,\phi_1,\phi_2\right)\equiv\psi\left\{\int_0^{\phi_1}\left[\sin\left(\psi\phi^2+\theta_z\right)(1+\varepsilon_0)\right]F_\phi\left(\phi,\theta_z,\hat{f}_{x2}^*,\hat{f}_y\right)d\phi\right.$$
$$\left.+\int_0^{\phi_2}\left[\sin\left(\psi\phi^2+\theta_z\right)(1+\varepsilon_0)\right]F_\phi\left(\phi,\theta_z,\hat{f}_{x2}^*,\hat{f}_y\right)d\phi\right\}=0 \tag{3.45}$$

$$\bar{\Gamma}_3\left(\hat{f}_{x2}^*,\hat{f}_y,\theta_z,\phi_1,\phi_2,\hat{u}_2^*\right)\equiv\psi\left\{\int_0^{\phi_1}\left\{\left[\cos\left(\psi\phi^2+\theta_z\right)(1+\varepsilon_0)\right]-1\right\}F_\phi\left(\phi,\theta_z,\hat{f}_{x2}^*,\hat{f}_y\right)d\phi\right.$$
$$\left.+\int_0^{\phi_2}\left\{\left[\cos\left(\psi\phi^2+\theta_z\right)(1+\varepsilon_0)\right]-1\right\}F_\phi\left(\phi,\theta_z,\hat{f}_{x2}^*,\hat{f}_y\right)d\phi\right\}-\hat{u}_2^*=0 \tag{3.46}$$

where $\phi_1=\sqrt{\psi\left(\theta_1^*-\theta_z\right)}$, $\phi_2=\sqrt{\psi\left(\theta_2^*-\theta_z\right)}$ and the function F_ϕ is defined by

$$F_\phi(\phi,\theta_z;\hat{f}_{x2}^*,\hat{f}_y)=\frac{2\psi\phi}{\sqrt{i_\phi+\alpha j_\phi}} \tag{3.47}$$

$$i_\phi=2\hat{f}_{x2}^*\left(\cos\theta_z-\cos\left(\psi\phi^2+\theta_z\right)\right)-2\hat{f}_y\left(\sin\theta_z-\sin\left(\psi\phi^2+\theta_z\right)\right) \tag{3.48}$$

$$j_\phi=\frac{1}{2}\left(\hat{f}_{x2}^{*2}-\hat{f}_y^2\right)\left(\cos2\theta_z-\cos\left(2\psi\phi^2+2\theta_z\right)\right)-\hat{f}_{x2}^*\hat{f}_y\left(\sin2\theta_z-\sin\left(2\psi\phi^2+2\theta_z\right)\right) \tag{3.49}$$

It is clear that the two relations (3.36) and (3.37) equations implicitly define $\hat{f}_y$ and θ_z in terms of $\{f_{x2}^*,m_1^*,m_2^*,\theta_1^*,\theta_2^*\}$, i.e. $\hat{f}_y=\hat{f}_y(f_{x2}^*,m_1^*,m_2^*,\theta_1^*,\theta_2^*)$ and $\theta_z=\theta_z(f_{x2}^*,m_1^*,m_2^*,\theta_1^*,\theta_2^*)$. To obtain derivatives of $\hat{f}_y$ and θ_z with respect to $\{f_{x2}^*,m_1^*,m_2^*,\theta_1^*,\theta_2^*\}$, the implicit differentiations of (3.36) and (3.37) have been taken and this results in a system of linear equations

$$\left(\frac{\partial \overline{\mathbf{\Gamma}}_{yz}}{\partial \boldsymbol{a}}\right)\left[\frac{\partial \boldsymbol{a}}{\partial \boldsymbol{f}^{\mathrm{p}*}} \quad \frac{\partial \boldsymbol{a}}{\partial \boldsymbol{u}^*}\right] = \left[\frac{\partial \overline{\mathbf{\Gamma}}_{yz}}{\partial \boldsymbol{f}^{\mathrm{p}*}} \quad \frac{\partial \overline{\mathbf{\Gamma}}_{yz}}{\partial \boldsymbol{u}^*}\right] \tag{3.50}$$

where $\overline{\mathbf{\Gamma}}_{yz} = \begin{bmatrix} \overline{\Gamma}_y & \overline{\Gamma}_z \end{bmatrix}^T$, $\boldsymbol{a} = \begin{bmatrix} \hat{f}_y & \theta_z \end{bmatrix}^T$ and entries of matrices $\partial \overline{\mathbf{\Gamma}}_{yz}/\partial \boldsymbol{a}$, $\partial \overline{\mathbf{\Gamma}}_{yz}/\partial \boldsymbol{f}^{\mathrm{p}*}$ and $\partial \overline{\mathbf{\Gamma}}_{yz}/\partial \boldsymbol{u}^{\mathrm{p}*}$ are presented in Appendix B. The system of linear equations (3.50) can be solved to obtain $\partial \boldsymbol{a}/\partial \boldsymbol{f}^{\mathrm{p}*}$ and $\partial \boldsymbol{a}/\partial \boldsymbol{u}^*$.

Similarly, by taking derivative of (3.44)-(3.46) with respect to $\hat{u}_2^*, \theta_1^*$ and θ_2^* along with implicit functions $\hat{f}_y = \hat{f}_y(f_{x2}^*, m_1^*, m_2^*, \theta_1^*, \theta_2^*)$ and $\theta_z = \theta_z(f_{x2}^*, m_1^*, m_2^*, \theta_1^*, \theta_2^*)$ defined by (3.36) and (3.37), it leads to a system of linear equations for $\boldsymbol{k}^{\mathrm{p}*}$

$$\left(\frac{\partial \overline{\mathbf{\Gamma}}}{\partial \boldsymbol{f}^{\mathrm{p}*}} + \frac{\partial \overline{\mathbf{\Gamma}}}{\partial \boldsymbol{a}}\frac{\partial \boldsymbol{a}}{\partial \boldsymbol{f}^{\mathrm{p}*}} + \frac{\partial \overline{\mathbf{\Gamma}}}{\partial \boldsymbol{\Phi}}\frac{\partial \boldsymbol{\Phi}}{\partial \theta_z}\frac{\partial \theta_z}{\partial \boldsymbol{f}^{\mathrm{p}*}}\right)\boldsymbol{k}^{\mathrm{p}*} = -\frac{\partial \overline{\mathbf{\Gamma}}}{\partial \boldsymbol{u}^*} - \frac{\partial \overline{\mathbf{\Gamma}}}{\partial \boldsymbol{a}}\frac{\partial \boldsymbol{a}}{\partial \boldsymbol{u}^*} - \frac{\partial \overline{\mathbf{\Gamma}}}{\partial \boldsymbol{\Phi}}\left(\frac{\partial \boldsymbol{\Phi}}{\partial \boldsymbol{u}^*} + \frac{\partial \boldsymbol{\Phi}}{\partial \theta_z}\frac{\partial \theta_z}{\partial \boldsymbol{u}^*}\right) \tag{3.51}$$

where $\overline{\mathbf{\Gamma}} = \begin{bmatrix} \overline{\Gamma}_1 & \overline{\Gamma}_2 & \overline{\Gamma}_3 \end{bmatrix}^T$, $\boldsymbol{\Phi} = \begin{bmatrix} \phi_1 & \phi_2 \end{bmatrix}^T$ and entries of matrices $\partial \overline{\mathbf{\Gamma}}/\partial \boldsymbol{f}^{\mathrm{p}*}$, $\partial \overline{\mathbf{\Gamma}}/\partial \boldsymbol{a}$, $\partial \overline{\mathbf{\Gamma}}/\partial \boldsymbol{\Phi}$, $\partial \boldsymbol{\Phi}/\partial \theta_z$, $\partial \overline{\mathbf{\Gamma}}/\partial \boldsymbol{u}^*$ and $\partial \boldsymbol{\Phi}/\partial \boldsymbol{u}^*$ are given explicitly in Appendix B. The gradient matrix $\boldsymbol{k}^{\mathrm{p}*}$ can therefore be obtained by solving a system of linear equations (3.51).

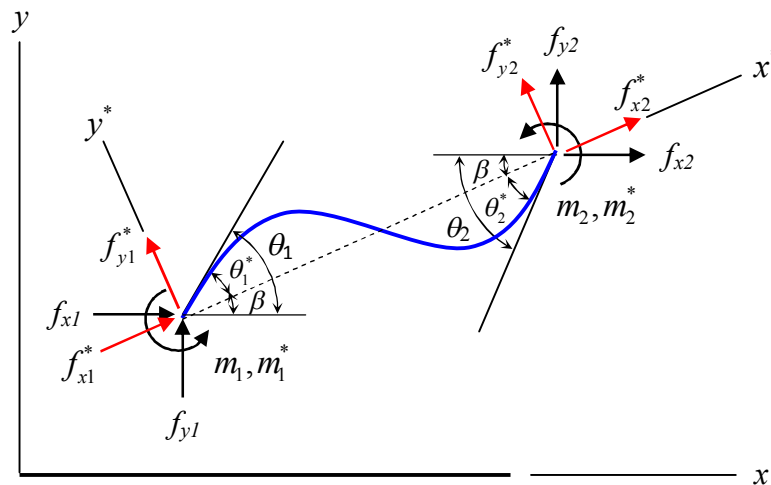### 3.3 Local Force-displacement Relation for Generic Element

Figure 3.4 Schematic of undeformed and deformed shape of generic member and the local coordinate system $\{x, y\}$ and co-rotational coordinate system $\{x^*, y^*\}$

Let's consider a generic member with its undeformed and deformed configurations shown in Figure 3.4 and let $\{x, y\}$ and $\{x^*, y^*\}$ denote the local coordinate system of the member in the undeformed state and its co-rotational coordinate system of the deformed member, respectively.

Now, let's define $\boldsymbol{f}^l = \{\hat{f}_{x1}, \hat{f}_{y1}, \hat{m}_1, \hat{f}_{x2}, \hat{f}_{y2}, \hat{m}_2\}$ and $\boldsymbol{u}^l = \{\hat{u}_1, \hat{v}_1, \theta_1, \hat{u}_2, \hat{v}_2, \theta_2\}$ as a vector of normalized end forces and moments and a vector of normalized end displacements and rotations observed in the $\{x, y\}$ system, respectively, and define $\boldsymbol{f}^* = \{\hat{f}_{x1}^*, \hat{f}_{y1}^*, \hat{m}_1^*, \hat{f}_{x2}^*, \hat{f}_{y2}^*, \hat{m}_2^*\}$ and $\boldsymbol{u}^* = \{\hat{u}_2^*, \theta_1^*, \theta_2^*\}$ a vector of normalized end forces and moments and a vector of normalized end displacements and rotations observed in the $\{x^*, y^*\}$ system, respectively. The normalized displacement $\boldsymbol{u}^*$ can be obtained in terms of $\boldsymbol{u}^l$ via the geometric consideration and results are given by

$$\theta_1^* = \theta_1 - \beta \tag{3.52}$$

$$\theta_2^* = \theta_2 - \beta \tag{3.53}$$

$$\hat{u}_2^* = (1 + \hat{u}_2 - \hat{u}_1)\cos\beta + (\hat{v}_2 - \hat{v}_1)\sin\beta - 1 \tag{3.54}$$

where β is the chord rotation defined by

$$(1 + \hat{u}_2 - \hat{u}_1)\sin\beta - (\hat{v}_2 - \hat{v}_1)\cos\beta = 0 \tag{3.55}$$

The normalized force and moment vector $\boldsymbol{f}^l$ in the local $\{x, y\}$ system can be readily related to a force and moment vector $\boldsymbol{f}^*$ in the $\{x^*, y^*\}$ system through standard coordinate transformation:

$$\boldsymbol{f}^l = \boldsymbol{T}(\beta)\boldsymbol{f}^* \tag{3.56}$$

where a transformation matrix $\boldsymbol{T}(\beta)$ is given by

$$T(\beta) = \begin{bmatrix} 0 & 0 & 0 & c_\beta & -s_\beta & 0 \\ 0 & 0 & 0 & s_\beta & c_\beta & 0 \\ 0 & 1 & 0 & 0 & 0 & 0 \\ c_\beta & 0 & 0 & 0 & 0 & -s_\beta \\ s_\beta & 0 & 0 & 0 & 0 & c_\beta \\ 0 & 0 & 1 & 0 & 0 & 0 \end{bmatrix} \tag{3.57}$$

in which $c_\beta = cos\beta$ and $s_\beta = sin\beta$. Since the member, when observed from the $\{x^*, y^*\}$ system, is identical to the simply-supported member, f^* and u^* can be related by the relation $f^* = f^*(u^*)$ obtained in section 3.1. Combining equation (3.56), $f^* = f^*(u^*)$ and $u^* = u^*(u^l)$ leads to the force-displacement relation in the local coordinate system:

$$f^l = f^l(u^l) = T(\beta) f^*(u^*(u^l)) \tag{3.58}$$

The relation (3.58) allows the end forces and moments to be computed for a given end displacements and rotations in the local coordinate system. By applying Taylor's series expansion to the nonlinear function f^l, it leads to the best linear approximation in the neighborhood of a given displacement vector u^{l0}:

$$f^l(u^l) \equiv f^l(u^{l0}) + k^l(u^{l0})(u^l - u^{l0}) \tag{3.59}$$

where k^l is the local element tangent stiffness matrix of the member given by

$$k^l = \frac{\partial T}{\partial \beta} f^* \frac{\partial \beta}{\partial u} + T k^* \frac{\partial u^*}{\partial u} \tag{3.60}$$

where matrices $\dfrac{\partial T}{\partial \beta}$, $\dfrac{\partial \beta}{\partial u}$ and $\dfrac{\partial u^*}{\partial u}$ are given in Appendix C.

3.4 Global Force-displacement Relation for Generic Element

Let φ be an angle indicating the orientation of the undeformed generic member with respect to the global coordinate system; more specifically, φ is an angle between the local $x-$ axis of the member and the global $X-$ axis of a structure. Also, let's define $\boldsymbol{f}^g = \{\hat{f}^g_{x1}, \hat{f}^g_{y1}, \hat{m}^g_1, \hat{f}^g_{x2}, \hat{f}^g_{y2}, \hat{m}^g_2\}$ and $\boldsymbol{u}^g = \left\{\hat{u}^g_1, \hat{v}^g_1, \theta^g_1, \hat{u}^g_2, \hat{v}^g_2, \theta^g_2\right\}$ as a vector of normalized end forces and moments and a vector of normalized end displacements and rotations observed in the $\{X, Y\}$ system, respectively. The force vectors $\boldsymbol{f}^g$ and $\boldsymbol{f}^l$ and the displacement vectors $\boldsymbol{u}^g$ and $\boldsymbol{u}^l$ can be related by following standard coordinate transformations:

$$\boldsymbol{f}^g = \boldsymbol{Q}^T \boldsymbol{f}^l \quad ; \quad \boldsymbol{u}^l = \boldsymbol{Q}\boldsymbol{u}^g \tag{3.61}$$

where Q is the transformation matrix given by

$$\boldsymbol{Q} = \begin{bmatrix} \cos\varphi & \sin\varphi & 0 & 0 & 0 & 0 \\ -\sin\varphi & \cos\varphi & 0 & 0 & 0 & 0 \\ 0 & 0 & 1 & 0 & 0 & 0 \\ 0 & 0 & 0 & \cos\varphi & \sin\varphi & 0 \\ 0 & 0 & 0 & -\sin\varphi & \cos\varphi & 0 \\ 0 & 0 & 0 & 0 & 0 & 1 \end{bmatrix} \tag{3.62}$$

From the force-displacement relation in the local coordinate system (3.58) along with (3.61), the force-displacement relation for a member in the global coordinate system can be obtained as

$$\boldsymbol{f}^g = \boldsymbol{f}^g\left(\boldsymbol{u}^g\right) = \boldsymbol{Q}^T \boldsymbol{f}^l\left(\boldsymbol{Q}\boldsymbol{u}^g\right) \tag{3.63}$$

The relation (3.63) allows the end forces and moments of a member in the global coordinate system to be computed once the end displacements and rotations in the global coordinate system are known. Again, by applying Taylor's series expansion, the best linear approximation of $\boldsymbol{f}^g$ in the neighborhood of a vector $\boldsymbol{u}^{g0}$ takes the form

$$\boldsymbol{f}^g\left(\boldsymbol{u}^g\right) \equiv \boldsymbol{f}^g\left(\boldsymbol{u}^{g0}\right) + \boldsymbol{k}^g\left(\boldsymbol{u}^{g0}\right)\left(\boldsymbol{u}^g - \boldsymbol{u}^{g0}\right) \tag{3.64}$$

where $\boldsymbol{k}^g$ is the global element tangent stiffness matrix of the member given in terms of $\boldsymbol{k}^l$ by

$$\boldsymbol{k}^g = \boldsymbol{Q}^T \boldsymbol{k}^l \boldsymbol{Q} \tag{3.65}$$

3.5 Load-displacement Relation for Structure

Let a given structure be discretized into m straight and prismatic members and let $\boldsymbol{P}$ and $\boldsymbol{U}$ be a force vector collecting all nodal loads and a displacement vector collecting all nodal degrees of freedom of the structure. By enforcing static equilibrium and continuity at all nodes, the force vector $\boldsymbol{P}$ can be directly related to all global element force vectors $\boldsymbol{f}^{g1}$, $\boldsymbol{f}^{g2}$, ..., $\boldsymbol{f}^{gm}$ and the displacement vector $\boldsymbol{U}$ can be directly related to all global element displacement vectors $\boldsymbol{u}^{g1}$, $\boldsymbol{u}^{g2}$, ..., $\boldsymbol{u}^{gm}$ via standard direct assembly procedure, i.e.

$$\boldsymbol{P} = \text{Direct assembly of } \{\boldsymbol{f}^{g1}, \boldsymbol{f}^{g2}, \boldsymbol{f}^{g3}, ..., \boldsymbol{f}^{gm}\} \tag{3.66}$$

$$\boldsymbol{U} = \text{Direct assembly of } \{\boldsymbol{u}^{g1}, \boldsymbol{u}^{g2}, \boldsymbol{u}^{g3}, ..., \boldsymbol{u}^{gm}\} \tag{3.67}$$

By applying the relation (3.63) for all members along with (3.66) and (3.67), it leads to the load-displacement relation for a structure:

$$\boldsymbol{P} = \boldsymbol{P}(\boldsymbol{U}) \tag{3.68}$$

For a given displacement vector $\boldsymbol{U}$, the relation (3.68) ensures that the load vector $\boldsymbol{P}$ can be computed. More specifically, the relation (3.67) is utilized first to disassemble $\boldsymbol{U}$ into $\boldsymbol{u}^{g1}$, $\boldsymbol{u}^{g2}$, ..., and $\boldsymbol{u}^{gm}$; next, the relation (3.63) is applied for all members to compute $\boldsymbol{f}^{g1}$, $\boldsymbol{f}^{g2}$, ..., and $\boldsymbol{f}^{gm}$; and, finally, the relation (3.66) is utilized to assemble $\boldsymbol{f}^{g1}$, $\boldsymbol{f}^{g2}$, ..., and $\boldsymbol{f}^{gm}$ into $\boldsymbol{P}$. By applying Taylor's series expansion to (3.68), the best linear approximation of $\boldsymbol{P}$ in the neighborhood of a vector $\boldsymbol{U}^0$ takes the form

$$\boldsymbol{P}(\boldsymbol{U}) \equiv \boldsymbol{P}(\boldsymbol{U}^0) + \boldsymbol{K}^T(\boldsymbol{U}^0)(\boldsymbol{U} - \boldsymbol{U}^0) \tag{3.69}$$

where $\boldsymbol{K}^T$ is the structure tangent stiffness matrix that can be obtained by a direct assembly of $\boldsymbol{k}^{g1}$, $\boldsymbol{k}^{g2}$, …, and $\boldsymbol{k}^{gm}$, i.e.

$$\boldsymbol{K}^T = \text{Direct assembly of } \{\boldsymbol{k}^{g1}, \boldsymbol{k}^{g2}, \boldsymbol{k}^{g3}, ..., \boldsymbol{k}^{gm}\} \tag{3.70}$$

The best linear approximation (3.70) plays an important role in the Newton-Raphson iterative scheme to determine the displacement vector $\boldsymbol{U}$ for a given load vector $\boldsymbol{P}$.

3.6 Determination of Internal Forces

Once the displacement vector $\boldsymbol{U}$ is solved, the internal resultant forces at any cross section of any member can readily be obtained by following procedures indicated below. First, the force and displacement at both ends of a member in the co-rotational coordinate system, i.e. $\boldsymbol{f}^*$ and $\boldsymbol{u}^*$, are obtained from the last converged iteration. Next, the displacements $\bar{u}$ and $\bar{v}$ and the rotation $\bar{\theta}$ at any cross section $\bar{S} \in (0, L)$ can be computed from the relations (3.18)-(3.20). Finally, by introducing a fictitious cut at $\bar{S}$ and then considering equilibrium of the left portion (see its free body diagram in Figure 3.5), it leads to expressions for the bending moment $\bar{m}$, the internal force resultant in the x^*-direction $\bar{f}_x$ and the internal force resultant in the y^*-direction $\bar{f}_y$ at the cross section $\bar{S}$ as
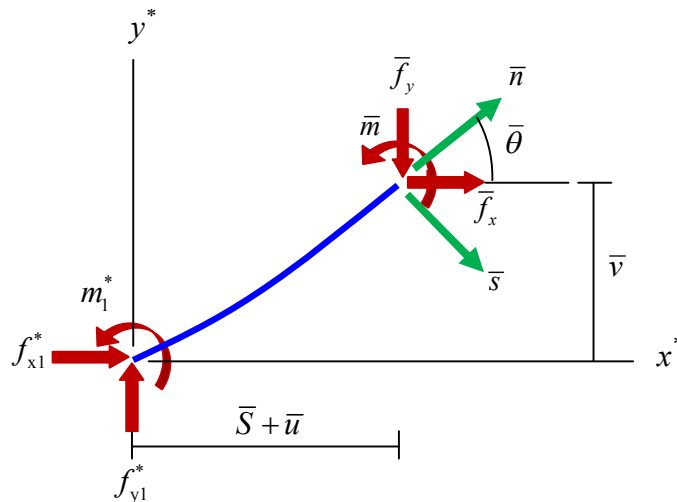
Figure 3.5 Free body diagram of a left portion of member resulting from a cut at $\bar{S}$

$$\hat{\bar{f}}_x = -\hat{\bar{f}}_{x1}^*$$

(3.71)

$$\hat{\bar{f}}_y = \hat{\bar{f}}_{y1}^*$$

(3.72)

$$\hat{\bar{m}} = -\hat{m}_1^* - \hat{\bar{f}}_{x1}^* \hat{\bar{v}} + \hat{\bar{f}}_{y1}^* \left(\bar{\xi} + \hat{\bar{u}} \right)$$

(3.73)

where $\hat{\bar{f}}_x = \bar{f}_x L^2 / EI$, $\hat{\bar{f}}_y = \bar{f}_y L^2 / EI$, $\hat{\bar{m}} = \bar{m}L / EI$ and $\bar{\xi} = \bar{S} / L$. The axial force resultant, denoted by $\bar{n}$, and the shear force resultant, denoted by $\bar{s}$, can subsequently be obtained as follows:

$$\hat{\bar{n}} = \hat{\bar{f}}_x \cos \bar{\theta} - \hat{\bar{f}}_y \sin \bar{\theta}$$

(3.74)

$$\hat{\bar{s}} = \hat{\bar{f}}_x \sin \bar{\theta} + \hat{\bar{f}}_y \cos \bar{\theta}$$

(3.75)

where $\hat{\bar{n}} = \bar{n}L^2 / EI$ and $\hat{\bar{s}} = \bar{s}L^2 / EI$.

CHAPTER IV

SOLUTION PROCEDURE

In this chapter, components essential for the solution procedure and the development of an in-house computer code (e.g. numerical integration, procedure to determine the end forces and moments due to the prescribed end displacement and rotations in the co-rotational coordinate system, nonlinear solver by Newton-Raphson method, etc.) are briefly discussed.

4.1 Numerical Integration

All integrals involved in the key governing equations are relatively complex and cannot directly be integrated to obtain regular functions. Nevertheless, integrands of all integrals, after performing variable transformations for the case of double-curvature members, are well-behaved and contain no singularity within their range of integration. In the present study, standard Gaussian quadrature (e.g. Hamming, 1987; Chapra and Canale, 1990) is employed to accurately and efficiently evaluate those involved integrals.

4.2 Procedure to Determine f^* for Prescribed u^*

Determination of f^* for a given u^* is a crucial step in the evaluation of load residuals in Newton-Raphson iteration (e.g. Hamming, 1987; Chapra and Canale, 1990) and it requires to solve a system of nonlinear algebraic equations (3.29)-(3.32) for a single curvature member and (3.36)-(3.37) and (3.44)-(3.46) for a double curvature member. Procedures based on Newton-Raphson iteration are implemented to achieve this particular task as indicated below.

1) Start by choosing an appropriate initial guess $f^{*(k)}$ with $k = 0$

2) Evaluate the residual $\mathbf{\Gamma}^{(k)} = \begin{bmatrix} \Gamma_1 & \Gamma_2 & \Gamma_3 \end{bmatrix}$ for a single curvature member and $\overline{\mathbf{\Gamma}}^{(k)} = \begin{bmatrix} \overline{\Gamma}_1 & \overline{\Gamma}_2 & \overline{\Gamma}_3 \end{bmatrix}$ for a double curvature member at $f^{*(k)}$ and given u^*

3) Check convergence $\left\|\mathbf{\Gamma}^{(k)}\right\| < Tol$ or $\left\|\overline{\mathbf{\Gamma}}^{(k)}\right\| < Tol$. If it is satisfied, stop the iteration; otherwise, go to step 4)

4) Obtain the gradient matrix $\partial\mathbf{\Gamma}/\partial\boldsymbol{f}^{*}$ or $\partial\overline{\mathbf{\Gamma}}/\partial\boldsymbol{f}^{*}$ at $\boldsymbol{f}^{*(k)}$ and given $\boldsymbol{u}^{*}$

5) Solve a system of linear equations $0 = \mathbf{\Gamma}^{(k)} + \dfrac{\partial\mathbf{\Gamma}}{\partial\boldsymbol{f}^{*}}\left(\boldsymbol{f}^{*(k+1)} - \boldsymbol{f}^{*(k)}\right)$ or

$0 = \overline{\mathbf{\Gamma}}^{(k)} + \dfrac{\partial\overline{\mathbf{\Gamma}}}{\partial\boldsymbol{f}^{*}}\left(\boldsymbol{f}^{*(k+1)} - \boldsymbol{f}^{*(k)}\right)$ to obtain $\boldsymbol{f}^{*(k+1)}$ and then go to step 2)

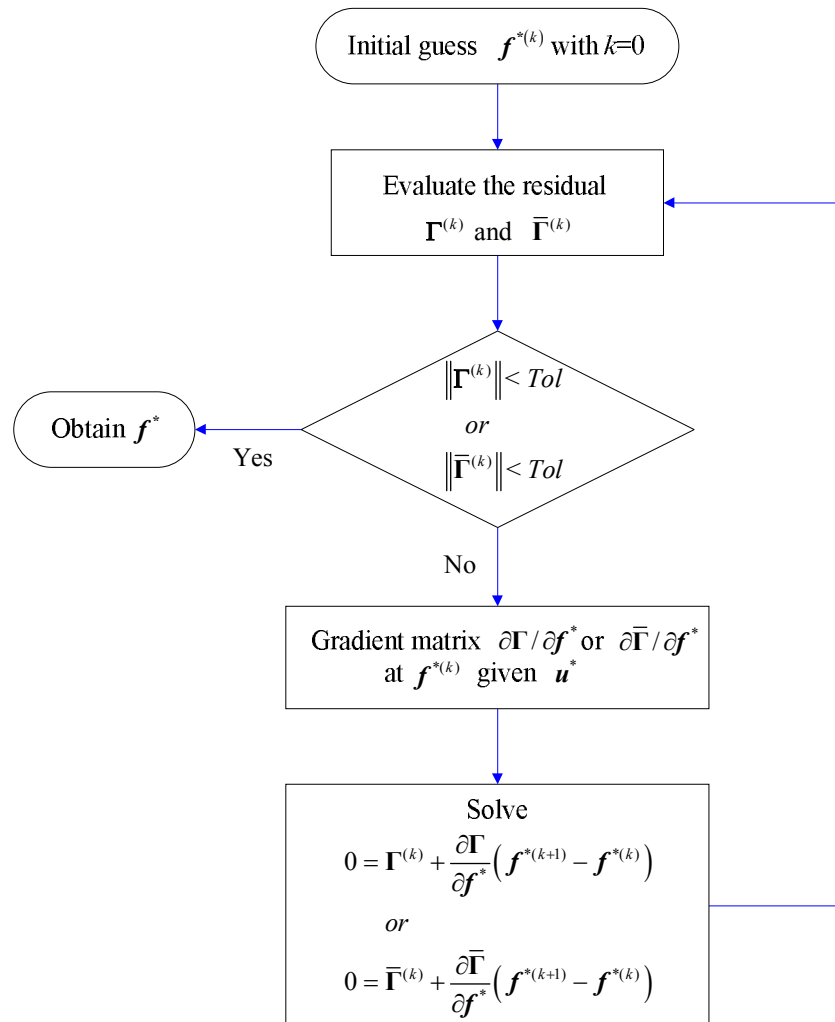The above procedures can also be presented in a form of a flowchart as shown in Figure 4.1.

Figure 4.1 Flowchart of procedures to determine for given $\boldsymbol{f}^{*}$ for a given $\boldsymbol{u}^{*}$

4.3 Solution Procedure by Newton-Raphson Method

To solve a system of nonlinear algebraic equations $\mathbf{P} = \mathbf{P(U)}$ for a given $\mathbf{P}$, Newton-Raphson method is utilized. Procedures to obtain the solution $\mathbf{U}^* + \Delta\mathbf{U}$ for the given load vector $\mathbf{P}^* + \Delta\mathbf{P}$ where $\mathbf{U}^*$ is a converged displacement vector associated with $\mathbf{P}^*$ from the previous step, $\Delta\mathbf{P}$ is the prescribed load increment in the current step, and $\Delta\mathbf{U}$ is the displacement increment to be determined, are summarized as follows:

1) Start by choosing an appropriate initial guess $\Delta U^{(k)}$ with $k = 0$

2) Obtain the total displacement vector $U^{(k)} = U^* + \Delta U^{(k)}$

3) Disassemble $U^{(k)}$ to obtain the global end displacement vector for each member $u^{g(k)}$

4) Obtain the local end displacement vector for each member $u^{l(k)}$ from the first relation of (3.61)

5) Obtain the end displacement vector in the co-rotational coordinate system for each member $u^{*(k)}$ from the relations (3.52)-(3.55)

6) Utilize procedures presented in the section 4.2 to determine the force vector $f^{*(k)}$ for each member from the known $u^{*(k)}$

7) Compute the gradient matrix k^{p*} for each member using results obtained from sections 3.1 and 3.2

8) Obtain local force vector $f^{l(k)}$ and local element tangent stiffness matrix $k^{l(k)}$ for each member using the relations (3.56) and (3.60), respectively

9) Obtain global force vector $f^{g(k)}$ and global element tangent stiffness matrix $k^{g(k)}$ for each member using the relations (3.61) and (3.65), respectively

10) Assembly global force vector $f^{g(k)}$ and global element tangent stiffness matrix $k^{g(k)}$ for all members to obtain $P\left(U^{(k)}\right)$ and for $K^{T(k)}$

11) Compute load residual vector $\boldsymbol{R}^{(k)} = \boldsymbol{P} + \Delta\boldsymbol{P} - \boldsymbol{P}\left(\boldsymbol{U}^{(k)}\right)$ and check convergence from $\left\|\boldsymbol{R}^{(k)}\right\| / \left\|\boldsymbol{P} + \Delta\boldsymbol{P}\right\| < Tol$. If it is satisfied, $\boldsymbol{U}^{(k)}$ becomes the solution and the iteration is terminated; otherwise, go to step 12)

12) Update the displacement increment $\Delta\boldsymbol{U}^{(k+1)}$ by solving a system of linear algebraic equations $\boldsymbol{R}^{(k)} = \boldsymbol{K}^{T(k)}\Delta\boldsymbol{U}^{(k+1)}$ and then go to step 2)

The above solution procedures can be presented clearly in a form of a flowchart as shown in Figure 4.2.
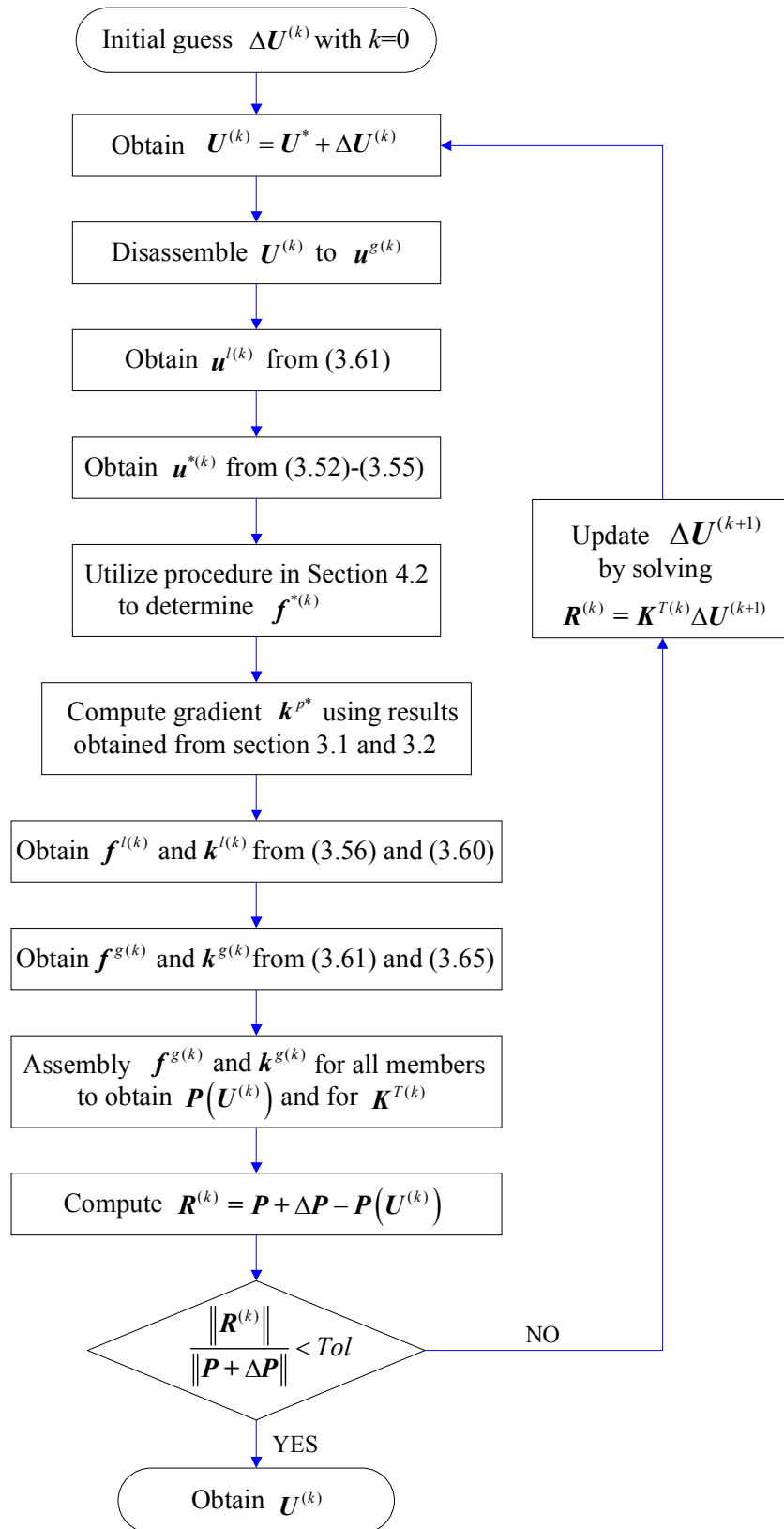
Figure 4.2 Flowchart of solution procedures by Newton-Raphson method

4.4 Structure of Implemented Computer Code

The implemented in-house computer code consists of three main parts including input routine, processing routine and output routine as shown in Figure 4.3.

In the input routine, essential data including the geometry of the structure (i.e. nodal coordinates and member connectivity), constraints against movements, cross sectional properties (i.e. area *A* and moment of inertia *I*), Young's modulus *E*, and nodal load data and number of load steps, must be provided.

The processing routine involves the complete nonlinear analysis. The given load data is sub-divided into several load steps and, for each load step, the nodal displacement vector is obtained using the procedure shown in the section 4.3. The routine is terminated when all load steps are considered.

The output routine is implemented to capable of post-processing the reactive forces, internal forces at any point within the structure, and the deformed shape of a structure. Once nodal displacements and rotations are solved, quantities of interest within the member can readily be computed. For instance, the displacement and rotation at any interior point of a member can be obtained using the relations (3.21)-(3.23) and all internal forces can be obtained by using the method of sections along with the enforcement of equilibrium in the deformed state.
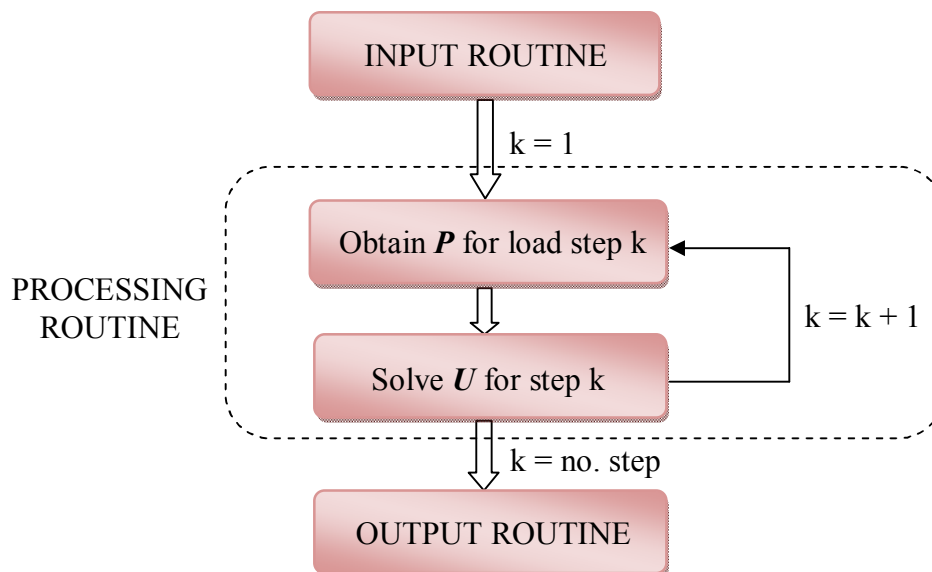

Figure 4.3 Structure of implemented in-house computer code

CHAPTER V

NUMERICAL RESULTS

In this chapter, numerical results for various examples are presented to demonstrate the efficiency and accuracy of the current technique. The formulation and implementation are tested by comparing the predicted solutions with those from a reliable finite element code. For numerical experiments of the first two problems, a series of meshes is adopted to construct the approximate solutions with the primary aim to show no dependency of numerical solutions on the level of discretization. The last two examples, a one-story portal frame and a multi-story frame, are considered to demonstrate capability of the proposed technique to treat structures consisting of multiple members.

5.1 Cantilever Beam Subjected to Two Moments and Axial Force

Consider a cantilever beam of length 2L, Young's modulus E, moment of inertia I, and cross sectional area A. The beam is subjected to two opposite concentrated moments, 1.5M at the mid-span and M at the tip, and the axial force P at the tip of beam as shown schematically in Figure 5.1(a). In the analysis, three meshes consisting of 2, 4 and 8 elements are adopted as shown in Figure 5.1(b).

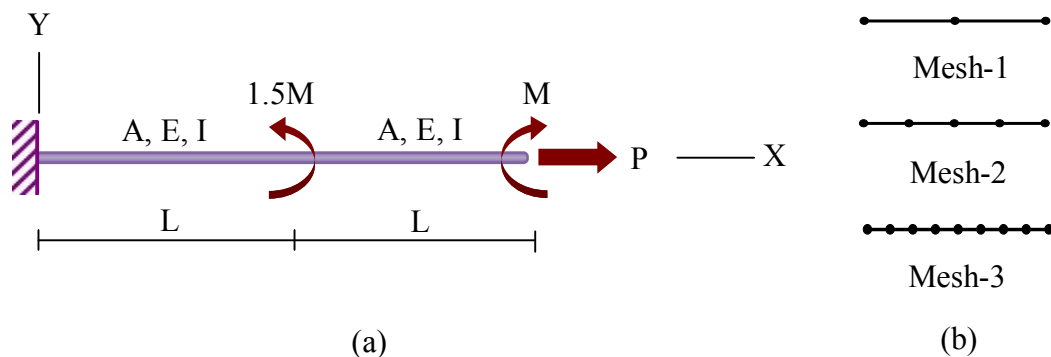(a)   (b)

Figure 5.1 (a) Schematic of cantilever beam subjected to two moments and axial forces and (b) three meshes adopted in the analysis.

The deformed shapes of the beam for $\alpha = \mathrm{I}/\mathrm{AL}^2 = 0$ (inextensible case), 0.5, 1 with $\hat{\mathrm{P}} = \mathrm{PL}^2/\mathrm{EI} = 0.2$ and $\hat{\mathrm{m}} = \mathrm{ML}/\mathrm{EI} \in \{2,4,6\}$ are shown in Figure 5.2 along with results obtained from the reliable FEM package. To ensure the accuracy of the benchmark solution, a sufficiently fine mesh (confirmed by a convergence test) is utilized to generate such reference solution. It is evident that results obtained from the current technique are identical for all three meshes and they exhibit excellent agreement with the benchmark solution for all three values of normalized moment $\hat{\mathrm{m}}$ considered. It should be noted that the predicted solutions exhibit mesh independent due to the use of exact governing equations in the evaluation of load residuals in the Newton-Ralphson iterative scheme. This crucial feature allows the reduction of number of elements used in the analysis to save the computational resources. It is also important to point out that using inextensibility assumption ($\alpha = 0$ or $\mathrm{A} \rightarrow \infty$) in the modeling can lead to results of significant difference from those for the more realistic, extensible case ($\alpha > 0$ or A is infinite).
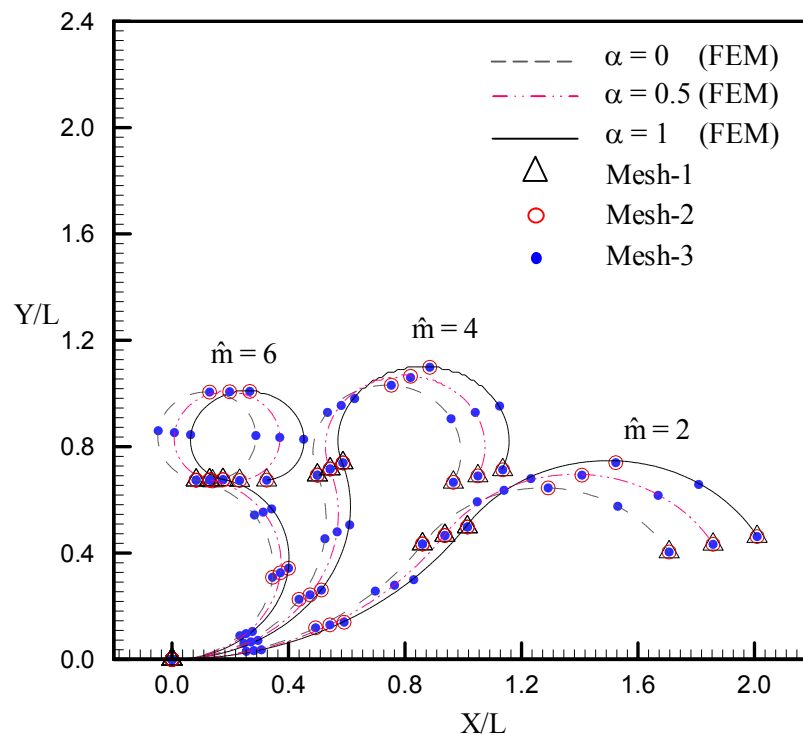

Figure 5.2 Deformed shapes of cantilever beam subjected to two moments and axial force with $\hat{\mathrm{P}} = 0.2$

5.2 T-Frame Subjected to Moments and Axial forces

Next, let's consider a T-frame consisting of a single column and two beams as shown schematically in Figure 5.3(a). The beams and the column are of the same length L, Young's modulus E, the moment of inertia I and the cross-sectional area A. The given frame is subjected to three concentrated moments $\{M_1, M_2, M_3\}$ and the axial forces P at the beam ends. In the analysis, the three moments are chosen such that $M_1 = M_2$ and $M_3 = -2.5M_1$ and three meshes consisting of 3, 6 and 12 members are adopted as shown in Figure 5.3(b).

The deformed shapes of the T-frame obtained from the analysis are reported in Figure 5.4 for $\alpha = I/AL^2 \in \{0, 0.5, 1\}$, $\hat{P} = PL^2/EI = 0.2$ and $\hat{m} = M_1L/EI \in \{2, 6\}$ along with results obtained from the FEM. Again, numerical results obtained from all three meshes are highly accurate (as compared with the benchmark solutions) and, again, exhibit mesh independence. For this particular structure, only three members (two beams and one column) are sufficient in the discretization. Similar to the previous case, the extensibility condition strongly influences the deformed shape of the structure.
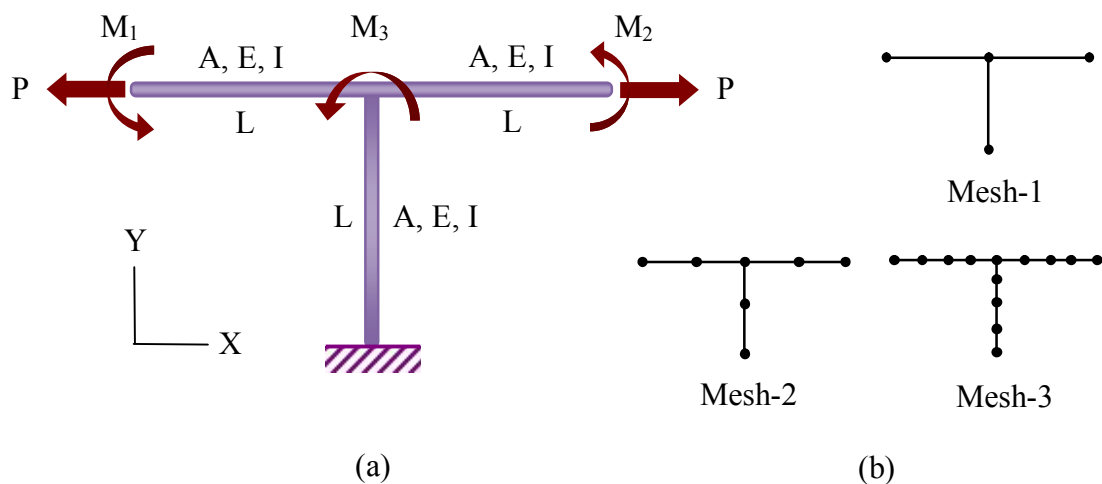

Figure 5.3 (a) T-frame subjected to three concentrated moments and axial forces and (b) three meshes adopted in the analysis
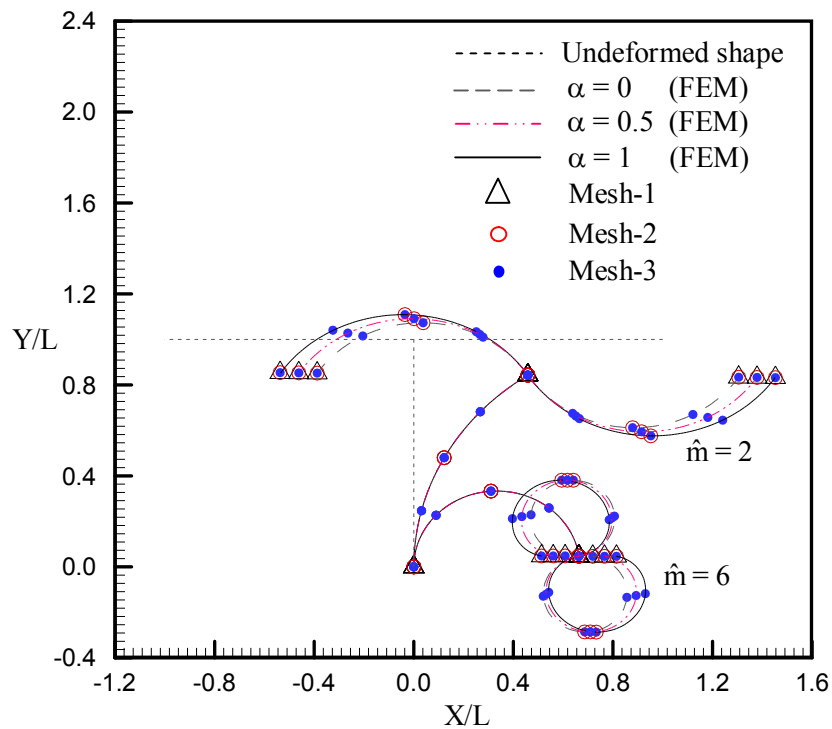
Figure 5.4 Deformed shapes of T-frame subjected to three concentrated moments and

normalized axial force $\hat{P} = 0.2$

5.3 Propped Cantilever Beam Subjected to End Loads

Next, let's consider a propped cantilever beam of length L, Young's modulus E, the moment of inertia I and the cross sectional area A as shown in Figure 5.5(a). The beam is fully fixed at the left end whereas the right end is restrained against the movement in the vertical direction and subjected to the end moment M and axial compressive force P. Due to the beam configuration and loading conditions, only one member is needed in the discretization as shown in Figure 5.5(b).

The deformed shapes of the beam obtained from the analysis are reported in Figure 5.6 for $\alpha = I/AL^2 = 0.005$ and different values of $\hat{P} = PL^2/EI$ and $\hat{m} = M_1 L/EI$. Again, to validate the computed solutions, converged results obtained from the FEM are plotted in the same graph. It is evident from this set of results that highly accurate numerical solutions are obtained with use of a single member in the discretization. It is also worth noting that the displacement and rotation at any interior point can readily be obtained via the post-processing equations (e.g. equations (3.18)-

(3.20)) once all unknowns at both ends of the member are determined. Results of such post-process are also reported in Figure (5.6) and, again, they are in very good agreement with the FEM solution. It can also be concluded from this set of results that increase of the axial compressive force P for a fixed end moment M results in the larger displacement and rotation.
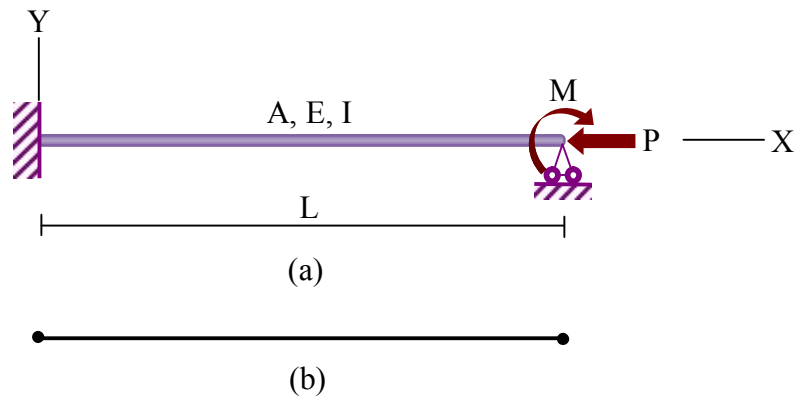

(a)

(b)

Figure 5.5 (a) Propped cantilever beam subjected to end moment M and axial compressive force P and (b) mesh used in the analysis
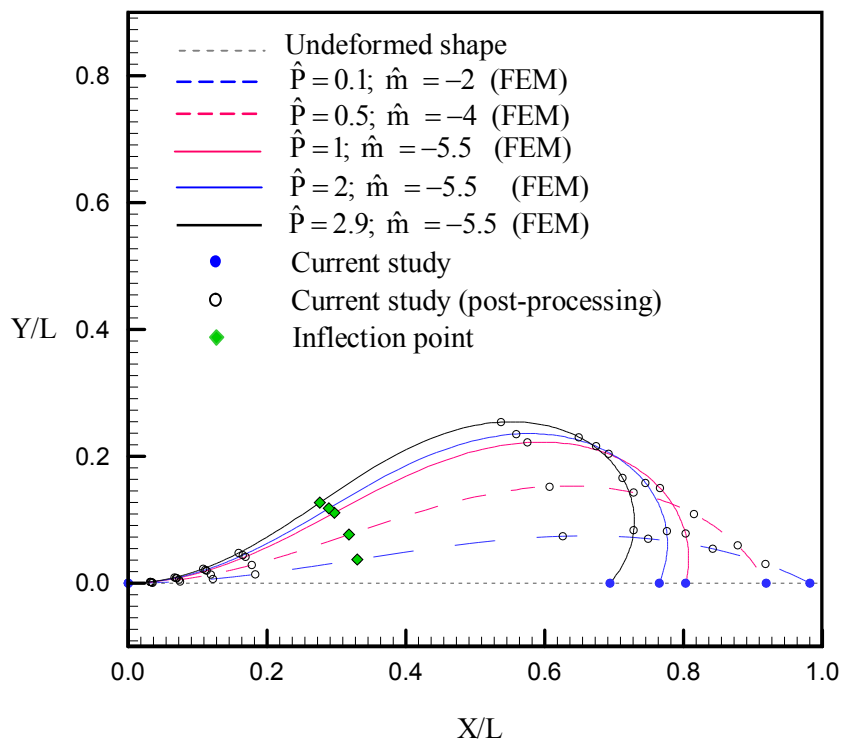

Figure 5.6 Deformed shapes of propped cantilever beam subjected to end moment and axial compressive force

In addition, the axial force, the shear force and the bending moment along the member are obtained and reported along with those generated by the linear elastic analysis in Figures 5.7, 5.8, and 5.9, respectively. It is evident that results obtained from the proposed technique show significant deviation from the linear solution and such difference increases as the magnitude of applied loads becomes larger. This is due mainly to that the deformed configuration of the member at larger loads is significantly different from the undeformed configuration and this also boosts the influence of the axial-bending interaction. In particular, the axial force and shear force obtained from the linear analysis are constant throughout the member (due to that equilibrium is enforced in the undeformed state) whereas those obtained from the large displacement and rotation analysis vary nonlinearly along member due to the significant change of the member axis. This similar trend was also observed in the case of the bending moment. In addition, as the compressive force P increases for a fixed moment M, the bending moment within the member becomes larger and this behavior cannot be predicted from the linear analysis.
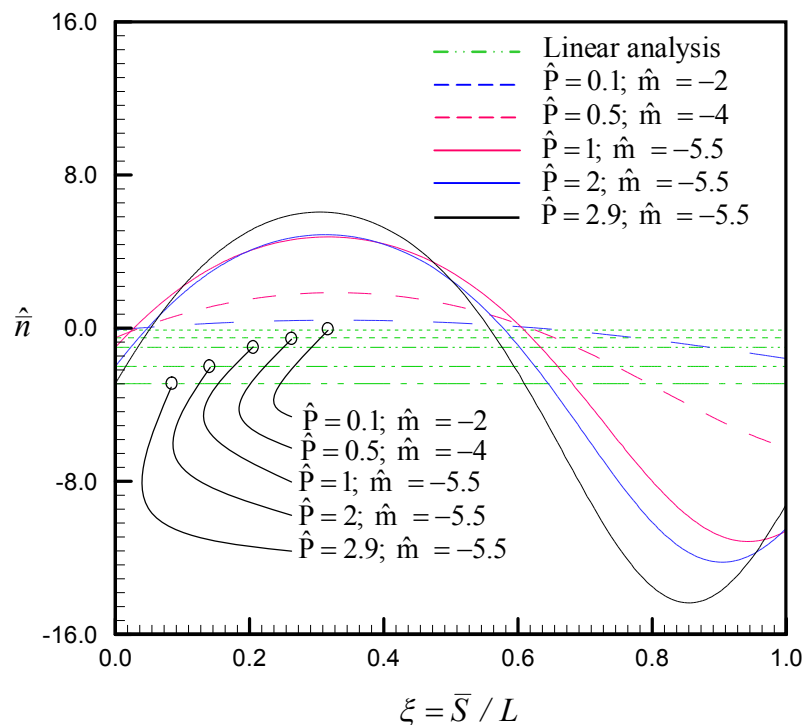

Figure 5.7 Normalized axial force diagram of propped cantilever beam subjected to end moment and axial compressive force
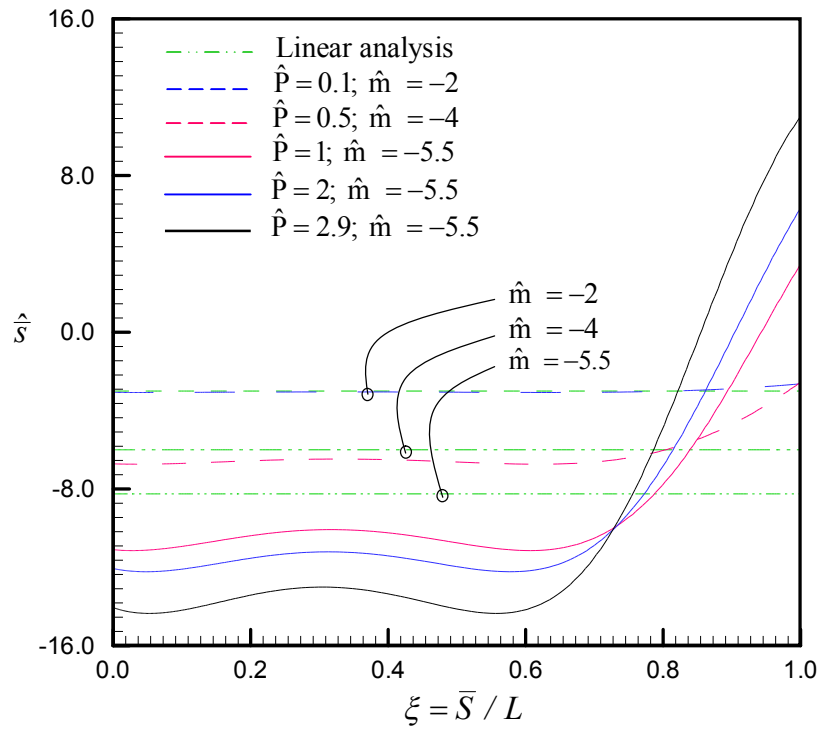
Figure 5.8 Normalized shear force diagram of propped cantilever beam subjected to end moment and axial compressive force
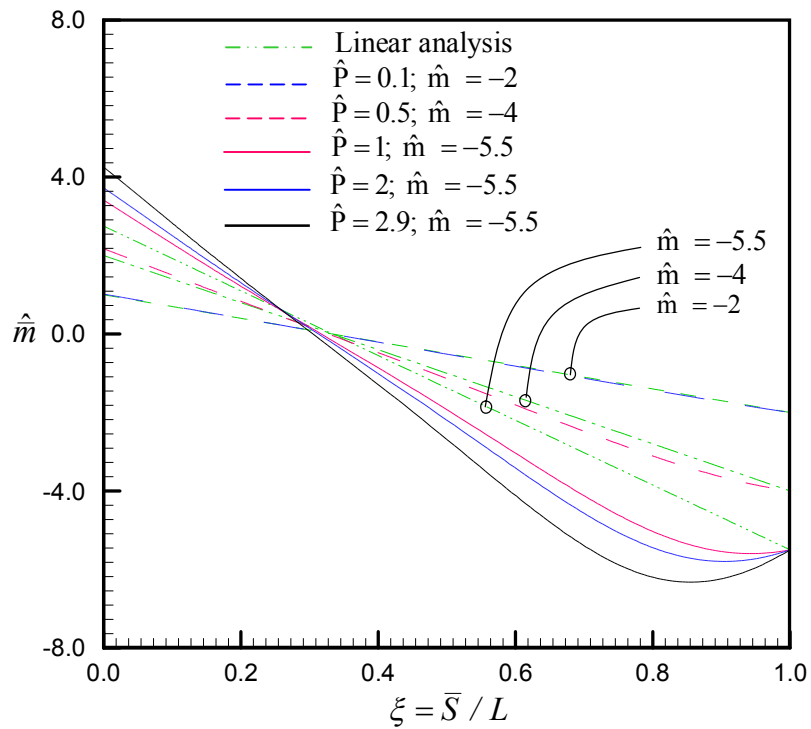

Figure 5.9 Normalized bending moment diagram of propped cantilever beam subjected to end moment and axial compressive force

5.4 One-story Portal Frame Subjected to Horizontal and Vertical Forces

Let's consider, next, a one-story portal frame consisting of two columns and beam as shown in Figure 5.10(a). The beam and the two columns are of the same length L, Young's modulus E, the moment of inertia I and the cross sectional area A. The frame is fully fixed at the base and subjected to a horizontal concentrated force P and two identical vertical forces V at the top of the column. In the analysis, the frame is discretized into three members (i.e. two columns and one beam) as shown in Figure 5.10(b) and the horizontal and vertical forces are chosen to be sufficiently large, i.e. $\hat{P} = PL^2/EI = 15$ and $\hat{V} = VL^2/EI = -5$, to ensure that the structure undergoes the large displacement and large rotation.
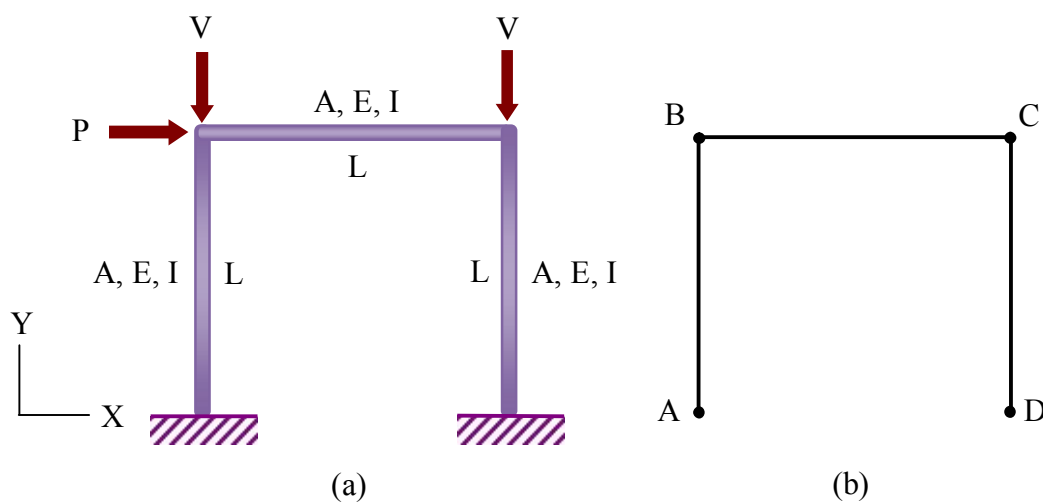
Figure 5.10 (a) One-story portal frame subjected to both horizontal and vertical forces at the top of columns and (b) mesh used in the analysis

The deformed shapes of the frame for $\alpha = I/AL^2 = 0$ (inextensible case), $\alpha = I/AL^2 \in \{0.005, 0.001\}$ (extensible case), $\hat{P} = 15$ and $\hat{V} = -5$ are shown in Figure 5.11 along with the benchmark solutions generated by the FEM. Interior points obtained from the post-process and the location of the inflection point in each member are also reported. It is evident that results obtained from current technique are almost indistinguishable from those obtained from the FEM. In addition, results for the extensible case exhibit significant deviation from those for the inextensible case.
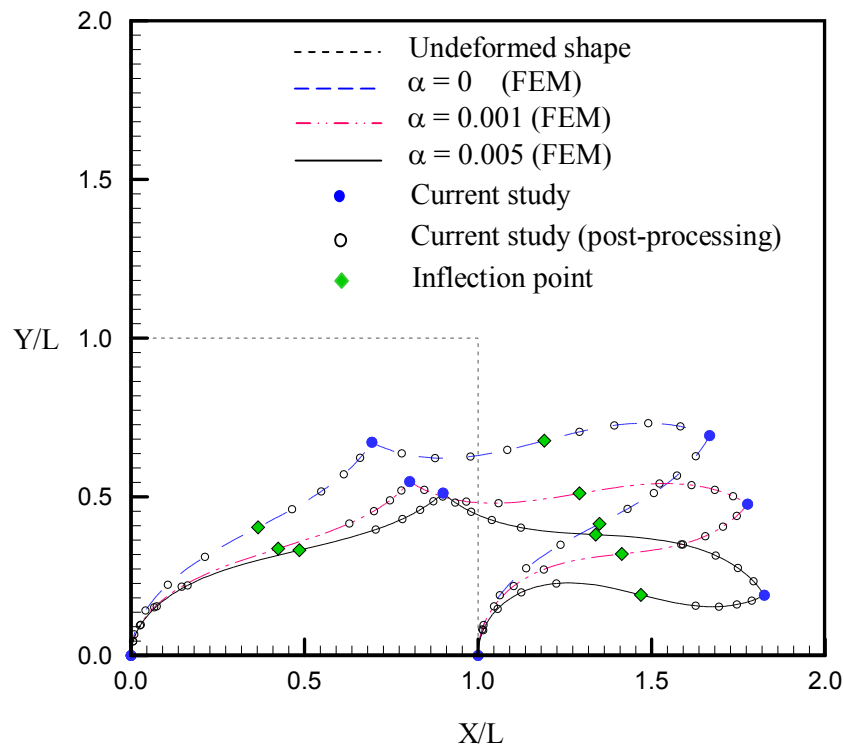
Figure 5.11 Deformed shapes of one-story portal frame subjected to both horizontal and vertical forces at the top of columns

Again, to demonstrate the behavior of the internal forces developed within this particular frame under the given applied forces, diagrams of the axial force, the shear force and the bending moment for three members (i.e. members AB, BC and CD) obtained from the current technique are reported in Figures 5.12-5.13 along with those from the linear elastic analysis. It is apparent from this set of results that the axial force and shear force predicted by the current technique possess highly nonlinear variation along all three members and are very different from those obtained from linear elastic analysis which are found constant within each member. For the bending moment, the discrepancy between results obtained from the two techniques is obviously less than the axial and shear forces; however, this level of difference is still sufficiently large to indicate the incapability of the linear analysis to model structures under large displacement and rotation.

Figure 5.12 Normalized axial forces diagram for member AB of one-story portal frame subjected to both horizontal and vertical forces at the top of columns

Figure 5.13 Normalized shear forces diagram for member AB of one-story portal frame subjected to both horizontal and vertical forces at the top of columns

Figure 5.14 Normalized bending moment diagram for member AB of one-story portal frame subjected to both horizontal and vertical forces at the top of columns
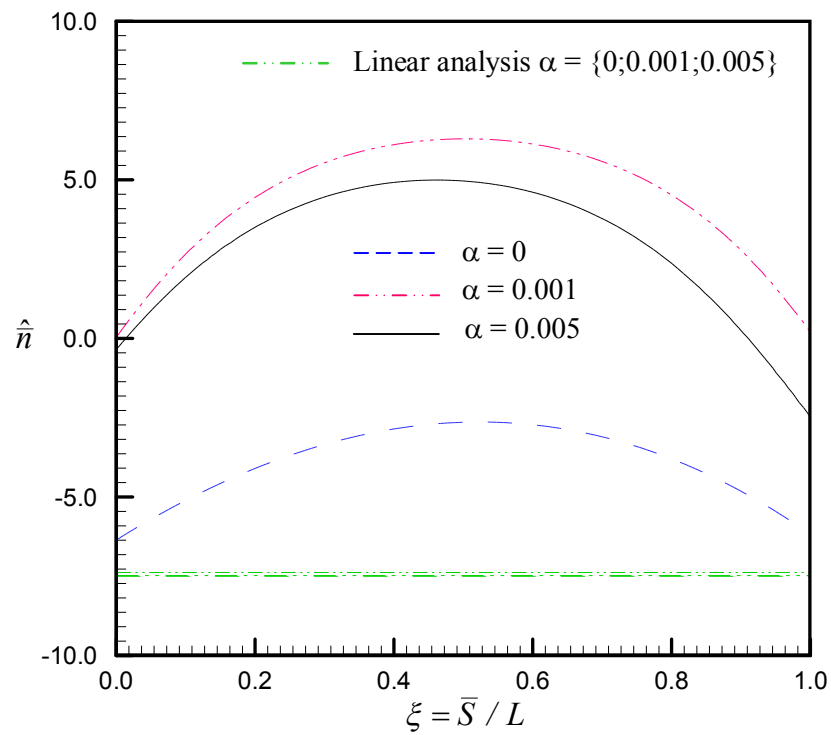
Figure 5.15 Normalized axial force diagram for member BC of one-story portal frame subjected to both horizontal and vertical forces at the top of columns
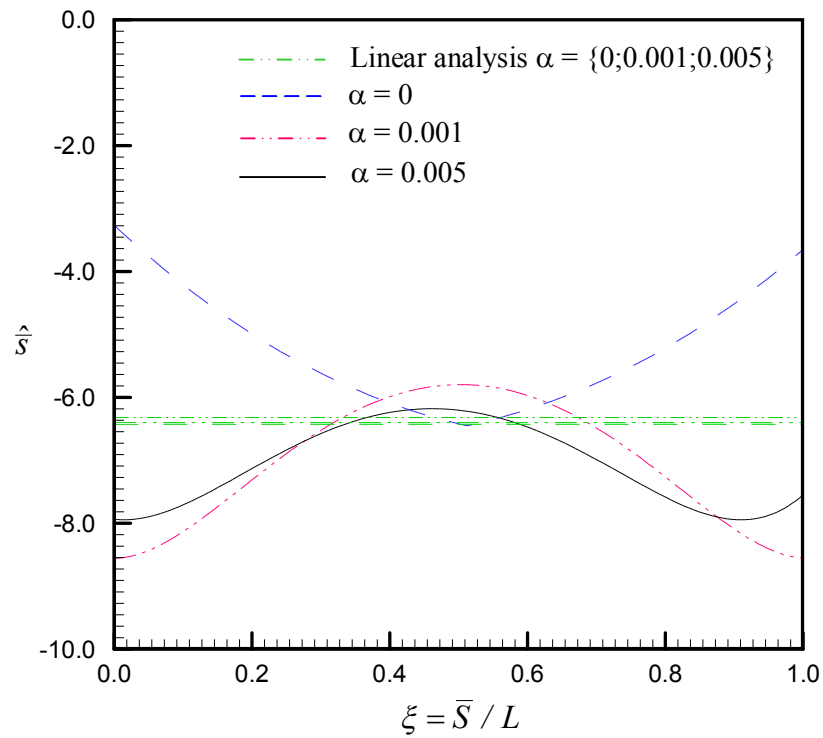
Figure 5.16 Normalized shear force diagram for member BC of one-story portal frame subjected to both horizontal and vertical forces at the top of columns
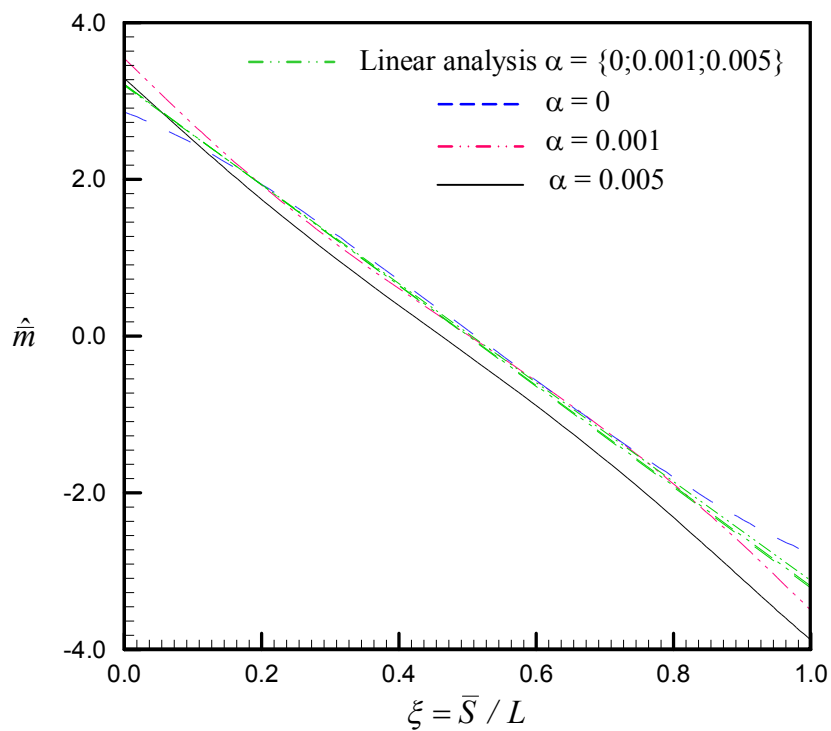
Figure 5.17 Normalized bending moment diagram for member BC of one-story portal frame subjected to both horizontal and vertical forces at the top of columns
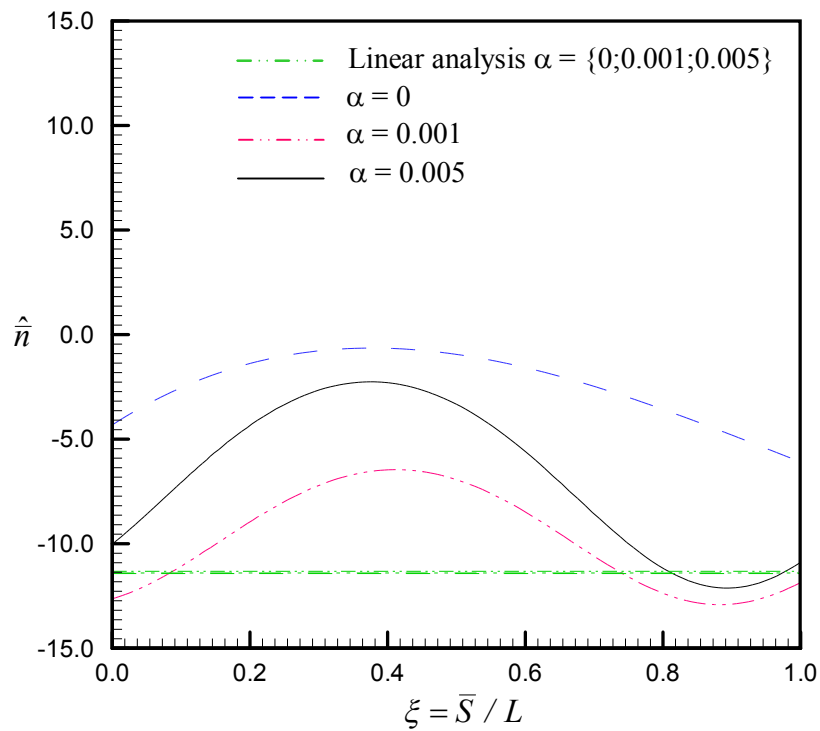
Figure 5.18 Normalized axial force diagram for member CD of one-story portal frame subjected to both horizontal and vertical forces at the top of columns
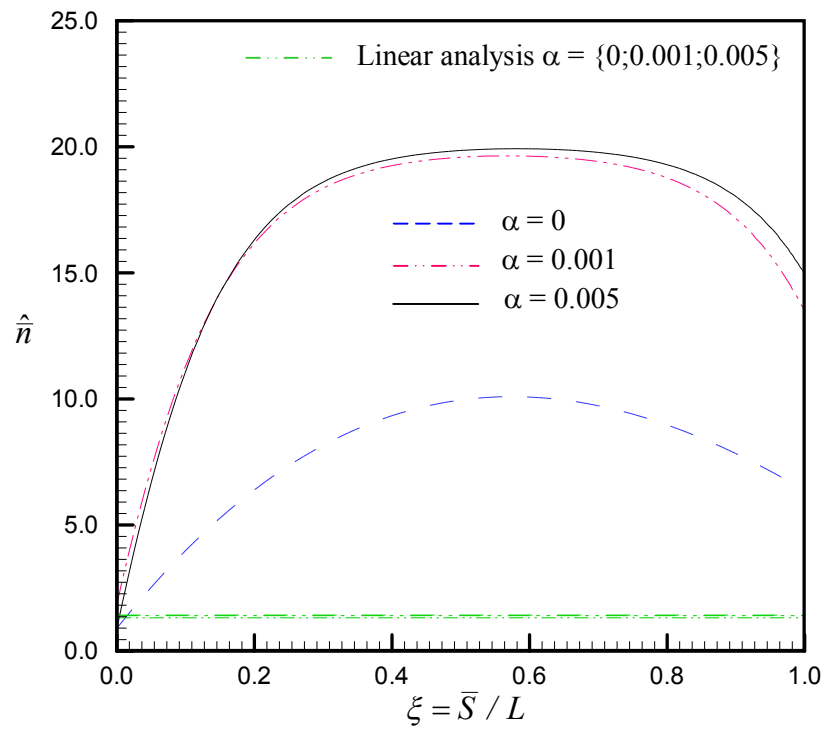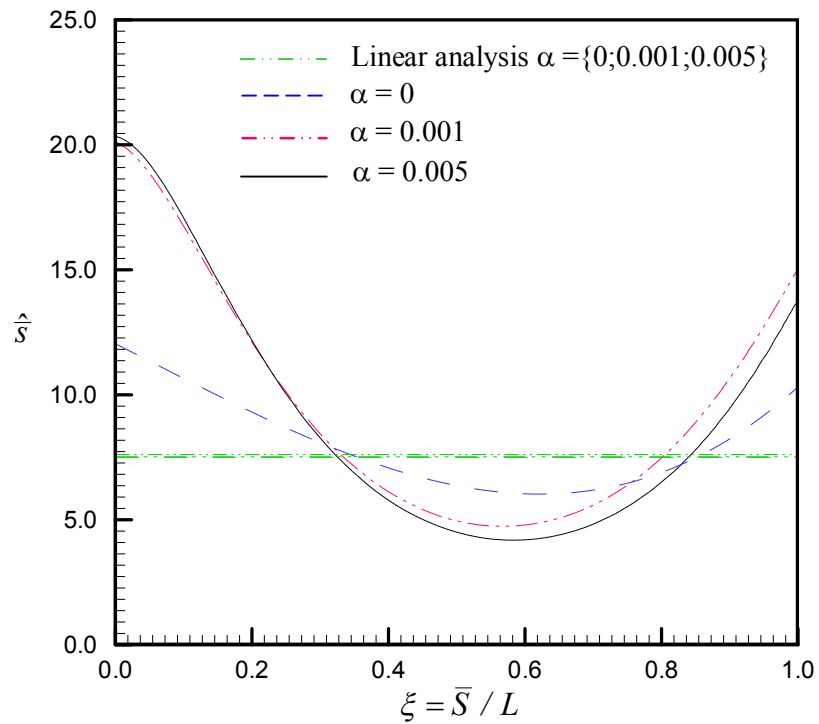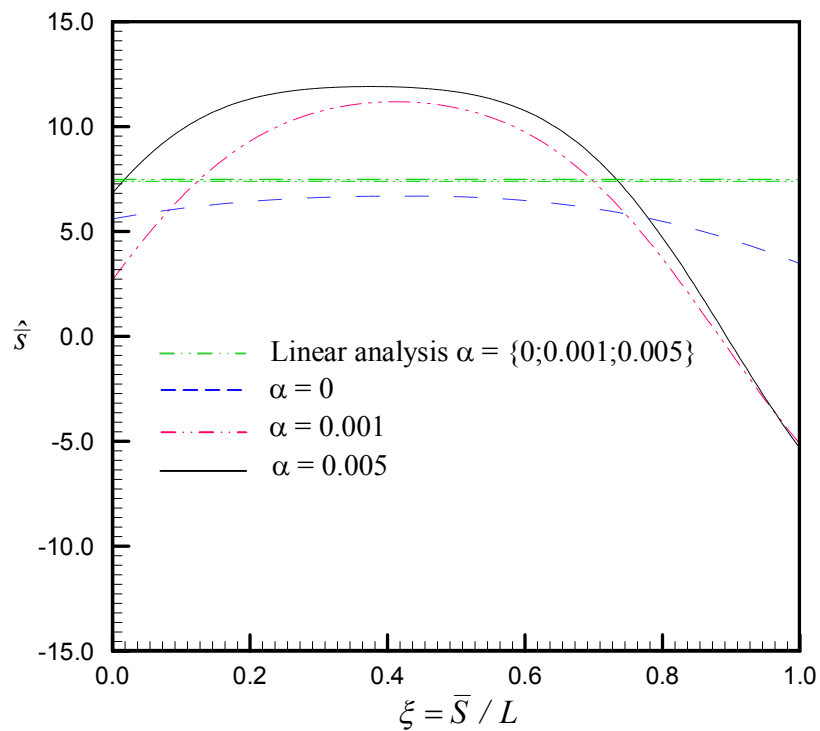

Figure 5.19 Normalized shear force diagram for member CD of one-story portal frame subjected to both horizontal and vertical forces at the top of columns
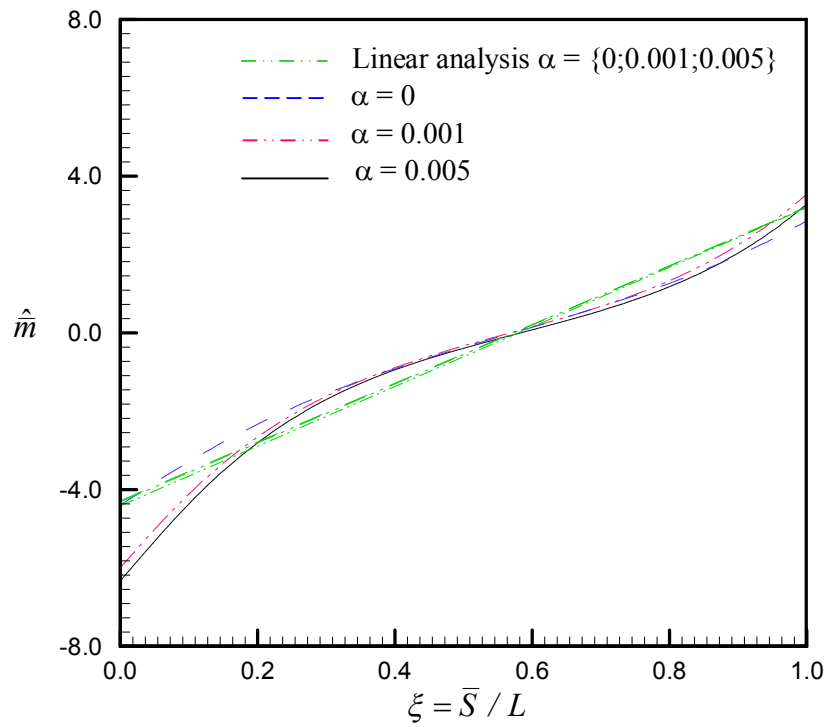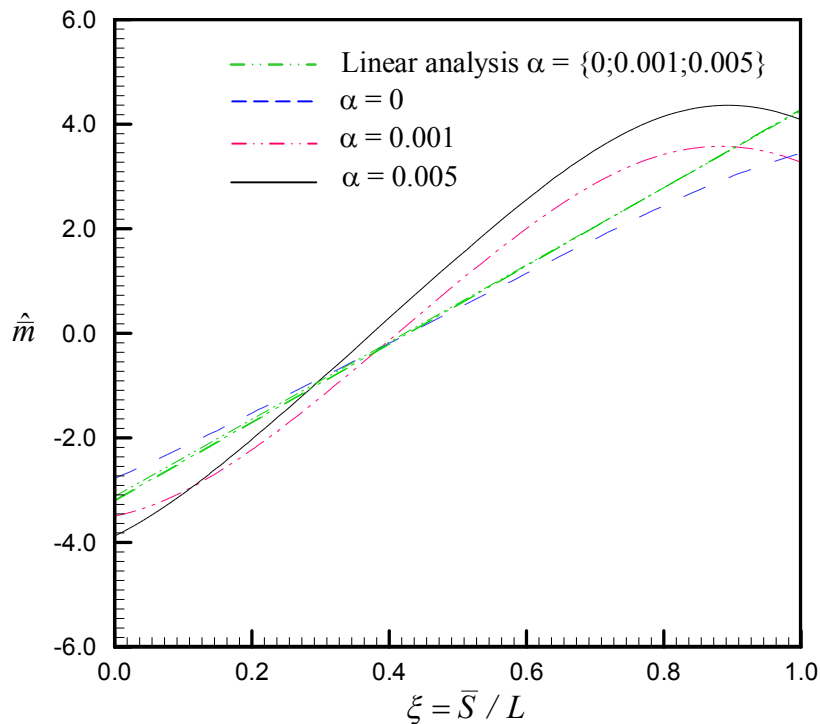
Figure 5.20 Normalized bending moment diagram for member CD of one-story portal frame subjected to both horizontal and vertical forces at the top of columns

5.5 Multi-Story Frame Subjected to Lateral and Vertical Forces

As a final example, let's consider a more complex boundary value problem associated with a multi-story frame subjected to the lateral forces P and vertical forces V as shown in Figure 5.15(a). All columns and beams are assumed prismatic and have the same length L, moment of inertial I, cross sectional area A and Young's modulus E. The base of the frame is fully restrained against both the displacement and rotation. In the analysis, the frame is discretized into only 12 members consisting of eight columns and four beams as shown in Figure 5.15(b).

The deformed shapes of the frame for three values of the extensibility parameter $\alpha = I/AL^2 \in \{0, 0.001, 0.005\}$ and a fixed level of applied loads $\hat{V} = 0.1$ and $\hat{P} = 2$ are shown in Figure 5.16. Results are shown at all nodes and certain points within the member (resulting from the post-process). The magnitude of both the lateral and vertical loads is chosen to be sufficiently large simply to demonstrate the capability of the current technique to accurately model highly geometric nonlinearity. Results for all three cases are compared with those obtained from the FEM and good

agreement between those solutions is observed. In addition, with the high level of applied loads (or, equivalently, structure undergoing large displacement and rotation), the extensibility parameter α significantly affects the deformed shape of the frame. In particular, as α increases, the structure experiences more severe displacement.

(a)   (b)
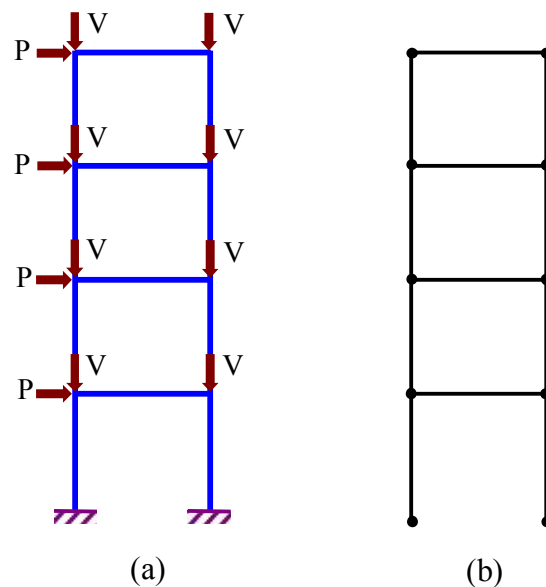
Figure 5.21 (a) Multi-story frame under lateral forces P and vertical forces V and (b) mesh used in the analysis
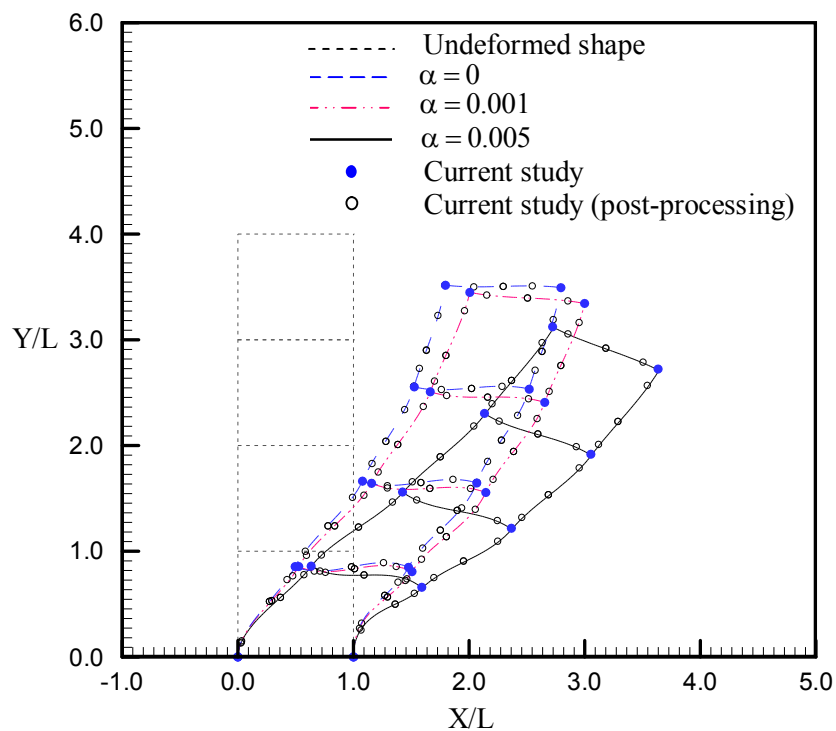
Figure 5.22 Deformed shapes of multi-story frame under lateral and vertical forces

CHAPTER VI

CONCLUSSIONS AND REMARKS

An efficient and accurate semi-analytical technique based upon the co-rotational formulation and the direct stiffness strategy has been developed for the large displacement and rotation analysis of two-dimensional, linearly elastic, extensible frames. The mathematical model has been constructed based on the exact kinematics among the displacement, rotation and curvature. A direct integration technique has been employed to transform a set of governing nonlinear ordinary differential equations into an equivalent set of nonlinear algebraic equations governing the end forces and displacements for a simply-supported member. Essential results for this particular member have been established and used as a basis along with the co-rotational technique to form the force-displacement relation and element tangent stiffness matrix in the local coordinate system. Standard coordinate transformations and the assembly procedure have been adopted to derive the load-displacement relation and the corresponding tangent stiffness matrix for a structure. The crucial features of the proposed technique include that (i) the tangent stiffness matrices are obtained exactly from the exact governing equations; (ii) the residual load vector is evaluated exactly from the exact governing equations; and (iii) the direct stiffness strategy is adopted to treat frames of general geometry and arbitrary nodal loads.

An in-house computer code has been successfully implemented for both single and double curvature members. Standard Gaussian quadrature has been adopted to evaluate all involved integrals and Newton-Raphson method has been used to construct a solution of a system of nonlinear algebraic equations. To verify both the formulation and implementation, extensive numerical experiments for various frame structures have been performed and computed solutions are compared with those obtained from a reliable finite element package. Results from such verification indicate that the proposed technique yields highly accurate numerical solutions; in

particular, such solutions are comparable to the analytical solution without refining the discretization.

Due to the high accuracy of the developed technique and its vast capabilities to treat structures of general geometry, it offers an attractive alternative to be employed in the analysis of two-dimensional frames undergoing large displacement and rotation. In addition, it can also be used to generate accurate benchmark solutions for comparison purposes. As the final remark, the current investigation is still restricted to structures made of linearly elastic materials and this limitation narrows its applications to a class of structures undergoing large deformation beyond the linear regime, e.g. in the collapse and failure analysis under severe loading conditions. Extension of the current technique to incorporate the material nonlinearity and the inertia effect to predict dynamic responses should significantly enhance the modeling capability and, at the same time, poses very challenging research problems.

REFERENCES

Banerjee, A., Bhattacharaya, B., and Mallik, A.K. (2008). Large deflection of cantilever beams with geometric non-linearity: Analytical and numerical approaches. International Journal of Non-Linear Mechanics 43: 366-376.

Chapra, S.C., and Canale, R.P. (1990). Numerical Methods for Engineeers. New York: Mc Graw-Hill.

Chen, L. (2010). An integral approach for large deflection cantilever beams. International Journal of Non-Linear Mechanics 45: 301-305.

Chucheepsakul, S., Srinil, N., and Petchpeart, P. (2003). A variational approach for three-dimensional model of extensible marine cables with specified top tension. Applied Mathematical Modeling 27: 781-803.

Dado, M., Al-Sadder, S., and Abuzeid, O. (2004). Post-buckling behavior of two elastica columns linked with a rotational spring. International Journal of Non-Linear Mechanics 39: 1579-1587.

Dado, M. and Al-Sadder, S. (2006). The elastic spring behavior of a rhombus frame constructed from non-prismatic beams under large deflection. International Journal of Mechanical Sciences 48: 958-968.

Frank Pai, P. (2007). Highly Flexible Structures: Modeling, Computation, and Experimentation. Virginia: AIAA Education Series.

Hamming, R. (1987). Numerical Methods for Scientists and Engineers. New York: Dover Publications.

Henderson, B.W. (1990). Boeing condor raises UAV performance levels. Aviation Week & Space Technology 132(17): 36-38.

Hu, Y.J., Zhu, Y., and Cheng, C.J. (2008). DQEM for large deformation analysis of structure with discontinuity conditions and initial displacements. Engineering Structures 30: 1473-1487.

Klubjaidai, W. and Chucheepsakul, S. (2008). Post-buckling of circular arch elastic subjected to end forces. The 13th National Convention on Civil Engineering 13: STR 164-169.

Lee, K. (2001). Post-buckling of uniform cantilever column under a combined load. International Journal of Non-Linear Mechanics 36: 813-816.

Li, S.-R. and Zhou, Y.-H. (2005). Post-buckling of a hinged-fixed beam under uniformly distributed follower forces. Mechanics Research Communications 32: 359-367.

Madhusudan, B.P., Rajeev, V.R., and Rao, B.N. (2003). Post-buckling of cantilever columns having variable cross section under a combined load. International Journal of Non-Linear Mechanics 38: 1513-1522.

Magnusson, A., Ristinmaa, M., and Ljung, C. (2001). Behavior of the extensible elastic solution. International Journal of Solids and Structures 38: 8441-8457

Mazzilli, C.E.N. (2009). Buckling and post-buckling of extensible rods revisited: A multiple-scale solution. International Journal of Non-Linear Mechanics 44: 200-208.

Ohtsuki, A. and Ellyin, F. (2000). Large deflection analysis of a square frame with rigid joints. Thin-Walled Structures 38: 79-91.

Rao, B. and Rao, G. (1989). Large deflections of a cantilever beam subjected to a rotational distributed loading. Forschung im Ingenieurwesen Bd. 55 Nr. 4

Rungamornrat, J. and Tangnovarad, P. (2011). Analysis of linearly elastic inextensible frames undergoing large displacement and rotation. Journal of Mathematical Problems in Engineering Article in Press.

Saha, S. and Ali, A.R.M. (2009). Thermal buckling and post-buckling characteristics of external slender elastic rods. Journal of Mechanical Engineering 40(1): 1-8.

Sepahi, O., Forouan, M.R., and Malekzadeh, P. (2010). Post-buckling analysis of variable cross-section cantilever beams under combined load via differential quadrature method. KSCE Journal of Civil Engineering 14(2): 207-214.

Sepahi, O., Forouan, M.R., and Malekzadeh, P. (2010). Differential quadrature application in post-buckling analysis of a hinged-fixed elastica under terminal forces and self-weight. Journal of Mechanical Science and Technology 24: 331-336.

Shatarat, N., Al-Sadder, S., Katkhuda, H., Qablan, H., and Shatnawi, A. (2009). Behavior of a rhombus frame of non-linear elastic material under large deflection. International Journal of Mechanical Sciences 51: 166-177.

Shirong, L. and Changjun, C. (2000). Analysis of thermal post-buckling of heated elastic rods. Applied Mathematics and Mechanics 21(2): 133-140.

Shirong, L., Changjun, C., and You, H.Z. (2003). Thermal post-buckling of an elastic beams subjected to a transversely non-uniform temperature rising. Applied Mathematics and Mechanics 24(5): 514-520.

Shvartsman, B.S. (2007). Large deflections of a cantilever beam subjected to a follower force. Journal of sound and vibration 304: 969-973.

Shvartsman, B.S. (2009). Direct method for analysis of flexible cantilever beam subjected to two follower forces. International Journal of Non-linear Mechanics 44: 249-252.

Suwansheewasiri, A. and Chucheepsakul, S. (2004). Buckling and post-buckling analysis of elastic frames under non-follower forces by elliptic integral method. The 9th National Convention on Civil Engineering 9: STR 138-143.

Timoshenko, S.P. (1953). History of Strength of Materials. New York: McGraw-Hill.

Timoshenko, S.P. and Gere, J.M. (1972). Theory of Elastic Stability, 2nd Edition New York: McGraw-Hill.

Vaz, M.A. and Solano, M.A. (2003). Post-buckling analysis of slender elastic rods subjected to uniform thermal loads. Journal of Thermal Stresses 26: 847-860.

Wang, C.Y. (1997). Post-buckling of a clamped-simply supported elastica. International Journal of Non-Linear Mechanics 32: 1115-1122.

Wang, J., Chen, J.K., and Liao, S. (2008). An explicit solution of the large deformation of a cantilever beam under point load at the free tip. Journal of Computational and Applied Mathematics 212: 320-330.

APPENDICES

APPENDIX A

The matrices $\partial\Gamma_y/\partial\boldsymbol{f}^{p*}, \partial\Gamma_y/\partial\hat{f}_y$ and $\partial\Gamma_y/\partial\boldsymbol{u}^*$ on the right hand side of equations (3.33) can be expresses as

$$\frac{\partial\Gamma_y}{\partial\boldsymbol{f}^{p*}} = \begin{bmatrix} \dfrac{\partial\Gamma_y}{\partial\hat{f}_{x2}^*} & \dfrac{\partial\Gamma_y}{\partial\hat{m}_1^*} & \dfrac{\partial\Gamma_y}{\partial\hat{m}_2^*} \end{bmatrix} \quad ; \quad \frac{\partial\Gamma_y}{\partial\boldsymbol{u}^*} = \begin{bmatrix} \dfrac{\partial\Gamma_y}{\partial\hat{u}_2^*} & \dfrac{\partial\Gamma_y}{\partial\theta_1^*} & \dfrac{\partial\Gamma_y}{\partial\theta_2^*} \end{bmatrix} \tag{A.1}$$

Similarly, the matrices $\partial\Gamma/\partial\boldsymbol{f}^{p*}$, $\partial\Gamma/\partial\hat{f}_y$ and $\partial\Gamma/\partial\boldsymbol{u}^*$ on the equations (3.34) can be expresses as

$$\frac{\partial\Gamma}{\partial\boldsymbol{f}^{p*}} = \begin{bmatrix} \dfrac{\partial\Gamma_1}{\partial\hat{f}_{x2}^*} & \dfrac{\partial\Gamma_1}{\partial\hat{m}_1^*} & \dfrac{\partial\Gamma_1}{\partial\hat{m}_2^*} \\[2ex] \dfrac{\partial\Gamma_2}{\partial\hat{f}_{x2}^*} & \dfrac{\partial\Gamma_2}{\partial\hat{m}_1^*} & \dfrac{\partial\Gamma_2}{\partial\hat{m}_2^*} \\[2ex] \dfrac{\partial\Gamma_3}{\partial\hat{f}_{x2}^*} & \dfrac{\partial\Gamma_3}{\partial\hat{m}_1^*} & \dfrac{\partial\Gamma_3}{\partial\hat{m}_2^*} \end{bmatrix} \tag{A.2}$$

$$\frac{\partial\Gamma}{\partial\hat{f}_y} = \begin{bmatrix} \dfrac{\partial\Gamma_1}{\partial\hat{f}_y} & \dfrac{\partial\Gamma_2}{\partial\hat{f}_y} & \dfrac{\partial\Gamma_3}{\partial\hat{f}_y} \end{bmatrix}^T \tag{A.3}$$

$$\frac{\partial\Gamma}{\partial\boldsymbol{u}^*} = \begin{bmatrix} \dfrac{\partial\Gamma_1}{\partial\hat{u}_2^*} & \dfrac{\partial\Gamma_1}{\partial\theta_1^*} & \dfrac{\partial\Gamma_1}{\partial\theta_2^*} \\[2ex] \dfrac{\partial\Gamma_2}{\partial\hat{u}_2^*} & \dfrac{\partial\Gamma_2}{\partial\theta_1^*} & \dfrac{\partial\Gamma_2}{\partial\theta_2^*} \\[2ex] \dfrac{\partial\Gamma_3}{\partial\hat{u}_2^*} & \dfrac{\partial\Gamma_3}{\partial\theta_1^*} & \dfrac{\partial\Gamma_3}{\partial\theta_2^*} \end{bmatrix} \tag{A.4}$$

All entries appearing in (A.1)-(A.4) are given explicitly by

$$\frac{\partial\Gamma_y}{\partial\hat{f}_{x2}^*} = A_1 \tag{A.5}$$

$$\frac{\partial \Gamma_y}{\partial \hat{m}_1^*} = -2\hat{m}_1^* \tag{A.6}$$

$$\frac{\partial \Gamma_y}{\partial \hat{m}_2^*} = 2\hat{m}_2^* \tag{A.7}$$

$$\frac{\partial \Gamma_y}{\partial \theta_1^*} = C_1 \tag{A.8}$$

$$\frac{\partial \Gamma_y}{\partial \theta_2^*} = C_2 \tag{A.9}$$

$$\frac{\partial \Gamma_y}{\partial f_y} = B_1 \tag{A.10}$$

$$\frac{\partial \Gamma_1}{\partial \hat{f}_{x2}^*} = -\psi \frac{1}{2} \int_{\theta_1^*}^{\theta_2^*} A F^3 d\theta \tag{A.11}$$

$$\frac{\partial \Gamma_2}{\partial \hat{f}_{x2}^*} = \psi \int_{\theta_1^*}^{\theta_2^*} (\alpha \cos\theta \sin\theta) F - \frac{(1+\varepsilon_0)\sin\theta}{2} A F^3 d\theta \tag{A.12}$$

$$\frac{\partial \Gamma_3}{\partial \hat{f}_{x2}^*} = \psi \int_{\theta_1^*}^{\theta_2^*} (\alpha \cos^2\theta) F - \frac{\left[(1+\varepsilon_0)\cos\theta - 1\right]}{2} A F^3 d\theta \tag{A.13}$$

$$\frac{\partial \Gamma_1}{\partial \hat{m}_2^*} = -\psi \int_{\theta_1^*}^{\theta_2^*} F^3 \hat{m}_2^* d\theta \tag{A.14}$$

$$\frac{\partial \Gamma_2}{\partial \hat{m}_2^*} = -\psi \int_{\theta_1^*}^{\theta_2^*} \left[\sin\theta(1+\varepsilon_0)\right] F^3 \hat{m}_2^* d\theta \tag{A.15}$$

$$\frac{\partial \Gamma_3}{\partial \hat{m}_2^*} = -\psi \int_{\theta_1^*}^{\theta_2^*} \left[\cos\theta(1+\varepsilon_0) - 1\right] F^3 \hat{m}_2^* d\theta \tag{A.16}$$

$$\frac{\partial \Gamma_1}{\partial \hat{f}_y} = \frac{1}{2}\psi \int_{\theta_1^*}^{\theta_2^*} B F^3 d\theta \tag{A.17}$$

$$\frac{\partial \Gamma_2}{\partial \hat{f}_y} = \psi \int_{\theta_1^*}^{\theta_2^*} F + \frac{(1+\varepsilon_0)\sin\theta}{2} BF^3 d\theta \tag{A.18}$$

$$\frac{\partial \Gamma_3}{\partial \hat{f}_y} = \psi \int_{\theta_1^*}^{\theta_2^*} (-\alpha \sin\theta \cos\theta) F + \frac{\left[(1+\varepsilon_0)\cos\theta - 1\right]}{2} BF^3 d\theta \tag{A.19}$$

$$\frac{\partial \Gamma_3}{\partial \hat{u}_2^*} = -1 \tag{A.20}$$

$$\frac{\partial \Gamma_1}{\partial \theta_1^*} = -\psi F_1 \tag{A.21}$$

$$\frac{\partial \Gamma_2}{\partial \theta_1^*} = -\psi F_1 (1+\varepsilon_1)\sin\theta_1^* \tag{A.22}$$

$$\frac{\partial \Gamma_3}{\partial \theta_1^*} = -\psi \left[(1+\varepsilon_1)\cos\theta_1^* - 1\right] F_1 \tag{A.23}$$

$$\frac{\partial \Gamma_1}{\partial \theta_2^*} = \psi \frac{1}{\hat{m}_2^*} \tag{A.24}$$

$$\frac{\partial \Gamma_2}{\partial \theta_2^*} = \psi \frac{(1+\varepsilon_2)\sin\theta_2^*}{\hat{m}_2^*} \tag{A.25}$$

$$\frac{\partial \Gamma_3}{\partial \theta_2^*} = \psi \frac{\left[(1+\varepsilon_2)\cos\theta_2^* - 1\right]}{\hat{m}_2^*} \tag{A.26}$$

$$\frac{\partial \hat{f}_y}{\partial \hat{u}_2^*} = \frac{\partial \Gamma_1}{\partial \hat{m}_1^*} = \frac{\partial \Gamma_2}{\partial \hat{m}_1^*} = \frac{\partial \Gamma_3}{\partial \hat{m}_1^*} = \frac{\partial \Gamma_1}{\partial \hat{u}_2^*} = \frac{\partial \Gamma_2}{\partial \hat{u}_2^*} = 0 \tag{A.27}$$

Where the functions F, F_1, A, A_1, B, B_1, C_1, C_2, ε_0, ε_1 and ε_2 are given by

$$F = \frac{1}{\sqrt{i+\alpha j}} \tag{A.28}$$

$$i = \hat{m}_2^{2*} + 2\hat{f}_{x2}^* (\cos\theta_2^* - \cos\theta) - 2\hat{f}_y (\sin\theta_2^* - \sin\theta) \tag{A.29}$$

$$j = \frac{1}{2}\left(\hat{f}_{x2}^{*2} - \hat{f}_y^2\right)(\cos 2\theta_2^* - \cos 2\theta) - \hat{f}_{x2}^* \hat{f}_y (\sin 2\theta_2^* - \sin 2\theta) \tag{A.30}$$

$$F_1 = \frac{1}{\sqrt{i_1 + \alpha j_1}} \tag{A.31}$$

$$i_1 = \hat{m}_2^{2*} + 2\hat{f}_{x2}^* \left(\cos\theta_2^* - \cos\theta_1^*\right) - 2\hat{f}_y \left(\sin\theta_2^* - \sin\theta_1^*\right) \tag{A.32}$$

$$j_1 = \frac{1}{2}\left(\hat{f}_{x2}^{*2} - \hat{f}_y^2\right)\left(\cos 2\theta_2^* - \cos 2\theta_1^*\right) - \hat{f}_{x2}^*\hat{f}_y\left(\sin 2\theta_2^* - \sin 2\theta_1^*\right) \tag{A.33}$$

$$A = 2\left(\cos\theta_2^* - \cos\theta\right) + \alpha\left[\hat{f}_{x2}^*\left(\cos 2\theta_2^* - \cos 2\theta\right) - \hat{f}_y\left(\sin 2\theta_2^* - \sin 2\theta\right)\right] \tag{A.34}$$

$$A_1 = 2\left(\cos\theta_2^* - \cos\theta_1^*\right) + \alpha\left[\hat{f}_{x2}^*\left(\cos 2\theta_2^* - \cos 2\theta_1^*\right) - \hat{f}_y\left(\sin 2\theta_2^* - \sin 2\theta_1^*\right)\right] \tag{A.35}$$

$$B = 2\left(\sin\theta_2^* - \sin\theta\right) + \alpha\left[\hat{f}_y\left(\cos 2\theta_2^* - \cos 2\theta\right) + \hat{f}_{x2}^*\left(\sin 2\theta_2^* - \sin 2\theta\right)\right] \tag{A.36}$$

$$B_1 = 2\left(\sin\theta_2^* - \sin\theta_1^*\right) + \alpha\left[\hat{f}_y\left(\cos 2\theta_2^* - \cos 2\theta_1^*\right) + \hat{f}_{x2}^*\left(\sin 2\theta_2^* - \sin 2\theta_1^*\right)\right] \tag{A.37}$$

$$C_1 = 2\hat{f}_{x2}^*\sin\theta_1^* + 2\hat{f}_y\cos\theta_1^* + \alpha\left[\left(\hat{f}_{x2}^{*2} - \hat{f}_y^2\right)\sin 2\theta_1^* + 2\hat{f}_{x2}^*\hat{f}_y\cos 2\theta_1^*\right] \tag{A.38}$$

$$C_2 = 2\hat{f}_{x2}^*\sin\theta_2^* + 2\hat{f}_y\cos\theta_2^* + \alpha\left[\left(\hat{f}_{x2}^{*2} - \hat{f}_y^2\right)\sin 2\theta_2^* + 2\hat{f}_{x2}^*\hat{f}_y\cos 2\theta_2^*\right] \tag{A.39}$$

$$\varepsilon_0 = \alpha\left(\hat{f}_{x2}^*\cos\theta - \hat{f}_y\sin\theta\right) \tag{A.40}$$

$$\varepsilon_1 = \alpha\left(\hat{f}_{x2}^*\cos\theta_1^* - \hat{f}_y\sin\theta_1^*\right) \tag{A.41}$$

$$\varepsilon_2 = \alpha\left(\hat{f}_{x2}^*\cos\theta_2^* - \hat{f}_y\sin\theta_2^*\right) \tag{A.42}$$

APPENDIX B

The entries of matrices $\partial\bar{\boldsymbol{\Gamma}}_{yz}/\partial\boldsymbol{a}$, $\partial\bar{\boldsymbol{\Gamma}}_{yz}/\partial\boldsymbol{f}^{\mathrm{p}*}$ and $\partial\bar{\boldsymbol{\Gamma}}_{yz}/\partial\boldsymbol{u}^{\mathrm{p}*}$ from equations (3.54) can be expresses as

$$
\frac{\partial\bar{\boldsymbol{\Gamma}}_{yz}}{\partial\boldsymbol{a}} =
\begin{bmatrix}
\dfrac{\partial\bar{\Gamma}_{y}}{\partial\hat{f}_{y}} & \dfrac{\partial\bar{\Gamma}_{y}}{\partial\theta_{z}} \\[3mm]
\dfrac{\partial\bar{\Gamma}_{z}}{\partial\hat{f}_{y}} & \dfrac{\partial\bar{\Gamma}_{z}}{\partial\theta_{z}}
\end{bmatrix}
\tag{B.1}
$$

$$
\frac{\partial\bar{\boldsymbol{\Gamma}}_{yz}}{\partial\boldsymbol{f}^{\mathrm{p}*}} =
\begin{bmatrix}
\dfrac{\partial\bar{\Gamma}_{y}}{\partial\hat{f}_{x2}^{*}} & \dfrac{\partial\bar{\Gamma}_{y}}{\partial\hat{m}_{1}^{*}} & \dfrac{\partial\bar{\Gamma}_{y}}{\partial\hat{m}_{2}^{*}} \\[3mm]
\dfrac{\partial\bar{\Gamma}_{z}}{\partial\hat{f}_{x2}^{*}} & \dfrac{\partial\bar{\Gamma}_{z}}{\partial\hat{m}_{1}^{*}} & \dfrac{\partial\bar{\Gamma}_{z}}{\partial\hat{m}_{2}^{*}}
\end{bmatrix}
\tag{B.2}
$$

$$
\frac{\partial\bar{\boldsymbol{\Gamma}}_{yz}}{\partial\boldsymbol{u}^{\mathrm{p}*}} =
\begin{bmatrix}
\dfrac{\partial\bar{\Gamma}_{y}}{\partial\hat{u}_{2}^{*}} & \dfrac{\partial\bar{\Gamma}_{y}}{\partial\theta_{1}^{*}} & \dfrac{\partial\bar{\Gamma}_{y}}{\partial\theta_{2}^{*}} \\[3mm]
\dfrac{\partial\bar{\Gamma}_{z}}{\partial\hat{u}_{2}^{*}} & \dfrac{\partial\bar{\Gamma}_{z}}{\partial\theta_{1}^{*}} & \dfrac{\partial\bar{\Gamma}_{z}}{\partial\theta_{2}^{*}}
\end{bmatrix}
\tag{B.3}
$$

Similarly, the matrices $\partial\bar{\boldsymbol{\Gamma}}/\partial\boldsymbol{f}^{\mathrm{p}*}$, $\partial\bar{\boldsymbol{\Gamma}}/\partial\boldsymbol{a}$, $\partial\bar{\boldsymbol{\Gamma}}/\partial\boldsymbol{\Phi}$, $\partial\boldsymbol{\Phi}/\partial\theta_{z}$, $\partial\bar{\boldsymbol{\Gamma}}/\partial\boldsymbol{u}^{*}$ and $\partial\boldsymbol{\Phi}/\partial\boldsymbol{u}^{*}$ on the equations (3.58) can be expresses as

$$
\frac{\partial\bar{\boldsymbol{\Gamma}}}{\partial\boldsymbol{f}^{\mathrm{p}*}} =
\begin{bmatrix}
\dfrac{\partial\bar{\Gamma}_{1}}{\partial\hat{f}_{x2}^{*}} & \dfrac{\partial\bar{\Gamma}_{1}}{\partial\hat{m}_{1}^{*}} & \dfrac{\partial\bar{\Gamma}_{1}}{\partial\hat{m}_{2}^{*}} \\[3mm]
\dfrac{\partial\bar{\Gamma}_{2}}{\partial\hat{f}_{x2}^{*}} & \dfrac{\partial\bar{\Gamma}_{2}}{\partial\hat{m}_{1}^{*}} & \dfrac{\partial\bar{\Gamma}_{2}}{\partial\hat{m}_{2}^{*}} \\[3mm]
\dfrac{\partial\bar{\Gamma}_{3}}{\partial\hat{f}_{x2}^{*}} & \dfrac{\partial\bar{\Gamma}_{3}}{\partial\hat{m}_{1}^{*}} & \dfrac{\partial\bar{\Gamma}_{3}}{\partial\hat{m}_{2}^{*}}
\end{bmatrix}
\tag{B.4}
$$

$$\frac{\partial \overline{\mathbf{\Gamma}}}{\partial \boldsymbol{a}} = \begin{bmatrix} \dfrac{\partial \overline{\Gamma}_1}{\partial \hat{f}_y} & \dfrac{\partial \overline{\Gamma}_2}{\partial \hat{f}_y} & \dfrac{\partial \overline{\Gamma}_3}{\partial \hat{f}_y} \\[3mm] \dfrac{\partial \overline{\Gamma}_1}{\partial \theta_z} & \dfrac{\partial \overline{\Gamma}_2}{\partial \theta_z} & \dfrac{\partial \overline{\Gamma}_3}{\partial \theta_z} \end{bmatrix}^{T} \tag{B.5}$$

$$\frac{\partial \overline{\mathbf{\Gamma}}}{\partial \boldsymbol{\Phi}} = \begin{bmatrix} \dfrac{\partial \overline{\Gamma}_1}{\partial \phi_1} & \dfrac{\partial \overline{\Gamma}_2}{\partial \phi_1} & \dfrac{\partial \overline{\Gamma}_3}{\partial \phi_1} \\[3mm] \dfrac{\partial \overline{\Gamma}_1}{\partial \phi_2} & \dfrac{\partial \overline{\Gamma}_2}{\partial \phi_2} & \dfrac{\partial \overline{\Gamma}_2}{\partial \phi_2} \end{bmatrix}^{T} \tag{B.6}$$

$$\frac{\partial \boldsymbol{\Phi}}{\partial \theta_z} = \begin{bmatrix} \dfrac{\partial \phi_1}{\partial \theta_z} & \dfrac{\partial \phi_2}{\partial \theta_z} \end{bmatrix}^{T} \tag{B.7}$$

$$\frac{\partial \overline{\mathbf{\Gamma}}}{\partial \boldsymbol{u}^{*}} = \begin{bmatrix} \dfrac{\partial \overline{\Gamma}_1}{\partial \hat{u}_2^{*}} & \dfrac{\partial \overline{\Gamma}_1}{\partial \theta_1^{*}} & \dfrac{\partial \overline{\Gamma}_1}{\partial \theta_2^{*}} \\[3mm] \dfrac{\partial \overline{\Gamma}_2}{\partial \hat{u}_2^{*}} & \dfrac{\partial \overline{\Gamma}_2}{\partial \theta_1^{*}} & \dfrac{\partial \overline{\Gamma}_2}{\partial \theta_2^{*}} \\[3mm] \dfrac{\partial \overline{\Gamma}_3}{\partial \hat{u}_2^{*}} & \dfrac{\partial \overline{\Gamma}_3}{\partial \theta_1^{*}} & \dfrac{\partial \overline{\Gamma}_3}{\partial \theta_2^{*}} \end{bmatrix} \tag{B.8}$$

$$\frac{\partial \boldsymbol{\Phi}}{\partial \boldsymbol{u}^{p*}} = \begin{bmatrix} \dfrac{\partial \phi_1}{\partial \hat{u}_2^{*}} & \dfrac{\partial \phi_1}{\partial \theta_1^{*}} & \dfrac{\partial \phi_1}{\partial \theta_2^{*}} \\[3mm] \dfrac{\partial \phi_2}{\partial \hat{u}_2^{*}} & \dfrac{\partial \phi_2}{\partial \theta_1^{*}} & \dfrac{\partial \phi_2}{\partial \theta_2^{*}} \end{bmatrix} \tag{B.9}$$

All entries appearing in (B.1)-(B.9) are given explicitly by

$$\frac{\partial \overline{\Gamma}_y}{\partial \hat{f}_{x2}^{*}} = \overline{\mathrm{A}}_1 \tag{B.10}$$

$$\frac{\partial \overline{\Gamma}_z}{\partial \hat{f}_{x2}^{*}} = \overline{\mathrm{A}}_2 \tag{B.11}$$

$$\frac{\partial \overline{\Gamma}_y}{\partial \hat{m}_1^{*}} = -2\hat{m}_1^{*} \tag{B.12}$$

$$\frac{\partial \overline{\Gamma}_z}{\partial \hat{m}_2^*} = -2\hat{m}_2^* \tag{B.13}$$

$$\frac{\partial \overline{\Gamma}_y}{\partial \theta_1^*} = \overline{C}_1 \tag{B.14}$$

$$\frac{\partial \overline{\Gamma}_z}{\partial \theta_2^*} = \overline{C}_2 \tag{B.15}$$

$$\frac{\partial \overline{\Gamma}_y}{\partial \hat{f}_y} = \overline{B}_1 \tag{B.16}$$

$$\frac{\partial \overline{\Gamma}_z}{\partial \hat{f}_y} = \overline{B}_2 \tag{B.17}$$

$$\frac{\partial \overline{\Gamma}_y}{\partial \theta_z} = \frac{\partial \overline{\Gamma}_z}{\partial \theta_z} = \overline{C}_z \tag{B.18}$$

$$\frac{\partial \overline{\Gamma}_1}{\partial \hat{f}_{x2}^*} = -\frac{1}{2}\psi \int_0^{\phi_1} \frac{\psi 2\phi \overline{D}}{\sqrt{\overline{H}^3}}\, d\phi - \frac{1}{2}\psi \int_0^{\phi_2} \frac{\psi 2\phi \overline{D}}{\sqrt{\overline{H}^3}}\, d\phi \tag{B.19}$$

$$\frac{\partial \overline{\Gamma}_2}{\partial \hat{f}_{x2}^*} = +\psi \int_0^{\phi_1} \frac{\psi 2\phi\left(\alpha \sin\Theta \cos\Theta\right)}{\sqrt{\overline{H}}} - \frac{\psi 2\phi\left[\sin\Theta\left(1+\overline{\varepsilon}_0\right)\right]\overline{D}}{2\sqrt{\overline{H}^3}}\, d\phi$$
$$+\psi \int_0^{\phi_2} \frac{\psi 2\phi\left(\alpha \sin\Theta \cos\Theta\right)}{\sqrt{\overline{H}}} - \frac{\psi 2\phi\left[\sin\Theta\left(1+\overline{\varepsilon}_0\right)\right]\overline{D}}{2\sqrt{\overline{H}^3}}\, d\phi \tag{B.20}$$

$$\frac{\partial \overline{\Gamma}_3}{\partial \hat{f}_{x2}^*} = +\psi \int_0^{\phi_1} \frac{\psi 2\phi\left(\alpha \cos^2\Theta\right)}{\sqrt{\overline{H}}} - \frac{\psi 2\phi\left[\cos\Theta\left(1+\overline{\varepsilon}_0\right)-1\right]\overline{D}}{2\sqrt{\overline{H}^3}}\, d\phi$$
$$+\psi \int_0^{\phi_2} \frac{\psi 2\phi\left(\alpha \cos^2\Theta\right)}{\sqrt{\overline{H}}} - \frac{\psi 2\phi\left[\cos\Theta\left(1+\overline{\varepsilon}_0\right)-1\right]\overline{D}}{2\sqrt{\overline{H}^3}}\, d\phi \tag{B.21}$$

$$\frac{\partial \overline{\Gamma}_1}{\partial \hat{f}_y} = +\frac{1}{2}\psi \int_0^{\phi_1} \frac{\psi 2\phi \overline{E}}{\sqrt{\overline{H}^3}}\, d\phi + \frac{1}{2}\psi \int_0^{\phi_2} \frac{\psi 2\phi \overline{E}}{\sqrt{\overline{H}^3}}\, d\phi \tag{B.22}$$

$$\frac{\partial \overline{\Gamma}_2}{\partial \hat{f}_y} = +\psi \int_0^{\phi_1} \frac{-\psi 2\phi \left(\alpha \sin^2 \Theta \right)}{\sqrt{\overline{H}}} + \frac{\psi 2\phi \left[\sin \Theta \left(1 + \overline{\varepsilon}_0 \right) \right] \overline{E}}{2\sqrt{\overline{H}^3}} d\phi$$
$$+ \psi \int_0^{\phi_2} \frac{-\psi 2\phi \left(\alpha \sin^2 \Theta \right)}{\sqrt{\overline{H}}} + \frac{\psi 2\phi \left[\sin \Theta \left(1 + \overline{\varepsilon}_0 \right) \right] \overline{E}}{2\sqrt{\overline{H}^3}} d\phi \qquad (B.23)$$

$$\frac{\partial \overline{\Gamma}_3}{\partial \hat{f}_y} = +\psi \int_0^{\phi_1} \frac{-\psi 2\phi \left(\alpha \sin \Theta \cos \Theta \right)}{\sqrt{\overline{H}}} + \frac{\psi 2\phi \left[\cos \Theta \left(1 + \overline{\varepsilon}_0 \right) - 1 \right] \overline{E}}{2\sqrt{\overline{H}^3}} d\phi$$
$$+ \psi \int_0^{\phi_2} \frac{-\psi 2\phi \left(\alpha \sin \Theta \cos \Theta \right)}{\sqrt{\overline{H}}} + \frac{\psi 2\phi \left[\cos \Theta \left(1 + \overline{\varepsilon}_0 \right) - 1 \right] \overline{E}}{2\sqrt{\overline{H}^3}} d\phi \qquad (B.24)$$

$$\frac{\partial \overline{\Gamma}_1}{\partial \theta_z} = -\frac{1}{2} \psi \int_0^{\phi_1} \frac{\psi 2\phi \overline{L}}{\sqrt{\overline{H}^3}} d\phi - \frac{1}{2} \psi \int_0^{\phi_2} \frac{\psi 2\phi \overline{L}}{\sqrt{\overline{H}^3}} d\phi \qquad (B.25)$$

$$\frac{\partial \overline{\Gamma}_2}{\partial \theta_z} = +\psi \int_0^{\phi_1} \frac{\overline{M}}{\sqrt{\overline{H}}} - \frac{\psi 2\phi \left[\sin \Theta \left(1 + \overline{\varepsilon}_0 \right) \right] \overline{L}}{2\sqrt{\overline{H}^3}} d\phi$$
$$+ \psi \int_0^{\phi_2} \frac{\overline{M}}{\sqrt{\overline{H}}} - \frac{\psi 2\phi \left[\sin \Theta \left(1 + \overline{\varepsilon}_0 \right) \right] \overline{L}}{2\sqrt{\overline{H}^3}} d\phi \qquad (B.26)$$

$$\frac{\partial \overline{\Gamma}_3}{\partial \theta_z} = +\psi \int_0^{\phi_1} \frac{\overline{N}}{\sqrt{\overline{H}}} - \frac{\psi 2\phi \left[\cos \Theta \left(1 + \overline{\varepsilon}_0 \right) - 1 \right] \overline{L}}{2\sqrt{\overline{H}^3}} d\phi$$
$$+ \psi \int_0^{\phi_2} \frac{\overline{N}}{\sqrt{\overline{H}}} - \frac{\psi 2\phi \left[\cos \Theta \left(1 + \overline{\varepsilon}_0 \right) - 1 \right] \overline{L}}{2\sqrt{\overline{H}^3}} d\phi \qquad (B.27)$$

$$\frac{\partial \overline{\Gamma}_1}{\partial \phi_1} = \frac{2\phi_1}{\sqrt{\overline{H}_1}} \qquad (B.28)$$

$$\frac{\partial \overline{\Gamma}_2}{\partial \phi_1} = \frac{2\phi_1 \left[\sin \Theta_1 \left(1 + \overline{\varepsilon}_1 \right) \right]}{\sqrt{\overline{H}_1}} \qquad (B.39)$$

$$\frac{\partial \overline{\Gamma}_3}{\partial \phi_1} = \frac{2\phi_1 \left[\cos \Theta_1 \left(1 + \overline{\varepsilon}_1 \right) - 1 \right]}{\sqrt{\overline{H}_1}} \qquad (B.30)$$

$$\frac{\partial \overline{\Gamma}_1}{\partial \phi_2} = \frac{2\phi_2}{\sqrt{\overline{H}_2}} \tag{B.31}$$

$$\frac{\partial \overline{\Gamma}_2}{\partial \phi_2} = \frac{2\phi_2 \left[\sin \Theta_2 \left(1 + \overline{\varepsilon}_2 \right) \right]}{\sqrt{\overline{H}_2}} \tag{B.32}$$

$$\frac{\partial \overline{\Gamma}_3}{\partial \phi_2} = \frac{2\phi_2 \left[\cos \Theta_2 \left(1 + \overline{\varepsilon}_2 \right) - 1 \right]}{\sqrt{\overline{H}_2}} \tag{B.33}$$

$$\frac{\partial \phi_1}{\partial \theta_z} = -\psi \frac{1}{2\sqrt{(\theta_1 - \theta_z)\psi}} \tag{B.34}$$

$$\frac{\partial \phi_2}{\partial \theta_z} = -\psi \frac{1}{2\sqrt{(\theta_2 - \theta_z)\psi}} \tag{B.35}$$

$$\frac{\partial \overline{\Gamma}_3}{\partial \hat{u}_2^*} = -1 \tag{B.36}$$

$$\frac{\partial \phi_1}{\partial \theta_1^*} = +\psi \frac{1}{2\sqrt{(\theta_1 - \theta_z)\psi}} \tag{B.37}$$

$$\frac{\partial \phi_2}{\partial \theta_2^*} = +\psi \frac{1}{2\sqrt{(\theta_2 - \theta_z)\psi}} \tag{B.38}$$

$$\frac{\partial \overline{\Gamma}_z}{\partial \hat{m}_1^*} = \frac{\partial \overline{\Gamma}_y}{\partial \hat{m}_2^*} = \frac{\partial \overline{\Gamma}_z}{\partial \theta_1^*} = \frac{\partial \overline{\Gamma}_y}{\partial \theta_2^*} 0 \tag{B.19}$$

$$\frac{\partial \overline{\Gamma}_1}{\partial \hat{u}_2^*} = \frac{\partial \overline{\Gamma}_2}{\partial \hat{u}_2^*} = \frac{\partial \overline{\Gamma}_y}{\partial \hat{u}_2^*} = \frac{\partial \overline{\Gamma}_z}{\partial \hat{u}_2^*} = \frac{\partial \overline{\Gamma}_1}{\partial \hat{m}_1^*} = \frac{\partial \overline{\Gamma}_2}{\partial \hat{m}_1^*} = \frac{\partial \overline{\Gamma}_3}{\partial \hat{m}_1^*} = \frac{\partial \overline{\Gamma}_1}{\partial \hat{m}_2^*} = \frac{\partial \overline{\Gamma}_2}{\partial \hat{m}_2^*} = \frac{\partial \overline{\Gamma}_3}{\partial \hat{m}_2^*} = 0 \tag{B.40}$$

$$\frac{\partial \overline{\Gamma}_1}{\partial \theta_1^*} = \frac{\partial \overline{\Gamma}_2}{\partial \theta_1^*} = \frac{\partial \overline{\Gamma}_3}{\partial \theta_1^*} = \frac{\partial \overline{\Gamma}_1}{\partial \theta_2^*} = \frac{\partial \overline{\Gamma}_2}{\partial \theta_2^*} = \frac{\partial \overline{\Gamma}_3}{\partial \theta_2^*} = \frac{\partial \phi_1}{\partial \hat{u}_2^*} = \frac{\partial \phi_2}{\partial \hat{u}_2^*} = \frac{\partial \phi_1}{\partial \theta_2^*} = \frac{\partial \phi_2}{\partial \theta_1^*} = 0 \tag{B.41}$$

Where the functions $\Theta, \Theta_1, \Theta_2, \overline{H}, \overline{H}_1, \overline{H}_2, \overline{A}_1, \overline{A}_2\ B_1,\ \ \overline{B}_2, \overline{C}_1, \overline{C}_2, \overline{C}_z, \overline{D}, \overline{E}, \overline{L}, \overline{M},$ $\overline{N}, \overline{\varepsilon}_0, \overline{\varepsilon}_1$ and $\overline{\varepsilon}_2$ are given by

$$\Theta = \left(\psi\phi^2 + \theta_z\right), \ \Theta_1 = \left(\psi\phi_1^2 + \theta_z\right) \text{ and } \Theta_2 = \left(\psi\phi_2^2 + \theta_z\right) \tag{B.42}$$

$$\overline{H} = i_\phi + \alpha\, j_\phi \tag{B.43.1}$$

$$i_\phi = 2\hat{f}_{x2}^* \left(\cos\theta_z - \cos\Theta\right) - 2\hat{f}_y \left(\sin\theta_z - \sin\Theta\right) \tag{B.43.2}$$

$$j_\phi = \frac{1}{2}\left(\hat{f}_{x2}^{*2} - \hat{f}_y^2\right)\left(\cos 2\theta_z - \cos 2\Theta\right) - \hat{f}_{x2}^* \hat{f}_y \left(\sin 2\theta_z - \sin 2\Theta\right) \tag{B.43.3}$$

$$\overline{H}_1 = i_{\phi 1} + \alpha\, j_{\phi 1} \tag{B.44.1}$$

$$i_{\phi 1} = 2\hat{f}_{x2}^* \left(\cos\theta_z - \cos\Theta_1\right) - 2\hat{f}_y \left(\sin\theta_z - \sin\Theta_1\right) \tag{B.44.2}$$

$$j_{\phi 1} = \frac{1}{2}\left(\hat{f}_{x2}^{*2} - \hat{f}_y^2\right)\left(\cos 2\theta_z - \cos 2\Theta_1\right) - \hat{f}_{x2}^* \hat{f}_y \left(\sin 2\theta_z - \sin 2\Theta_1\right) \tag{B.44.3}$$

$$\overline{H}_2 = i_{\phi 2} + \alpha\, j_{\phi 2} \tag{B.45.1}$$

$$i_{\phi 2} = 2\hat{f}_{x2}^* \left(\cos\theta_z - \cos\Theta_2\right) - 2\hat{f}_y \left(\sin\theta_z - \sin\Theta_2\right) \tag{B.45.2}$$

$$j_{\phi 1} = \frac{1}{2}\left(\hat{f}_{x2}^{*2} - \hat{f}_y^2\right)\left(\cos 2\theta_z - \cos 2\Theta_2\right) - \hat{f}_{x2}^* \hat{f}_y \left(\sin 2\theta_z - \sin 2\Theta_2\right) \tag{B.45.3}$$

$$\overline{A}_1 = 2\left(\cos\theta_1 - \cos\theta_z\right) + \alpha\left[\hat{f}_{x2}^* \left(\cos 2\theta_1 - \cos 2\theta_z\right) - \hat{f}_y \left(\sin 2\theta_1 - \sin 2\theta_z\right)\right] \tag{B.46}$$

$$\overline{A}_2 = 2\left(\cos\theta_z - \cos\theta_2\right) + \alpha\left[\hat{f}_{x2}^* \left(\cos 2\theta_2 - \cos 2\theta_z\right) - \hat{f}_y \left(\sin 2\theta_2 - \sin 2\theta_z\right)\right] \tag{B.47}$$

$$\overline{B}_1 = 2\left(\sin\theta_z - \sin\theta_1\right) - \alpha\left[\hat{f}_y \left(\cos 2\theta_1 - \cos 2\theta_z\right) + \hat{f}_{x2}^* \left(\sin 2\theta_1 - \sin 2\theta_z\right)\right] \tag{B.48}$$

$$\overline{B}_2 = 2\left(\sin\theta_z - \sin\theta_2\right) - \alpha\left[\hat{f}_y \left(\cos 2\theta_2 - \cos 2\theta_z\right) + \hat{f}_{x2}^* \left(\sin 2\theta_2 - \sin 2\theta_z\right)\right] \tag{B.49}$$

$$\overline{C}_1 = -2\hat{f}^*_{x2}\sin\theta_1 - 2\hat{f}_y\cos\theta_1 - \alpha\left[\left(\hat{f}^{*2}_{x2} - \hat{f}^2_y\right)\sin 2\theta_1 + 2\hat{f}^*_{x2}\hat{f}_y\cos 2\theta_1\right] \tag{B.50}$$

$$\overline{C}_2 = -2\hat{f}^*_{x2}\sin\theta_2 - 2\hat{f}_y\cos\theta_2 - \alpha\left[\left(\hat{f}^{*2}_{x2} - \hat{f}^2_y\right)\sin 2\theta_2 + 2\hat{f}^*_{x2}\hat{f}_y\cos 2\theta_2\right] \tag{B.51}$$

$$\overline{C}_z = 2\hat{f}^*_{x2}\sin\theta_z + 2\hat{f}_y\cos\theta_z + \alpha\left[\left(\hat{f}^{*2}_{x2} - \hat{f}^2_y\right)\sin 2\theta_z + 2\hat{f}^*_{x2}\hat{f}_y\cos 2\theta_z\right] \tag{B.52}$$

$$\overline{D} = 2\cos\theta_z - 2\cos\Theta + \alpha\left[\hat{f}^*_{x2}\left(\cos 2\theta_z - \cos 2\Theta\right) - \hat{f}_y\left(\sin 2\theta_z - \sin 2\Theta\right)\right] \tag{B.53}$$

$$\overline{E} = 2\cos\theta_z - 2\cos\Theta + \alpha\left[\hat{f}^*_{x2}\left(\cos 2\theta_z - \cos 2\Theta\right) - \hat{f}_y\left(\sin 2\theta_z - \sin 2\Theta\right)\right] \tag{B.54}$$

$$\overline{L} = -2\hat{f}^*_{x2}\left(\sin\theta_z - \sin\Theta\right) - 2\hat{f}_y\left(\cos\theta_z - \cos\Theta\right)$$
$$- \alpha\left[\left(\hat{f}^{*2}_{x2} - \hat{f}^2_y\right)\left(\sin 2\theta_z - \sin 2\Theta\right) + 2\hat{f}^*_{x2}\hat{f}_y\left(\cos 2\theta_z - \cos 2\Theta\right)\right] \tag{B.55}$$

$$\overline{M} = \psi 2\phi\cos\Theta + \psi 2\phi\alpha\left[\hat{f}^*_{x2}\left(\cos^2\Theta - \sin^2\Theta\right) - 2\hat{f}_y\sin\Theta\cos\Theta\right] \tag{B.56}$$

$$\overline{N} = -\psi 2\phi\sin\Theta - \psi 2\phi\alpha\left[\hat{f}_y\left(\cos^2\Theta - \sin^2\Theta\right) + 2\hat{f}^*_{x2}\cos\Theta\sin\Theta\right] \tag{B.57}$$

$$\overline{\varepsilon}_0 = \alpha\left(\hat{f}^*_{x2}\cos\Theta - \hat{f}_y\sin\Theta\right) \tag{B.58}$$

$$\overline{\varepsilon}_1 = \alpha\left(\hat{f}^*_{x2}\cos\Theta_1 - \hat{f}_y\sin\Theta_1\right) \tag{B.59}$$

$$\overline{\varepsilon}_2 = \alpha\left(\hat{f}^*_{x2}\cos\Theta_2 - \hat{f}_y\sin\Theta_2\right) \tag{B.60}$$

APPENDIX C

From equations (3.59)-(3.62) and (3.64), the entries of matrices $\partial \boldsymbol{T} / \partial \beta$, $\partial \beta / \partial \boldsymbol{u}$ and $\partial \boldsymbol{u}^* / \partial \boldsymbol{u}$ can be obtain as

$$\frac{\partial \boldsymbol{T}}{\partial \beta} = \begin{bmatrix} 0 & 0 & 0 & -s_\beta & -c_\beta & 0 \\ 0 & 0 & 0 & c_\beta & -s_\beta & 0 \\ 0 & 0 & 0 & 0 & 0 & 0 \\ -s_\beta & 0 & 0 & 0 & 0 & -c_\beta \\ c_\beta & 0 & 0 & 0 & 0 & -s_\beta \\ 0 & 0 & 0 & 0 & 0 & 0 \end{bmatrix} \tag{C.1}$$

$$\frac{\partial \beta}{\partial \boldsymbol{u}} = \begin{bmatrix} s_\beta / \hat{d}^* & -c_\beta / \hat{d}^* & 0 & -s_\beta / \hat{d}^* & c_\beta / \hat{d}^* & 0 \end{bmatrix} \tag{C.2}$$

$$\frac{\partial \boldsymbol{u}^*}{\partial \boldsymbol{u}} = \begin{bmatrix} -c_\beta & -s_\beta & 0 & c_\beta & s_\beta & 0 \\ -s_\beta / \hat{d}^* & c_\beta / \hat{d}^* & 1 & s_\beta / \hat{d}^* & -c_\beta / \hat{d}^* & 0 \\ -s_\beta / \hat{d}^* & c_\beta / \hat{d}^* & 0 & s_\beta / \hat{d}^* & -c_\beta / \hat{d}^* & 1 \end{bmatrix} \tag{C.3}$$

where $c_\beta = \cos \beta$, $s_\beta = \sin \beta$ and $\hat{d}^* = 1 + \hat{u}_2^*$

BIOGRAPHY

The author, Mr. Jongaphonh Douanevanh was born in Phonkheng Village, Saysettha District, Vientiane Capital, Lao P.D.R, on December 05, 1986. He graduated high school from Vientiane Secondary School in July 2003, and enrolled in Bachelor of Engineering in Civil Engineering at Department of Civil Engineering, Faculty of Engineering, National University of Laos (NUOL) at the same year. After graduation in August 2008, he has been working at Lao Brewery Company Limited for four months. He continued his master's degree in Civil Engineering at Chulalongkorn University in June 2009 under the AUN/SEED-Net (JICA) Scholarship. The major in his master's degree is structural engineering, which includes studies and researches in structural mechanics and with advanced mathematical techniques. His thesis aims to investigate the actual deformed behavior of structures. He successfully fulfilled the requirements for the Master of Engineering degree in October 2011.